Development of a moving bed reactor for thermochemical heat storage with $Ca(OH)_2$

A thesis accepted by the Faculty of Energy-, Process- and Bio-Engineering of the Universität Stuttgart to fulfil the requirements for the degree of Doctor of Engineering Sciences (Dr.-Ing.)

by

Aldo Miguel Cosquillo Mejia

born in Lima, Peru

Main referee: Prof. Dr. rer. nat. habil. André Thess

Co-referee: Prof. Mina Shahi

Date of oral exam: 19.12.2024

Institute for Building Energetics, Thermotechnology and Energy Storage

2024

Ich erkläre, dass ich abgesehen von den ausdrücklich bezeichneten Hilfsmitteln diese Dissertation selbstständig verfasst habe.

Köln, den 17.05.2024

Aldo Miguel Cosquillo Mejia

Acknowledgement

"Der Weg ist das Ziel", I could not agree more to this German saying when it comes to think of the time for this work. In this period, I did not only obtain academic knowledge but had also the chance to acquire valuable life experience and met people that made this journey very interesting. I would therefore like to spend a few words to acknowledge and thank the people who were directly or indirectly involved in this endeavour.

Prof. André Thess, for giving me the opportunity to do research at the Institute and for his insightful and positive feedback during the seminars of doctoral candidates.

I would also like to thank Prof. Mina Shahi for accepting to co-referee this thesis.

Dr. Matthias Schmidt, for his supervision and valuable guidance in multiple aspects during this work: in the lab during the experiments, on the board when thermodynamics seemed somewhat tricky and for always keeping a positive working environment.

Dr. Marc Linder for the great leadership, positive attitude to my results, constructive feedback and for the encouragement to further develop my scientific skills.

The whole TCS team. Kai, for all the help in the lab and for the encouragement towards the end of this work. Andreas for his professionalism and technical assistance in the lab. Viktor, for his insights in material selection and proposed solutions during the last stage of the experimental work. Venizelos, for sharing his experiences from his own test bench, suggesting solutions when technical issues appeared and for keeping a great working atmosphere in the group. Nicole, for showing me that hard work and perseverance can just make you stronger. Veronika, for her patience, guidance and also help with the language during my first months at DLR. Jonina, for her always welcoming and positive attitude, the permanent encouragement to professional growth and for her patience towards my German language skills. Many thanks to Inga, Marie, Alex, Eva, Hanna, Christian Brack, Mila, Jana, Andrea Gutierrez, Christian Weckerle and Michael for sharing their technical and scientific thinking during our peer-mentoring sessions or one-to-one discussions. Hannes Neckermann, for his valuable assistance during his Master Thesis.

My mother, who always encouraged me to take challenges, no matter how big they look or how far away I have to travel to beat them. Thank you for your visits and for the great Peruvian food you made here in Germany so that I didn't feel very homesick. My brothers and specially my only sister, who gave me examples of resilience. My brother Juan, the surgeon, the academic guy, the one I know feels proud every time he gets news of my achievements. Thank you for being always someone to look up to.

Andrea, for being the ears to my stories on the other side of the ocean, even though they sound rocket science sometimes. Thank you for giving me peace of mind, for your understanding and motivation.

Last but not least, to my father, who saw a great deal of this process and who would for sure be so proud to see this come true.

Table of Contents

Nomenclature

Symbols

T	Temperature	K
ρ	Density	m^3/kg
p	Pressure	kPa
H	Height of the packed bed	m
ΔH	Reaction enthalpy	kJ/mol
μ	Dynamic viscosity	Pa.s
v	Kinematic viscosity	m^2/s
a	Thermal diffusivity	m^2/s
U	Gas velocity	m/s
d_p	Particle diameter	m
ε	Fractional void	-
g	Gravity	m^2/s
α	Heat transfer coefficient	$W/m^2.K$
λ	Thermal conductivity	W/m. K
U_{mf}	Minimal fluidisation velocity	m/s
Re_{mf}	Reynolds minimal fluidisation	-
Re_{ψ}	Reynolds coefficient in void fraction	-
Nu	Nusselt number	-
Ar	Archimedes number	-
Pr	Prandtl number	-

Abbreviations

CAES	Compressed air energy storage
SMES	Superconducting magnetic energy storage
TES	Thermal energy storage
TCS	Thermochemical storage
CSP	Concentrated solar power
DSC	Differential scanning calorimetry
TGA	Thermogravimetric analysis
TA	Thermal analyser
CMC	carboxymethyl cellulose
EFP	easy-to-fluidise particles
SEM	Scanning electron microscope
XRD	X-ray diffraction

Kurzfassung

Die Verwendung des Reaktionssytems $Ca(OH)_2/CaO$ bietet mehrere Vorteile bei der Nutzung als Wärmespeichermaterial. Die thermochemische Reaktion hat eine hohe Energiedichte und bietet die Möglichkeit, die im chemischen Potential vorhandene Energie über lange Zeiträume und ohne Energieverluste zu speichern. Dies ist von besonderem Interesse, wenn es um saisonale Speicherung geht. Darüber hinaus sind die niedrigen Kosten des Materials, die erwiesene Zyklenstbilität und die allgemeine weltweite Verfügbarkeit als natürliche Ressource wirtschaftlich und nachhaltig attraktiv. Jedoch stellen die inhärenten Eigenschaften des pulverförmigen Ausgangsmaterials, z.B. die geringe Wärmeleitfähigkeit und die Tendenz zur Agglomeration, eine große Herausforderung bei der Konstruktion von Reaktoren dar. Eine kosteneffiziente Lösung ist die Entkopplung von Leistung und Kapazität, d.h. die Verwendung von Bewegtbettreaktoren. Aufgrund der ungünstigen Eigenschaften des Materials muss es jedoch modifiziert werden, um einen effizienten Wärme- und Stofftransport zu gewährleisten.

In dieser Arbeit wurden drei Reaktoren für die thermische Zyklierung von modifiziertem $Ca(OH)_2$ und die Demonstration des Bewegtbettkonzepts entwickelt und in Betrieb genommen. Das erste Design entspricht einer Reaktionskammer, die für die schnelle Zyklierung und die visuelle Echtzeitverfolgung des reagierenden Materials im technischen Maßstab ausgelegt ist. Nachfolgend trugen weitere Materialuntersuchungen mittels z.B. TGA, XRD und Druckkraftmessungen zu einer umfassenden Charakterisierung des Granulats bei. Zwei verschiedene Proben wurden in diesem Setup 20 Zyklen unterzogen: Granulate, die mit nanostrukturierten Al_2O_3-Partikeln beschichtet waren, und $Ca(OH)_2/CaCO_3$-Verbundstoffe. Der Betrieb des Reaktors wurde ebenso demonstriert wie ein vollständiger Umsatz des Granulats. Die positive Auswirkung der Al_2O_3-Beschichtung und des $CaCO_3$-Anteils im Kompositmaterial auf die Stabilisierung der Partikel wurde nachgewiesen. Gleichzeitig wurden keine Anzeichen von Agglomeration festgestellt.

Das zweite Design ist ein indirekt beheizter Reaktor mit einem Rohrbündel-Wärmetauscher. Nach 6 thermochemischen Zyklen, die mit zwei verschiedenen Proben durchgeführt wurden, CaO-Granulat, das in einer Keramikschale eingekapselt ist, sowie $Ca(OH)_2$-Granulat, das mit nanostrukturierten Al_2O_3-Partikeln beschichtet ist, wurde nachgewiesen, dass beide Modifikationen zur Stabilisierung der Partikel beitragen. Obwohl mit dem verkapselten Granulat das Bewegtbettkonzept des Reaktors technisch nachgewiesen wurde, war die Energiedichte des Materials deutlich geringer und ihr Umsatz unvollständig. Im Gegensatz dazu zeigte das beschichtete Granulat einen vollständigen Umsatz mit einer höheren Energiedichte als das Pulverspeichermaterial. Allerdings konnte die natürliche Volumenänderung des

Materials, infolge der chemischen Reaktion, nicht verhindert werden was die Bewegung der Partikel durch den Reaktor erschwerte. Daher wurde unter Kombination der experimentellen Erkenntnisse mit dem indirekten Bewegtbettreaktor, und den charakterisierten Eigenschaften des Speichergranulats, ein neuartiges direkt beheiztes Reaktorkonzept entwickelt.

Bei der Konstruktion wurden zwei Hauptanliegen berücksichtigt: die Bereitstellung von genügend Wärmeenergie, um den Umsatz des Granulats anzutreiben und gleichzeitig die Fluidisierung des Bettes zu vermeiden. Die Vermeidung der Fluidisierung soll die mechanische Beanspruchung auf die Partikelstabilität des Granulats minimieren. Aufgrund der höheren Energiedichte wurden die mit Al_2O_3 beschichteten $Ca(OH)_2$-Granulate für einen 10-fachen thermochemischen Zyklus in diesem Reaktor ausgewählt. Neben dem vollständigen Umsatze des Speichergranulats wurde zum ersten Mal auch die Bewegung des Materials in diesem neu entwickelten Reaktorkonzept demonstriert. Darüber hinaus wurde entdeckt, dass die Wechselwirkung zwischen $Ca(OH)_2$ und Al_2O_3 eine Schicht erzeugt, die den Granulaten eine erhöhte Stabilität verleiht. Die Ergebnisse dieser Arbeit dienen als Ausgangspunkt für die Skalierung des Reaktorkonzepts zu einer Pilotanlage, die mit $Ca(OH)_2$ arbeitet, dass nach dem Ansatz der Partikelstabilisierung modifiziert wurde.

Abstract

The use of the reaction system $Ca(OH)_2/CaO$ offers several advantages as a heat storage system. For instance, as a thermochemical reaction it has a high energy density and offers the possibility to store the chemical potential energy for long periods of time without energy losses. This is of particular interest when seasonal storage applications are sought. Furthermore, its low cost, proven cyclability and generally worldwide availability as natural resource makes it economically and sustainably attractive. Nevertheless, the inherent properties of the base powder material e.g. low thermal conductivity and tendency to agglomerate present a major challenge when designing reactors. A cost-efficient solution is the detachment of the power and capacity i.e. the use of moving bed reactors. Nevertheless, due to the unfavourable characteristics of the material, it has to be subject of modifications to ensure efficient heat and mass transport.

In this thesis, three reactors were developed and set into operation for the thermal cycling of modified $Ca(OH)_2$ and demonstration of the moving bed concept. The first design corresponds to a reaction chamber designed for the rapid cycling and real-time tracking of the reacting material under technical scale. In addition, further material analysis (e.g. TGA, XRD and dynamometry) contributed to an extensive assessment of the granules. Two different samples were cycled 20 times in this setup: granules coated with Al_2O_3 nanostructured particles and $Ca(OH)_2/CaCO_3$ composites. The operation of the reactor was demonstrated as well as the full conversion of the granules. The positive effect on the particle stabilisation given by the Al_2O_3 coating and the $CaCO_3$ share in the composites was confirmed and at the same time no evidence of agglomeration was found.

The second design is an indirectly heated reactor with a tube bundle heat exchanger. After 6 thermochemical cycles conducted with two different samples, CaO granules encapsulated in a ceramic shell and $Ca(OH)_2$ granules coated with Al_2O_3 nanostructured particles, it was proven that both modifications contribute to the particle stabilisation. Although the encapsulated granules proved the moving bed concept of the reactor, the energy density was significantly lower and their conversion incomplete. In contrast, the coated granules displayed a complete conversion with energy density higher than the powder storage material. However, the natural change in dimensions of the reactive material, as a result of the thermal cycling, could not be prevented and therefore the movement of the bed was hindered. After combining the experimental results of the indirect moving bed reactor and the determined characteristics of the storage granules, a novel directly heated reactor concept was developed.

The lab scale reactor was designed taking into consideration two main concerns: to supply enough thermal energy to drive the conversion of the granules while avoiding the fluidisation of the bed. The latter condition seeks to minimise the mechanical impact on the particle stability of the granules. Due to the higher energy density, the $Ca(OH)_2$ granules coated with Al_2O_3 were selected for a 10-fold thermochemical cycle in this reactor. Besides the full conversion of the storage granules, the movement of the material in this novel reactor configuration was demonstrated for the first time. Furthermore, it was discovered that the interaction between $Ca(OH)_2$ and Al_2O_3 produces a layer that confers the enhanced stability of the granules. Therefore, the results of this work can be used as the starting point for the upscale of the reactor design towards a pilot facility that works with $Ca(OH)_2$ modified following the particle stabilisation approach.

1. Introduction

The route for a zero-net carbon emission future requires the rapid decarbonisation of the energy sources. One the one hand, the increasing installed capacity of renewable sources of energy e.g. photovoltaic, wind and solar thermal contributes to this goal, especially in the electricity sector. However, due to the intermittent availability of wind and solar irradiation, there is a mismatch between the energy supply and demand. Such discrepancy is compensated mostly by fossil-based systems. For this reason, in order to achieve a carbon-free energy system, cost-efficient storage technologies must be developed. Different energy storage systems have been developed according to the specific needs to be met. According to the form of energy stored they can be classified as mechanical (e.g. flywheels, pump hydroelectric and compressed air energy storage (CAES)), electric systems (e.g. supercapacitors and superconducting magnetic energy storage (SMES)), electrochemical systems (e.g. lithium-ion battery and flow battery), hydrogen storage and thermal energy storage (TES). Among them, the latter is of interest since heat accounts for almost half of the global energy consumption [1]. Table 1 presents a summary of the characteristics of some storage systems.

Table 1. Characteristics of different energy storage systems (adapted from Zhang et al. [2])

Energy storage system	Storage Mechanism	Storage period	Energy density (KWh/m^3)	Price per unit energy-stored (€/kWh)
Flywheels	Mechanical	Hour	20-80	100,000-400,000
Pumped hydro energy storage	Mechanical	Day – month	0.5 -1.5	10 – 70
Compressed air energy storage (CAES)	Mechanical	Day	3-6	2-140
Superconducting magnetic energy storage (SMES)	Electrical	Hour	0.2-2.5	63,000-750,000

Lithium-ion (Li – ion)	Conventional battery	Day – month	200 – 500	500 - 2000
Vanadium redox battery	Flow battery	Day-month	16-33	110-750
Hydrogen-based energy storage system	Chemical	Day – month	2.7 – 160 (at 1–700 bar)	2 – 15
Thermo-chemical storage (TCS)	Thermal	Hour - month	1120 - 250	8 - 100

The working mechanism of TES consists of transferring heat to a storage media (charge) and then release it when energy is needed (discharge) [3]. Depending on the storage material used, TES can be divided into three categories: sensible, latent and thermochemical storage. In sensible storage, the energy is stored by means of changing the temperature of the material. It has been extensively studied and thus has reached the highest level of maturity. One application can be found in concentrated solar power (CSP) plants where heat is stored during the daytime and the heat release is used to generate high-pressure steam for the power block and thus improve the dispatchability of electricity during unfavourable weather conditions or at night [4, 5]. Latent storage is based on heat absorption/release occurring when there is a phase change in the storage material. The third category corresponds to thermochemical storage, which utilises the potential high energy density in the reversible chemical reactions to store energy. Thus, the enthalpy of reaction is used on both endothermal and exothermal reaction to store or release energy respectively [6] (see Eq. 1).

$$A_{(s)} + B_{(g)} \rightleftharpoons AB_s + \Delta H \quad (1)$$

Unlike sensible and latent storage, which have limitations due to the heat losses, thermochemical storage displays the highest energy density and offers the possibility of storage without thermal losses for long periods of time [2]. Therefore, it can be used to bridge the seasonal heat supply and demand discrepancy and contribute in the decarbonisation of the heating sector.

Among the thermochemical storage systems, the following gas-solid reversible reaction is of high interest (Eq. 2):

$$Ca(OH)_2 + \Delta H \rightleftharpoons CaO + H_2O \quad (2)$$

One of the reasons for the interest in this reaction is the availability of the raw material. Calcium hydroxide is found in nature as limestone ($CaCO_3$) which is present in

bedrocks of Karst landscapes. This in principle confers this material the characteristic of being not toxic. Furthermore, unlike other minerals extracted only in a few locations [7], Karsts are fairly well distributed around the globe [8, 9]. In order to obtain calcium hydroxide, a series of reactions must take place. First, calcium carbonate from limestone is calcinated at high temperatures (> 900 °C) to obtain calcium oxide and CO_2 (Eq. 3). Then, water is added to form calcium hydroxide in an exothermal reaction (Eq. 4).

$$CaCO_3 + 182.1\ kJ/mol \rightarrow CaO + CO_2 \quad (3)$$

$$CaO + H_2O \rightleftharpoons Ca(OH)_2 + 104\ kJ/mol \quad (4)$$

Besides the high energy density, another advantage of this storage system is the low cost of the material. For these reasons, the material is regarded as a promising for thermal energy storage. However, the powder material displays inherent properties that require complex and costly reactor designs when upscaling is sought. Hence, in order to make the most of the competitive price of the powder material, the reactor (power) and storage (capacity) must be detached. This configuration requires the continuous or semi continuous movement of the storage particles through the reaction chamber. Given the challenges the material possesses and in order to achieve the movement of a reacting bed, different strategies at the material and reactor side must be applied. Therefore, the aim of this thesis is to develop and demonstrate the operation of a moving bed reactor for $Ca(OH)_2$ as storage material.

1.1. State of the technology

The $Ca(OH)_2/CaO$ storage system is of particular interest when seasonal heat storage applications are considered at domestic and industrial scale e.g. district heating. Here, the electricity and supply sector can be coupled by using the surplus of renewable electricity produced in summer to charge large volumes of storage material. Later, when the demand of heat rises in winter, the heat stored in the form of chemical potential can be utilised by performing the hydration of the storage material. In addition, the reaction has the potential to upgrade waste heat and therefore increase the efficiency of thermal industrial processes. For these reasons, a number of investigations have been carried out to characterise this thermochemical system, produce modifications to the material and to develop cost-efficient reactors which will be reviewed in this section.

1.1.1. Material characterisation

Thermodynamic equilibrium and reaction enthalpy

In a chemical reaction, the equilibrium is a state given when the concentration of reactants equalises to the concentration of products. The equilibrium indicates that the forward and backward reactions of a reversible reaction occur at the same rate. If the direction of the reaction wants to be driven, changes in the parameters of temperature or pressure must be applied. Several studies have been carried out to determine the thermodynamic equilibrium of $Ca(OH)_2$ /CaO. For instance, Schaube et al. [10] conducted a series of experiments in a TG analyser to collect data from the dehydration and hydration of $Ca(OH)_2$ /CaO at H_2O partial pressures of 4.3, 17.6, 35.5 and 96.6 kPa and derived an equilibrium equation in terms of pressure and temperature. Using the same method, Matsuda et al. [11] determined the equilibrium after performing experiments using lower H_2O partial pressures ranging from 1.2 to 16 kPa. Other authors designed their own set up to conduct the experiments. For example, Halstead and Moore [12] performed a series of pressure measurement during the dehydration and rehydration experiments. To this end, they developed a setup consisting of a quartz tube connected to a vacuum pump and supply of moist CO_2-free air. The values of pressure ranged from 2.5 to 89.5 kPa. Samms and Evans [13] used a steel vessel connected to a controlled temperature autoclave to supply steam at different pressures (100-5000 kPa) to measure the temperature resulted from the formation of $Ca(OH)_2$. In general, these experiments vary in the methods applied and experimental conditions which results in different equilibrium equations. The reaction enthalpy found in the afore mentioned experiments lays between 94.6 and 111.8 kJ/mol. Fig. 1 summarises the equilibrium lines from the experimental works described and compares them with the equilibrium line plotted from the tabulated values of Gibbs free enthalpy found in Barin [14]. For the calculations of equilibrium temperature in this work, the equation of Samms and Evans is used (Eq. 5).

$$\ln\left(p_{H_2O}[bar]\right) = -\frac{11375}{T\,[K]} + 14.574 \tag{5}$$

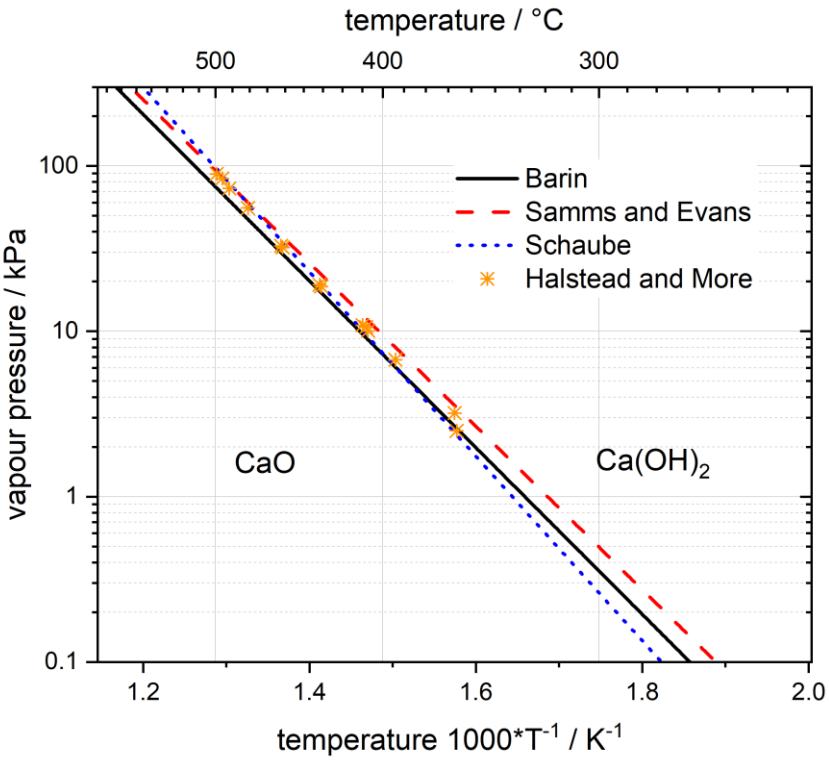

Fig. 1. Chemical equilibrium lines of the reaction $Ca(OH)_2 + \Delta H \rightleftharpoons CaO + H_2O$

Heat capacity and thermal conductivity

Schaube et al. [10] determined the heat capacity of $Ca(OH)_2$ and CaO by means of differential scanning calorimetry (DSC). The reported results correspond to temperatures between 25 and 500 °C and are in good accordance with the values found in the tables of JANAF [15] and Barin [14]. For instance, for $Ca(OH)_2$ the heat capacity ranges between 1.2 and 1.5 kJ/kg.K wheras for CaO, it lays from 0.75 to 0.9 kJ/kg.K. Regarding the heat conductivity, Schaube et al [16] and Ogura et al. [17] used different methods to experimentally determine values that range between 0.1 and 0.55 W/m.K. It was found that the heat conductivity increases when the powder is compressed and therefore displays a higher density. Despite this enhancement, the reached values are low and therefore the heat transfer remains challenging for the design of reactors.

Cycle stability

As mentioned before, the $Ca(OH)_2$/CaO system possesses high energy density. However, the decrease in the degree of conversion counterbalances this advantageous feature. For this reason, several studies focused on demonstrating the stability of the conversion over a large number of cycles. For instance, Schaube et al. [10] reported full conversion for powder $Ca(OH)_2$ over 100 cycles in a TGA device. Furthermore, Criado et al. [18] confirmed reversibility of the reaction by completing 32 cycles over calcined

limestone particles sized between 100 and 200 µm. The largest experimental series was carried out by Rosemary et al. [19], who conducted more than 1000 cycles over an 8-g $Ca(OH)_2$ sample in a self-design setup and reported steady conversion with values over 90 %. In addition, this study mentions the formation of $CaCO_3$ in the sample due to leaked-in CO_2 from ambient air in the reaction chamber.

CO_2 in the $Ca(OH)_2$/CaO reaction

The high energy density the $Ca(OH)_2$/CaO reaction displays can be negatively affected by the presence of CO_2 as this gas leads to the formation of $CaCO_3$. Hence, the energy density of the storage material results diminished. For this reason, several authors studied how the carbonation takes place. For instance, Criado et al. [20] demonstrated that the CO_2 carrying capacity of CaO increases with the temperature. Yan et al. [21] observed that under dry conditions the carbonation proceeds more easily for $Ca(OH)_2$ than CaO at low CO_2 levels (0.1 %), although with a share of $CaCO_3$ below 1.5 % of the total mass. Nevertheless, when the concentration of CO_2 is substantially higher in the gas mix (25 %), CaO reacts faster which results in the loss of almost half of the reactive material. They also discovered that the extent of the carbonation is larger under wet conditions and that longer hydration times result in increased values of $CaCO_3$. This is in agreement with Wang et al. [22], who demonstrated that the absorption of CO_2 in CaO is enhanced by the presence of H_2O. In summary, the presence of CO_2 is disadvantageous for the cycling stability of the $Ca(OH)_2$ /CaO storage system. For this reason, measures must be applied in order to avoid the carbonation of the storage material in either closed or open systems.

Reaction kinetics

The reaction kinetics of the dehydration and hydration of $Ca(OH)_2$/CaO plays an important role in the design of this thermochemical energy storage system. Thus, finding a mathematical expression that describes the reaction kinetics allows for the calculation of the heat and mass transfer and the upper limit of power in a reactor design. For this reason, multiple studies have been carried out in thermogravimetric analysers under vacuum conditions or using nitrogen or air atmosphere for the thermal decomposition of $Ca(OH)_2$. From the data obtained, empirical models associated to multiple reaction steps were proposed. For instance, Koga et al. [23] proposes a number of kinetic equations for the different steps occurring during the dissociation of reactants. Schaube et al. [10] and Mikhail et al. [24] proposed two reaction steps based on the degree of conversion of the sample. In general, the research proposes that a dehydration zone begins at the crystal surface and moves inward the particle [23-25] and that the presence of water vapor, the particle size, degree of compaction and sample temperature hinder the diffusion of water from the reactant [11, 18, 23, 25]. For describing the kinetics of hydration at high partial pressures of

water, Schaube et al. [10] proposed two equations, one for lower temperatures and another when the temperature is close to equilibrium. Criado et al. [18] proposed two reaction models that take into consideration the entire particle or the surface. In general, the amount of experimental data as well as the models derived is fairly extended due to the different methodologies and parameters used. For this reason, finding a unique mathematical expression that describes the kinetics of the reaction is still challenging.

Flowability

Fine powders like calcium hydroxide or oxide have a particle mean diameter of approximately 5 µm. Hence, the interparticle adhesion forces (e.g. Van der Waals forces) outweigh the gravitational forces which results in poor flowability [26]. Gollsch et al. [27] experimentally determined the flowability of powder $Ca(OH)_2$ in a ring shear. The results classified the material as "very cohesive" and "cohesive" which in turn challenges its use in moving or fluidised bed reactors.

1.1.2. Material modifications

Despite its multiple advantages as thermochemical storage, the powder $Ca(OH)_2/CaO$ has drawbacks such as low thermal conductivity and poor mechanical properties. For this reason, various modifications to the material have been investigated in order to enhance its performance e.g. by improving the thermal conductivity, enhancing the reaction kinetics or by conferring particle stabilisation.

Enhancement of the thermal conductivity

One of the modifications consists of doping the material with Al and Zn, expanded graphite or hexagonal boron nitride to enhance the thermal conductivity of the powder $Ca(OH)_2$ and thus accelerate the rate of decomposition [28-30] (see Fig.2). Funayama et al. used SiC-Si-based foam and honeycomb to increase the heat transfer of $Ca(OH)_2$ and thus achieved higher output [31, 32].

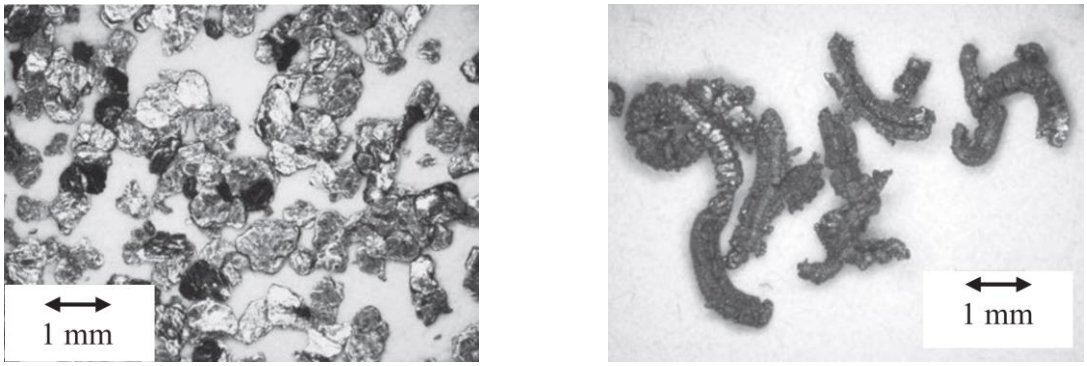

Fig. 2. Microscope images of expanded graphite precursor (left) and expanded graphite (right) [30]

Reaction kinetics enhancement

Other investigation groups focused on the modifications to enhance the kinetics of the dehydration and hydration by means of different additives. For instance, the use of salts based on Ni, Zn, Al, Li and Mg have been proved to accelerate the dehydration of $Ca(OH)_2$ and to lower the reaction temperature [33-35]. In the search for the same effect on $Ca(OH)_2$, Shkatulov and Aristov [36] conducted a screening of different salts and determined KNO_3 as the most suitable candidate which was later proved by the experimental investigation of Wang et al. [37]. Li et al. [38] demonstrated that this effect can also be achieved by doping $Ca(OH)_2$ with $ZrO(NO_3)_2$ while Bian et al. [39] used Ce and Mn to accelerate the hydration process of CaO. Kariya et al. [40, 41] used vermiculite and silicon carbide for this purpose (Fig. 3). During the hydration of these composites, the rate of reaction resulted higher than pure $Ca(OH)_2$, specially with the use of porous silicon carbide that improved the diffusion of steam.

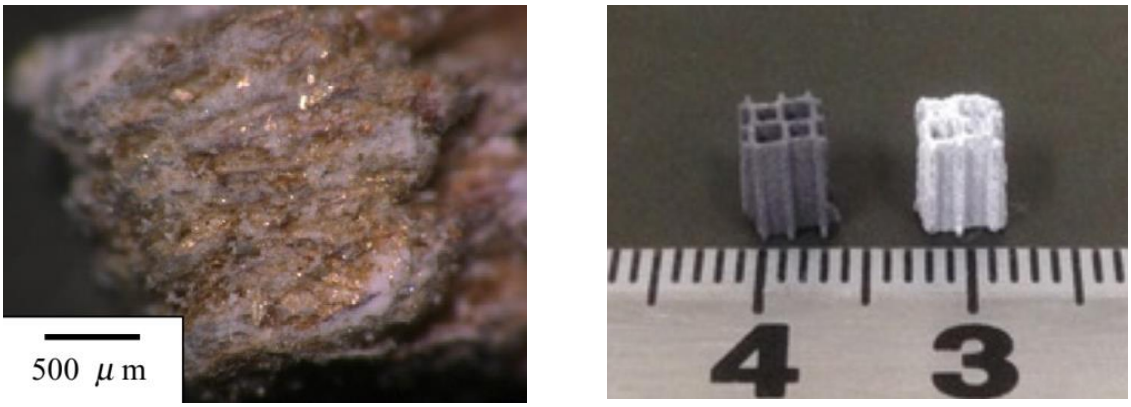

Fig 3. Left: Composite of vermiculite and $Ca(OH)_2$ [40]. Right: SiC support frame (left) and SiC frame containing CaO (right) [41].

Particle stabilisation

Stabilisation of powder $Ca(OH)_2$

In order to increase the mechanical properties and stabilise the particles of the storage material, different approaches have been investigated. For example, the use of nanostructured silica to coat the surface of $Ca(OH)_2$ particles proved to reduce their adhesive forces and therefore prevent agglomeration [42, 43] (Fig. 4) although with certain loss of reactivity under technical conditions [44]. Besides the SiO_2, Gollsch et al. [27] investigated the coating of host $Ca(OH)_2$ particles with nanostructured alumina. The flowability in the mix resulted improved, however it gradually decreased after thermochemical cycling. Another example is the use of frames to support powder $Ca(OH)_2$ [31, 32, 45] (Fig. 5).

Fig. 4. Left: Calcium hydroxide powder with 0.5 wt% additive after 4 cycles in the lab scale reactor [43]

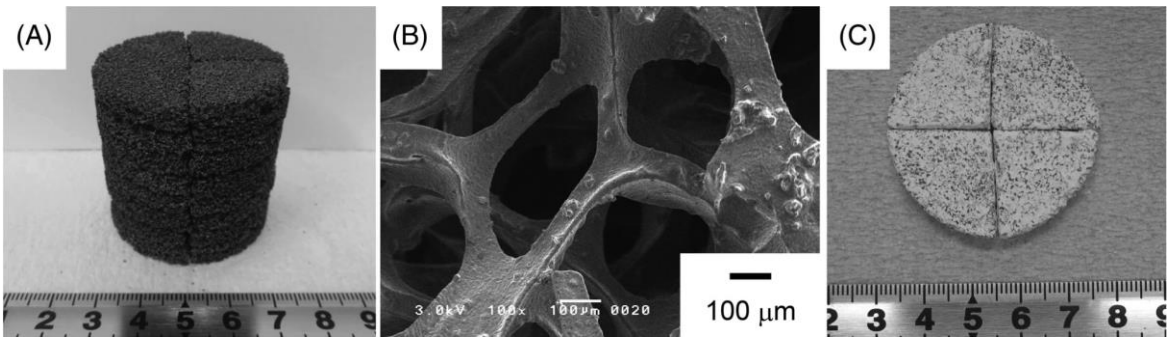

Fig. 5. A: Ceramic foam silicon carbide and silicon (SiC/Si); B: reticulate structure of the foam; C: composite material: foam with calcium hydroxide [32]

Use of binder matrix and composites

The use of binder matrix or the development of composites based on CaO has been subject of multiple research works. For instance, Criado et al. [46, 47] investigated the stabilisation of shaped CaO by inserting it in a binder matrix of sodium silicate. Although the mechanical stability increased significantly, the effect was progressively lost with the number of cycles. Sakellariou et al. [48] developed composites of CaO and kaolinite as binder to be subject of 20 thermal cycles in a TA device (Fig. 6). The mechanical stability of the samples resulted enhanced due to a Ca/Al/Si network structure in which CaO was contained. Similarly, Xia et al. [49], manufactured pelletised composites of CaO and carboxymethyl cellulose sodium (CMC-Na) to be the binder of vermiculite. Both CMC-Na and vermiculite built a structure in which the storage material was supported.

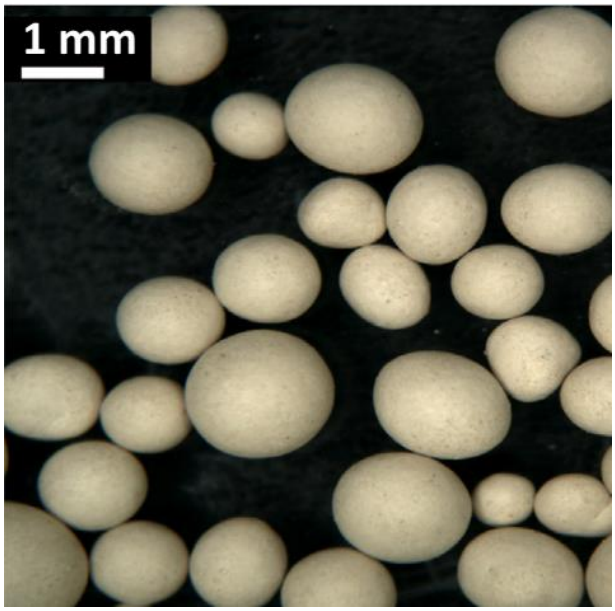

Fig. 6. Composite of Ca-Kaolinite pellets [48]

Macroencapsulation

Macroencapsulation is another method investigated to provide stability to the storage material. For example, Guo et al. [50] calcinated a mixture of $CaCO_3$ and CMC (carboxymethyl cellulose) to produce composite pellets that were later embedded in a silicon carbide matrix. The shelled pellets demonstrated to retain mechanical stability and relatively high storage density over 22 thermochemical cycles. Afflerbach et al. [51, 52], investigated the stabilisation effect of a ceramic shell on a CaO granule. After a 10-fold cycle experiment in a TA, the mechanical stability enhanced by the ceramic shell resulted slightly lowered by the thermal cycling (Fig. 7). In addition, the conversion was stable during the experiment series due to the permeability of the shell to water vapour. Due to the promising results, this modified material was tested in larger amounts in lab-scale reactors [53, 54] and the results are part of the present work.

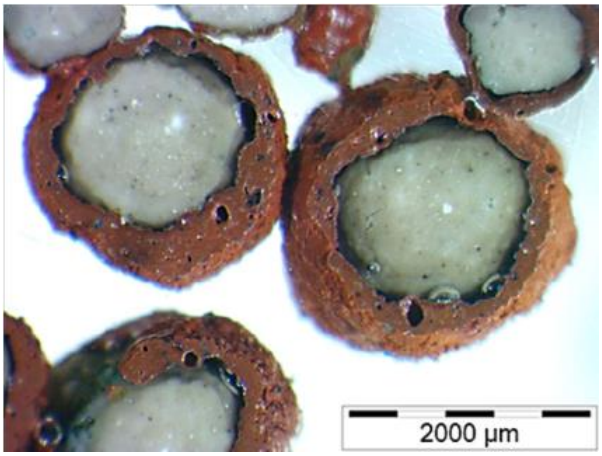

Fig. 7. Polished section of CaO granules encapsulated with oxide ceramic shell [52]

$Ca(OH)_2$ -based granules or pellets

Another approach investigated is the stabilisation of particles by shaping of $Ca(OH)_2$ powder into granules or pellets. For example, after a 17-fold cycle experimental series with $Ca(OH)_2$ pellets, Funayama et al. [55] discovered that the reactivity remained stable. However, the pellets displayed sintering and agglomeration occurred (Fig. 8). Fujii et al. [56] discovered that doping pellets with Al increases the dehydration rate and contributes to enhance their integrity. Yet this effect lasted only for one cycle.

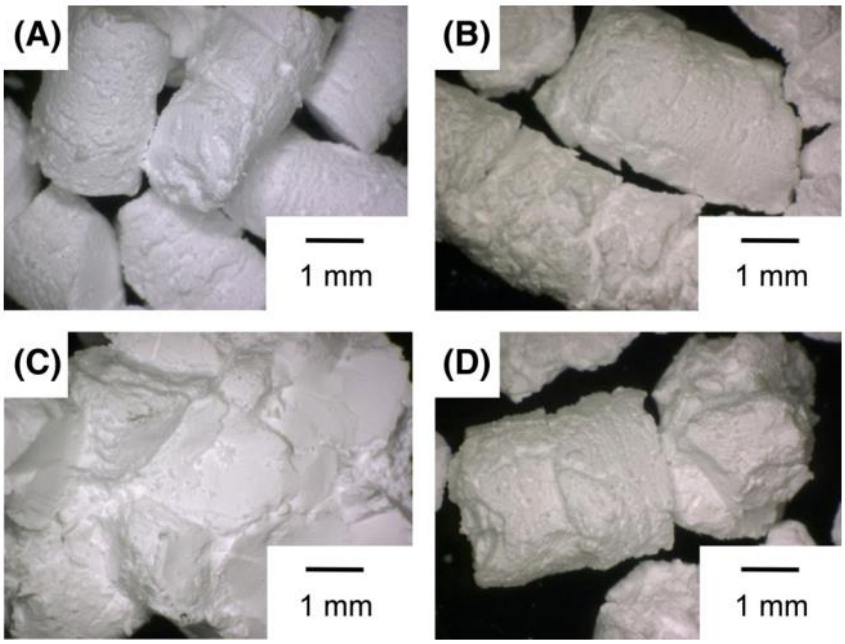

Fig 8. $Ca(OH)_2$ pellets before cycling (A); and after 17 cycles located at the top (B), in the middle (C) and bottom (D) of the reactor [55]

In order to enhance their mechanical stability, $Ca(OH)_2$ -doped pellets were coated with mesoporous alumina, dense silica and al-mesoporous silica gel. After 10 thermal cycles in TA, the mechanical strength resulted enhanced for the pellets coated with silica [57, 58]. Jashari et al. [59], used inorganic oxides as nanostructured additives to coat $Ca(OH)_2$ granules. After 5 thermal cycles in TA, the Al_2O_3-based coated samples (AEROXIDE® Alu C) demonstrated the highest performance among all the additives in terms of cycling stability, structural integrity and mechanical stability while maintaining high energy density (Fig. 9). Based on this outcome, Lucke et al. [60] optimised the Al_2O_3-coating process in terms of cost and resources to make the upscale viable. Further investigation on the performance of the coated storage granules at technical scale is detailed in this work.

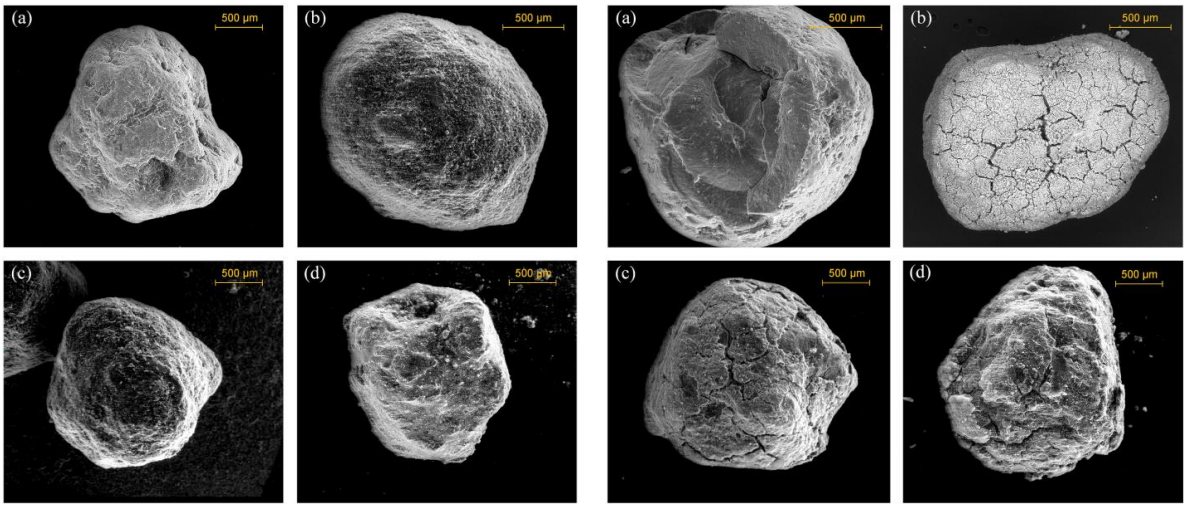

Fig. 9. Scanning electron microscope (SEM) micrographs of $Ca(OH)_2$ granules coated with different additives before (left) and after cycling (right): a) uncoated; b) Al_2O_3-based coating (AEROXIDE® Alu C); c) pyrogenic SiO_2-based coating (AEROSIL® 300); d) SiO_2+ Al_2O_3-based coating (AEROSIL® MOX 80) [59]

1.1.3. Reactors

Different reactors have been developed for the thermochemical cycling of $Ca(OH)_2/CaO$. Based on the flow pattern of the reacting bed, they can be classified into three categories: fixed or packed bed, moving bed, rotary kiln and fluidised bed [61, 62].

Fixed bed reactors

In fixed bed reactors, the storage material is allocated in a vessel and the reaction partner is supplied to or removed from the packed bed for its hydration or dehydration respectively. The concept can be divided into two categories: directly heated or indirectly heated, being the second the mostly used to study the thermochemical characteristics of the $Ca(OH)_2/CaO$ reaction. Schaube et al. [16] investigated the $Ca(OH)_2/CaO$ reaction theoretically and compared the direct and indirect heat transfer in a fixed bed reactor. In general, the low thermal conductivity of the material limits the heat transfer in an indirect concept. As a result, lower power levels are achieved. Conversely, a reactor in which the heat transfer fluid (HTF) and reaction gas flow through the reaction bed display high heat transfer and therefore high-power levels. Later, a fixed bed reactor was developed to study its thermal behaviour in terms of reaction rate, heat and mass transfer. After 25 cycles, the particle rate reaction was found to be the main limiting factor in this directly heated setup [63] (Fig. 10, left). Yan et al. [64] studied the charge and discharge process in a directly heated fixed bed. They discovered that the dehydration is faster at higher temperatures whereas the hydration rate increases either with lower set temperatures or higher gas pressures. In addition,

the experiments demonstrated that the Li-based doping in $Ca(OH)_2$ increased the storage efficiency. Schmidt et al. [65] demonstrated the feasibility of the $Ca(OH)_2/CaO$ system at technical relevant scale. Within the 10 cycles performed in an indirectly heated reactor, two operation modes were demonstrated by adjusting the mass flow of the HTF: peak power (7.5 kW_{th}) and nominal power (3 kW_{th}) (Fig. 10, right). Further investigation by the same group demonstrated the operation of charge and discharge at low gas pressures of 10 kPa and 8.7 kPa respectively [66]. Although the fixed bed reactor concept is in comparison easy to design and simulate, the operation can only be batch-wise. Therefore, the continuous mode that allows for the detachment of power and capacity is not possible under this concept.

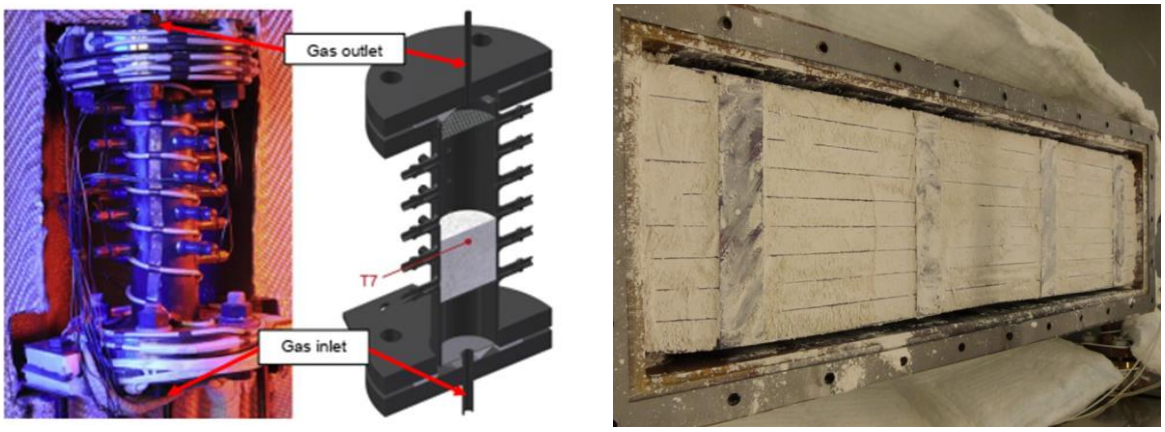

Fig. 10. Labs-scale fixed bed reactors. Left: directly heated [43, 63]. Right: indirectly heated [65].

Moving bed reactors

In a moving bed reactor, the storage material moves either continuously or semi-continuously through the reaction chamber. Unlike the fixed bed, this concept allows for the separation of the storage section and the reactor. For a continuous mode, the controlled feeding and withdrawal of storage material as well as the transport must be available. Schmidt et al. [67] developed a moving bed reactor and a test facility for the thermal cycling, transport and storage of 270 kg of powder $Ca(OH)_2$. In this indirectly heated reactor, a tube-bundle heat exchanger consisted of 158 tubes of 28 mm long and resulted in a heat transfer area of 5 m^2. The design allows for the heat transfer of 10 kW and a storage capacity of 100 kWh (Fig. 11, left). In order to improve the bulk behaviour of the storage material, $Ca(OH)_2$ was mixed with powder Al_2O_3 (12 % w/w). Although the enhancement in the flowability of the mix was demonstrated in cold state, the heat exchanger tubes resulted partly blocked after thermal cycling [68] (Fig. 11, right). The results of this study were used for the further development in the stabilisation of $Ca(OH)_2$ particles and a new reactor design was developed for the experimental investigation of the new material modifications (see section 2: Paper II).

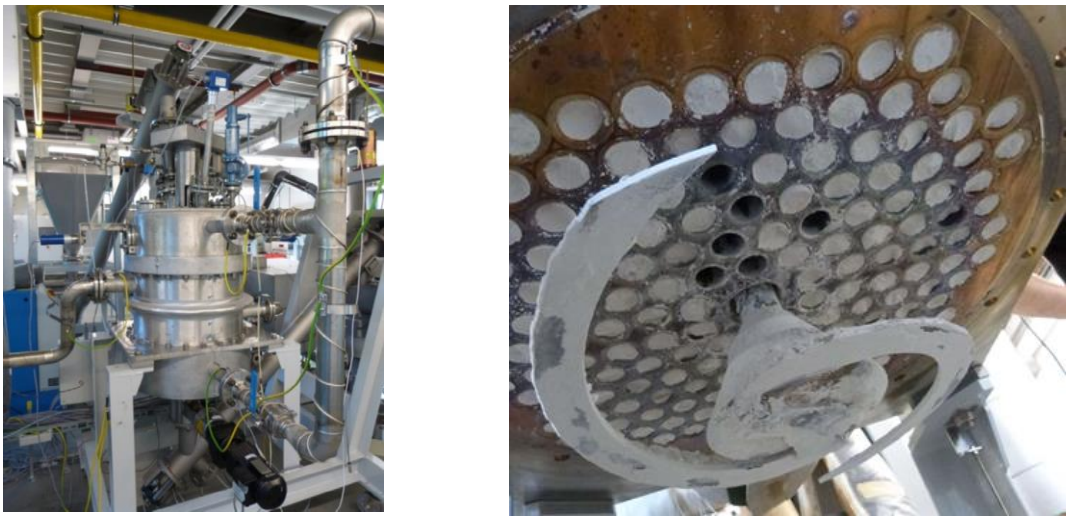

Fig. 11. Left: Moving bed reactor in test facility at DLR Cologne [67]. Right: State of heat exchangers of reactor after cycling.

Rotary kilns

The use of rotary kilns started in the 19th century for the production of cement. The basic layout is comprised of a tilted steel cylinder that stands on bearing rollers that with the action of a rotating motor enables the rotation. In order to investigate how the flow of the material in this reactor concept works, the transverse and longitudinal behaviour of the solid bed were studied. From them, flow regimes and residence time models were derived. The heat transfer takes place in the three known modes: conduction, radiation and convection. They stem from the interaction of different components in the system: the solids bed, the walls of the drum and the gas [69]. Neises et al. [70] demonstrated the feasibility of a solar heated rotary kiln to conduct the thermal reduction and oxidation of cobalt oxide (Fig. 12). Thirty cycles over a batch of solids were reduced at 900 °C on the sun side of the reactor and re-oxidised off-sun. The material displayed no degradation; however, complete conversion of the solids could not be achieved. Tescari et al. [71] developed a solar rotary kiln to calcine $CaCO_3$ in a continuous mode. The flowing bed of particles with a rate between 9 and 20 kg/h was heated up to 1000 °C by concentrated solar power and a maximum efficiency of 45 % was obtained. In order to improve the efficiency, the increase of the incident power and flow rate is proposed. Despite of the advantages this concept offers for a continuous flow of reacting thermochemical storage materials, the costs for preventive and eventual corrective maintenance of rotatory elements exposed to high temperatures opposes the low cost of the storage material in study. In addition, the low conversion achieved so far makes this concept economically unattractive.

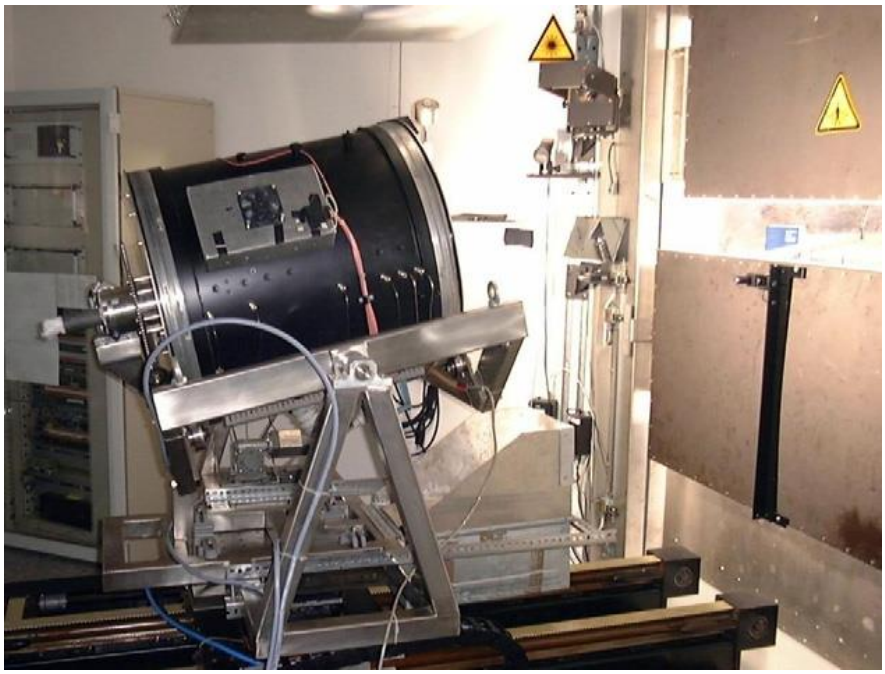

Fig. 12. Rotary Kiln in a solar furnace [70]

Fluidised bed reactors

In a fluidised bed, when gas streams through a powder bed, it creates a pressure drop that rises linearly with the increasing gas velocity. When the velocity rises until the point it causes that the upwards drag force equals the weight of the powder bed, the pressure drop reaches a maximum and an emulsion (gas/particles) is formed; this is known as minimum fluidisation velocity. If the gas velocity further increases, the pressure drop fluctuates and produces various types of fluidisation such bubbling, slugging and turbulent bed. Among them, the optimal heat transfer is obtained under bubbling conditions. However, applying higher gas velocities enlarges the bubbles size which leads to large pressure variations and affects the heat transfer. At even higher velocities the state of the bed can reach a diluted state and thus be taken by pneumatic transport [72, 73] (see Fig. 13). Depending on the fluidisation behaviour, bed particles can be classified in 4 groups (Geldart A, B, C and D) based on the difference between the particle and the gas density and the average particle diameter [74, 75] (see Fig. 14).

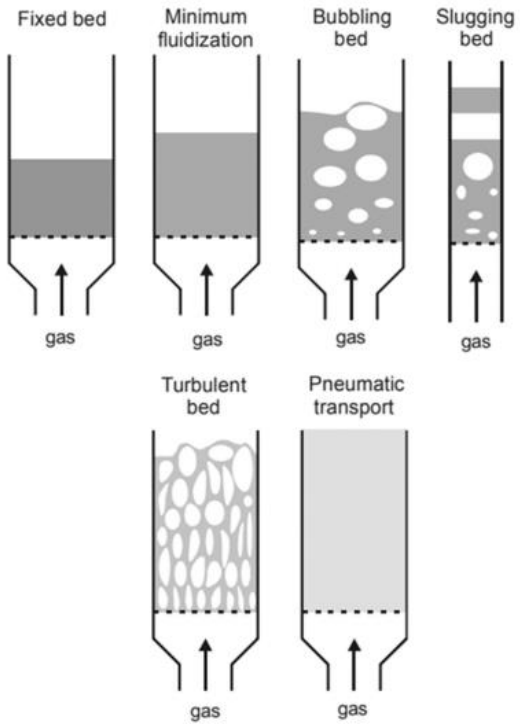

Fig. 13. Fluidised bed regimes [74]

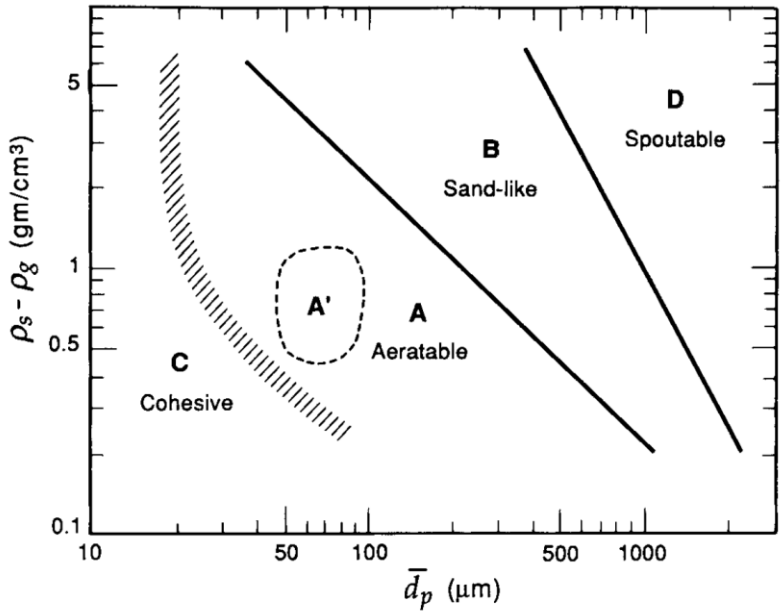

Fig. 14. The Geldart classification of particles for air at ambient conditions [75]

The design of a fluidised bed requires the calculation of the pressure drop and the conditions for minimal fluidisation. Ergun et al. [76] established that the pressure losses are dependent on fluid and particle properties. The pressure losses are related to viscous and kinetic energy losses are represented in the first and second terms of Eq. 6 respectively.

$$\frac{(-\Delta p)}{H} = 150\frac{\mu U}{d_p^2}\frac{(1-\varepsilon)^2}{\varepsilon^3} - 1{,}75\frac{\rho_f U^2}{d_p}\frac{(1-\varepsilon)}{\varepsilon^3} \quad (6)$$

Depending on the characteristics of the powder, hundreds of empirical correlations to predict the minimum fluidisation velocity (U_{mf}) are available. Anantharaman et al. [77], uses the following expression for the calculation:

$$U_{mf} = \frac{Re_{mf}\mu}{\rho d_p} \quad (7)$$

In this equation, the calculation of U_{mf} is in function of dimensionless numbers: Reynolds (Eq. 8) and Archimedes numbers (Eq. 9).

$$Re_{mf} = \left({K_1}^2 + K_2 Ar\right)^{0.5} - K_1 \quad (8)$$

where K_1 and K_2 are empirical constants.

$$Ar = \frac{g\rho\left(\rho_p - \rho\right){d_p}^3}{\mu^2} \quad (9)$$

where g is the gravitational acceleration, ρ is the gas density, ρ_p is the particle density, d_p is the particle diameter and μ is the gas viscosity.

As stated before, the rates of heat and mass transfer is one of the main advantages of gas-solid fluidised beds [74]. The heat transfer coefficient is in principle related to the heat conductivity of the gas (λ), the diameter of the particle (d_p) and the Nusselt number (Eq. 10) [78].

$$\alpha = \frac{Nu\lambda}{d_p} \quad (10)$$

The Nusselt number is also related to other gas properties such as Reynolds coefficient in void fraction (Re_ψ), Prandtl number (r), kinematic viscosity (v) and thermal diffusivity (a). Other factors like the minimal fluidisation velocity (U_{mf}), void fraction and particle diameter (d_p) play a role in the calculation. A detailed description of the calculation of the heat transfer coefficient for the bed of material in this work is presented in section 2 (paper III).

The use of fluidised beds for the hydration and dehydration of $Ca(OH)_2/CaO$ was first conceptualised by Criado et al. [79]. In the design, water vapour is the only agent of fluidisation in both discharge and charge processes. After assessment of the reactor concept and process associated, it was found that it is technically viable with a maximum power output of 100 MW_{th} for the hydration and a storage density of 260 kWh/m^3. Pardo et al. [80] investigated the feasibility of $Ca(OH)_2/CaO$ as

thermochemical storage in a fluidised bed reactor. In order to enhance the fluidisation of the powder bed, easy-to-fluidise particles (EFP) based on Al_2O_3 were mixed with powder $Ca(OH)_2$. After fluidisation tests in cold state, the solid mixture of $Al_2O_3/Ca(OH)_2$ were subject of 50 thermochemical cycles obtaining an energy density of 156 kWh/m^3. Further investigation was conducted in a 5.5 kW_{th} batch fluidised bed reactor operated at high gas velocities (0.3-0.5 m/s). The experimental results and the model developed to validate the results supported the upscale of a bubbling fluidised bed reactor concept [81]. A new conceptual design consisted of a bubbling fluidised bed reactor with a guided flow of the particles and immersed tubes as heat exchangers. This indirectly heated reactor required the use of calcined CaO and a gas distributor plate to ensure the fluidisation of the particles. A model suggests that 15 MW of thermal power can be achieved from a 100-m^3 reactor [82].

In summary, fluidised bed reactors have been demonstrated to obtain high heat transfer coefficients and be capable of upscaling and therefore achieve thermal power in the order of MW. However, this could be achieved with material that requires specific pre-treatment steps before thermal cycling. In addition, the use of ancillary equipment for the continuous gas flow increases the parasitic energy consumption.

Mechanically induced fluidised bed reactor

A different fluidised bed concept was developed by Risthaus et al. [83] (Fig. 15). Unlike the concepts mentioned before where gas velocities are used to agitate the bed, this reactor used a ploughshare mixer to mechanically induce the fluidisation of the bed of $Ca(OH)_2/CaO$ particles and thus overcome the low thermal conductivity of the powder material. In this regard, they found that the heat is rapidly distributed in the mechanically fluidised bed. In addition, effective heat transfer coefficients accounted for 156 and 243 W/m^2.K for hydration and dehydration respectively.

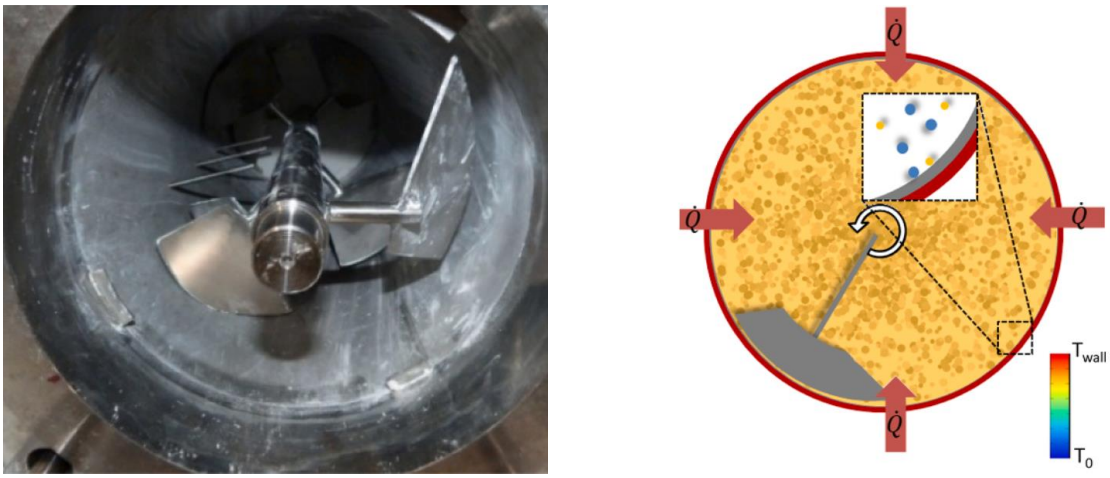

Fig. 15. Left: Ploughshare shaft in the reactor. Right: Heat input and rotation of the ploughshare mixer in the reactor [83].

1.2. Research objective

The high potential of $CaO/Ca(OH)_2$ for thermochemical heat storage is counterbalanced by the unfavourable properties it displays in its powder form e.g. low thermal conductivity, cohesivity and the tendency to form agglomerates after cycling. These drawbacks challenge the efforts to design reactors that detach power and capacity and therefore obtain high power densities. For this reason, different approaches have been studied to improve the bulk behaviour of $Ca(OH)_2$ and thus make it suitable for moving or fluidised bed reactors. Among these modifications, the particle stabilisation approach has been investigated and proved, although only at mg-scale. Thus, the first part of this work deals with the characterisation of granulated $Ca(OH)_2$ at technical scale as well as the experimental thermodynamic analysis of different reactor concepts. Based on the characterisation of the granules and the experimental analysis of the performance of a reactor, an adapted concept was derived and developed. It is by means of this novel setup, that the ultimate aim of decoupling power and capacity for the thermochemical heat storage of $Ca(OH)_2$ was achieved.

1.2.1. Scientific contributions

So far, multiple modifications under the particle stabilisation approach have been developed and successfully proved although under specific parameters and amounts that differ from the actual conditions in reactors. Hence, for a comprehensive and application-oriented assessment of stabilised material ($Ca(OH)_2$ storage granules), two conditions have to be met for their thermal cycling. First, the test bench must emulate the conditions of an actual reactor for the thermal cycling e.g. the amount of granules must be larger and able to form a bulk and the parameters used must be the same as in reactors. Furthermore, it must allow for the visualisation of the samples as they are reacting. Therefore, a directly heated reactor was developed for this purpose. **Paper I**, describes this setup. The main feature of the design is the use of a port view in combination with a high-resolution camera equipped with macro lens. Multiple photographs are taken along a 20-fold-cycle experimental series and then analysed using the image processing software ImageJ. This allows for the real-time and in-situ tracking of the state of the structural integrity of the granules. Hence, a qualitative assessment of the effect of the stabilisation method can be carried out and used for comparison. In addition, ex situ analysis takes place using dynamometry for the determination of mechanical strength, sieve analysis for the size distribution of particles and SEM for morphology analysis. The cycling stability is determined by TGA and further evaluated by XRD analysis. Overall, this method enables to observe the behaviour of the reacting bulk and to characterise it in technical scale, thus delivering important parameters for the design of the reactor (described in Paper III).

In order to meet industrial-scale power demand, large storage capacities are required. The moving bed reactor is one of the concepts that in principle allows for the separation of power and capacity. For this reason, in **Paper II**, a moving bed reactor is developed for preliminary testing of the characterised granules. In this reactor, the heat exchanger design corresponds to a tube bundle and preheated air supplies heat through the shell side of the tubes whereas the storage granules reside in the tube side. In order to demonstrate the functionality of the setup, two different samples are cycled six times. The reaction performance of both samples is analysed and compared upon reference granules. At the material side, the cycling stability is determined by TGA and the morphology through SEM. The moving bed function is tested at the end of the experiment series of each sample. The operational analysis of the reactor provides with design considerations for the development of a new reactor concept in which the flowability of the granules is enabled.

Based on the results described in Paper I and Paper II, a new reactor concept is developed. **Paper III**, describes the considerations for the design of a directly heated reactor as well as the operating parameters to be applied. In this reactor, the selection of gas velocity and temperature represent a challenge since a slight variation in the parameters can change the state of the reaction bed i.e. from stationary to a fluidising state. In this study, the samples are subject of a 10-fold thermochemical cycling to demonstrate the functionality of the reactor and to conduct the thermodynamic analysis of the concept. The characterisation of the cycled granules includes a number of analysis over the samples: mechanical strength by means of dynamometry, the size distribution of the particles through sieve analysis and the morphology by SEM. In addition, the cycling stability is determined by TGA and contrasted with phase composition using XRD. Finally, the gravity assisted movement of the bed is tested at the end of the experimental series (see Fig. 16).

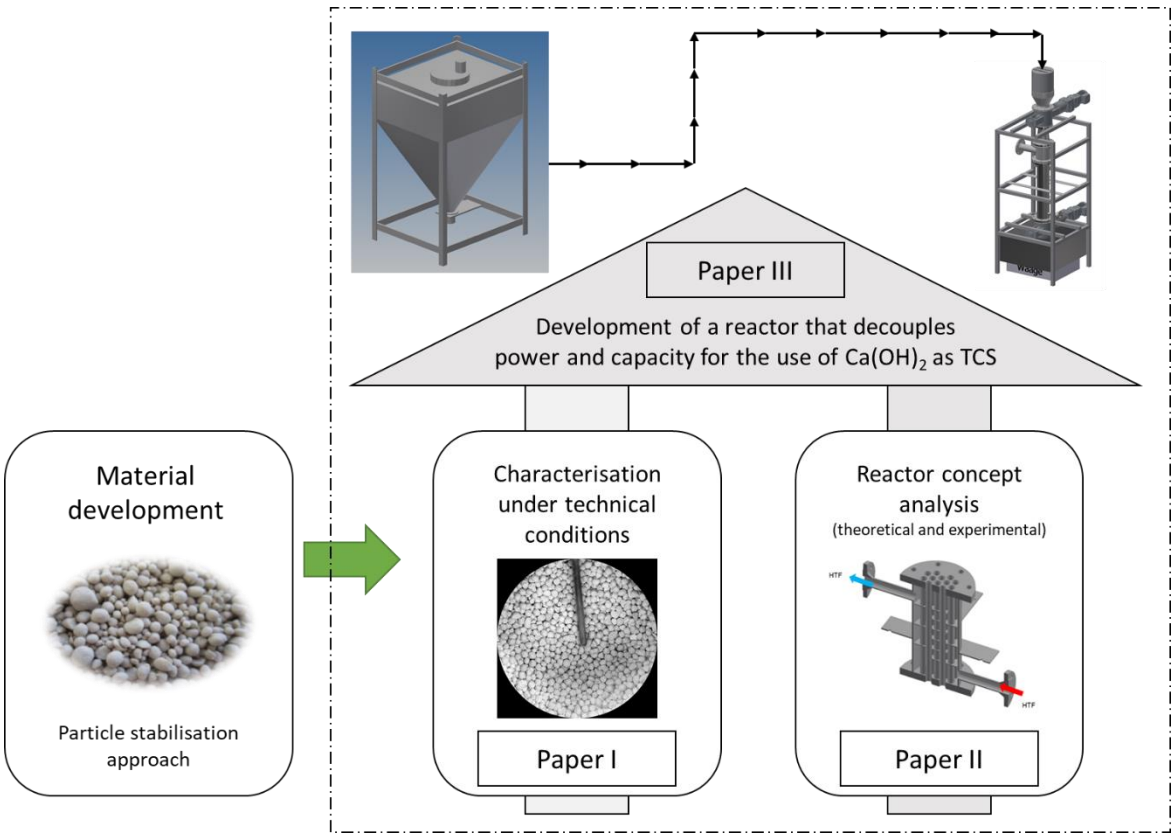

Fig. 16. Overview of the distribution of this work's scientific contributions towards the development of a moving bed reactor for the use of $Ca(OH)_2$ as TCS.

2. Publications

The following publications support the present thesis:

Paper I: Characterisation of modified material ($Ca(OH)_2$-based granules) under technical conditions

Aldo Cosquillo Mejia, Sandra Afflerbach, Marc Linder, Matthias Schmidt. "Real-time visualization and experimental analysis of stabilized $Ca(OH)_2$ granules for thermal energy storage", *Energy and Conversion Management: X*, 23, **2024**, DOI: 10.1016/j.ecmx.2024.100656

Contribution declaration: main author, conduction of the experimental work (except for SEM and XRD imaging) and data assessment.

Paper II: Preliminary tests in an indirectly heated reactor

Aldo Cosquillo Mejia, Sandra Afflerbach, Marc Linder, Matthias Schmidt. "Experimental analysis of encapsulated $CaO/Ca(OH)_2$ granules as thermochemical storage in a novel moving bed reactor", *Applied Thermal Engineering*, 169, **2020**. DOI: 10.1016/j.applthermaleng.2020.114961

Contribution declaration: main author, conduction of the experimental work (except for SEM imaging) and data assessment.

Paper III: Development of a lab-scale reactor

Aldo Cosquillo Mejia, Sandra Afflerbach, Marc Linder, Matthias Schmidt. "Development of a moving bed reactor for thermochemical heat storage based on granulated $Ca(OH)_2$", *Processes*, 10(1680), **2022**, DOI: 10.3390/pr10091680

Contribution declaration: main author, conduction of the experimental work (except for SEM and XRD imaging) and data assessment.

In addition, part of this work was published in the following contributions to international conferences:

Aldo Cosquillo Mejia, Marc Linder, Matthias Schmidt. "Development of a moving bed reactor for thermochemical energy storage with $Ca(OH)_2/CaO$", International Conference on Renewable Energy Storage (IRES), 2019, Düsseldorf, Germany, oral presentation.

Aldo Cosquillo Mejia, Marc Linder, Matthias Schmidt. "Modified $Ca(OH)_2$ for thermochemical heat storage: real time visualisation and analysis", Enerstock Conference, 2021, Ljubljana, Slovenia, oral presentation (online).

Aldo Cosquillo Mejia, Marc Linder, Matthias Schmidt. "Development of a moving bed reactor for thermochemical storage with novel encapsulated $Ca(OH)_2/CaO$", ISES Solar World Congress, 2021, Freiburg, Germany. Oral presentation (online).

Aldo Cosquillo Mejia, Sandra Afflerbach, Marc Linder, Matthias Schmidt. "Thermochemical cycling of $Ca(OH)_2$-based granules: real-time visualisation and analysis", Innovative Materials and Processes in Energy Systems conference (IMPRES), 2022, Barcelona, Spain. Oral presentation.

Aldo Cosquillo Mejia, Sandra Afflerbach, Marc Linder, Matthias Schmidt. "Development of a pilot plant for thermochemical storage with $Ca(OH)_2$-based granules", International Conference of Power Engineering, 2023, Kyoto, Japan. Oral presentation.

Paper I: Characterisation of modified material ($Ca(OH)_2$-based granules) under technical conditions

Energy Conversion and Management: X 23 (2024) 100656

Contents lists available at ScienceDirect

Energy Conversion and Management: X

journal homepage: www.sciencedirect.com/journal/energy-conversion-and-management-x

Real-time visualization and experimental analysis of stabilized $Ca(OH)_2$ granules for thermal energy storage

Aldo Cosquillo Mejia [a,*], Sandra Afflerbach [b], Marc Linder [c], Matthias Schmidt [a]

[a] German Aerospace Center – DLR e.V., Institute of Engineering Thermodynamics, Linder Höhe, 51147 Köln, Germany
[b] Helmut-Schmidt-University / University of the Federal Armed Forces Hamburg, Chair for Energy Engineering, Faculty for Mechanical and Civil Engineering, Holstenhofweg 85, 22043 Hamburg, Germany
[c] German Aerospace Center – DLR e.V., Institute of Engineering Thermodynamics, Pfaffenwaldring 38-40, 70569 Stuttgart, Germany

ARTICLE INFO

Keywords:
Particle stabilization
Calcium hydroxide
Al_2O_3 nanoparticles
$Ca(OH)_2/CaCO_3$ composites
Thermochemical storage
Mechanical stability

ABSTRACT

The reversible reaction $Ca(OH)_2 + 104.4$ kJ/mol ⇌ $CaO + H_2O$ offers several advantages as energy storage system. For example, it possesses a higher energy density than lead-acid or nickel–cadmium batteries. In addition, it has proven cyclability, low cost and worldwide availability. For this reason, it is suitable for seasonal heat storage applications. However, the raw powder material displays properties that represent a major challenge for the design of reactors that decouple power from capacity e.g. low thermal conductivity, cohesivity and tendency to form agglomerates. In order to overcome these drawbacks, different approaches to stabilize the $Ca(OH)_2/CaO$ particles have been investigated e.g. shaping, micro encapsulation, macroencapsulation, etc. The assessment of the stabilized products, however, has limitations in terms of amount of mass and reaction conditions as it is carried out in TA (thermal analyzer). Furthermore, it does not allow to analyze the structural decay and agglomeration of stabilized particles in-situ. For this reason, a more comprehensive assessment of a bulk of material under reactor conditions is necessary. In this work, a reaction chamber is developed to enable the observation of a bulk of storage material (0.1 L) during thermal cycling. Thus, two samples were subject of 20 cycles of dehydration and rehydration. The experiments were carried out at a temperature range of 350 °C – 500 °C and water vapor pressure of 0 – 1 bar. The analysis of images and post experiment tests (e.g. thermogravimetric analysis (TGA), dynamometry, X-ray diffraction (XRD) analysis) prove that the mechanical strength and structural integrity resulted enhanced for both samples. In addition, it allows to further understand the bulk behavior of $Ca(OH)_2$ granules and thus important implications for the design of technical scale reactors can be derived.

Introduction

The transition to a carbon–neutral energy matrix requires the rapid expansion of renewable energy sources in different sectors in the human society. Nevertheless, the stochastic behavior of the these energies and the consequent discrepancy between supply and demand present a big challenge for their consolidation [1]. Thereby, energy storage can be used to bridge the gap between the production and consumption of energy. Among different energy storage technologies, the storage system given by the reaction $Ca(OH)_2 + 104.4$ kJ/mol ⇌ $CaO + H_2O$ is regarded as promising due to the advantageous features it displays. The reaction offers a high energy density and fast kinetics [2,3]. In addition, it has been proved to be reversible over a large number of cycles [4], it is not toxic, inexpensive and generally worldwide available. As this is a thermochemical reaction, the charged material can be stored for long periods with virtually no heat losses [5]. Thus, it is suitable for seasonal heat storage applications [6,7]. Although the production of $Ca(OH)_2$ produces significant CO_2 emissions, the reversibility of the reaction and novel methods that simultaneously sequestrate CO_2 during the decarbonization of $CaCO_3$ [8] reduce its carbon footprint. Due to all these favorable properties, the reaction has been characterized and the thermodynamic properties described in several studies [2,9–11]. The feasibility of this storage system has been tested at larger scale in different reactor concepts. For instance, the functionality of the powder $Ca(OH)_2$ in a fixed bed reactor was confirmed [12–16]. However, given the low thermal conductivity of the material (0.1–0.5 W/m.K) [3,17–19], large

* Corresponding author.
E-mail address: aldo.cosquillo@dlr.de (A. Cosquillo Mejia).

https://doi.org/10.1016/j.ecmx.2024.100656
Received 8 April 2024; Received in revised form 24 June 2024; Accepted 27 June 2024
Available online 2 July 2024

and complex heat exchangers are required when the upscale to industrial-application capacities is considered. For this reason, other concepts that offer the possibility to detach the storage from the reactor have also been investigated. This is the case of the moving bed concept, which although proven functional, revealed major challenges that stem from the inherent properties of the powder storage material. For instance, the cycled material displayed the formation of agglomerates which hindered the movement of the bulk of material through the heat exchangers of the reactor [20,21] and at the same time affected negatively the heat and mass transport [22,23].

One of the approaches to improve the bulk properties of the storage material is to stabilize the particles which implies the modification of the base material under different techniques. For instance, Schmidt et al. [20] tested modified powder $Ca(OH)_2$ in a moving bed reactor. Additives based on alumina and silicon salts were mixed with the powder storage material to improve the flowability of the particles after cycling. The results showed that even though the reactor was operational, the improved flowability of the powder was not stable for several reaction cycles. Other investigations used larger particles specifically prepared to work in fluidized bed reactors. However, this could only be proved for a limited number of cycles [24,25]. The use of additives based on zinc, copper and aluminum to dope $Ca(OH)_2$ pellets proved to enhance the structural stability of the particles. However, this effect was lost after a few cycles [26,27]. Other approaches used $CaO/Ca(OH)_2$ as part of composites and as core material inside ceramic capsules [22,28–32]. They were reported to improve the mechanical stability after cycling [21]. However, such results were obtained after a complex process of preparation or at the expense of energy density.

The use of a small amount of nanostructured additives to stabilize larger $Ca(OH)_2$ particles has been investigated and proved successful in small scale [26,27,33,34]. For example, the coating of $Ca(OH)_2$ granules with Al_2O_3 nanostructured particles has been studied at larger scale in previous works of our research group [21]. Recently, a 10-fold thermochemical cycle using the coated granules was conducted in a moving bed reactor [35]. The analysis of the cycled granules shows that the mechanical stability improved. Although a large number of granules resulted fragmented, no agglomeration was observed. In addition, the movement of the bulk out of the reactor was reported for the first time. Nevertheless, the process of structural decay and agglomeration of the granules during the thermochemical cycling is still unclear. Therefore, for a comprehensive assessment of the functionality of the stabilized granules, they must undergo a larger number of cycles under reactor-like conditions. This could be in principle carried out in thermal analyzers (TA). However, the amount of sample such devices can hold is limited to mg-scale i.e. the study over a large bulk of granules cannot be realized. Furthermore, the tracking of the structural integrity of granules is restricted to post experimental analysis. For these reasons, a specific reaction chamber that emulates the conditions in a thermochemical reactor was designed.

In this work, a reaction chamber that allows for the rapid cycling of a bulk of $Ca(OH)_2$-based granules under technical conditions was developed. The design enables the real-time observation of the samples during the charge and discharge. Thus, the process of deterioration of the granules occurring during the reaction of the bulk, e.g. crack formation, fracturing and agglomeration, can be visually documented and later further analyzed. Two batches prepared under different stabilization approaches undergo 20 thermochemical cycles in the reaction chamber. The aim of this work is therefore to assess the mechanical properties and bulk behavior of the two samples along the experimental series. This includes the particle size distribution and the potential agglomeration of the granules. In addition, the crushing strength and the cycling stability of the samples are determined. The results will provide important information for the design of reactors that use $Ca(OH)_2$ as thermochemical storage material.

Methodology

Experimental setup

Visualization reaction chamber

Fig. 1 depicts the scheme of the setup used in this work. It consists of a 200-mm-long and 60-mm-diameter steel pipe with a cap welded at the bottom. A sight flange, equipped with a quartz glass, enables the visualization of the granules inside the chamber during the charge and discharge processes. The heat transfer fluid (HTF) and the reaction gas (water vapor) enter the reaction chamber through two separated inlets and mix in the lower zone which is filled with inert material (glass beads). Then, the air or air/steam mixture streams up through the storage granules and leaves through the gas outlet which is located at the upper section of the chamber, below the sight flange. Additionally, heating cords are attached to the outer walls of the setup and around the glass flange. In order to minimize heat losses, insulation wool covers the whole set up. Three thermocouples measure the temperatures in the center of the cross section of the reaction chamber at three different heights. The inlet temperature (T_{in}) is measured in the glass beads section and takes the temperature of the air volume flow and water vapor entering the chamber. The temperature of the storage material (T_{bulk}) is measured by a thermocouple located in the lower part of the bulk of the granules, above the glass beads. The third measurement point is installed right above the bulk of granules (T_{out}).

Test bench

Fig. 2 displays the schematic view of the test bench. It is comprised by:

- the heat transfer fluid (HTF) supply unit
- the visualization reaction chamber
- the reaction gas supply unit

In the HTF supply unit, ambient air is first compressed and dried. In the next step, the moisture and CO_2 of the air are removed in an adsorption drier. Before the air is supplied to the chamber, the volume flow is set by a mass flow controller (MFC) and then heated up by means of an electrical heater. At the reaction gas unit, water vapor is prepared in an evaporator, where the temperature is adjusted to the desired pressure. Once the water vapor pressure is reached, the flow rate is set by means of a second MFC and the valve that connects it and the evaporator is opened to allow the reaction gas to stream into the reaction chamber.

Materials

Uncoated granules (reference)

As reference material, commercially available granulated $Ca(OH)_2$ (Sorbacal® H90G) was supplied by Rheinkalk GmbH. The content of $Ca(OH)_2$ amounts to 92.9 wt% and granules with a diameter between 1.6 and 2 mm were used for the experiments (bulk density: 721 kg/m^3). See Fig. 3 (A).

Coated granules

Coated granules were produced by adding an adhesion promoting agent and nanostructured Al_2O_3 (supplied by Evonik Industries AG) to granulated $Ca(OH)_2$ (Sorbacal® H90G) in a mixer under co-current flow. The additive was added up to the point that all surfaces of the granules were thoroughly covered following the procedure described in [34,36]. Coated granules with a diameter between 1.6 and 2 mm were selected for the experimental series (bulk density: 822 kg/m^3). See Fig. 3 (B).

$Ca(OH)_2/CaCO_3$ composites

Composites of $Ca(OH)_2$ and $CaCO_3$ in the form of granules were supplied by Rheinkalk GmbH. The content of $Ca(OH)_2$ corresponds to

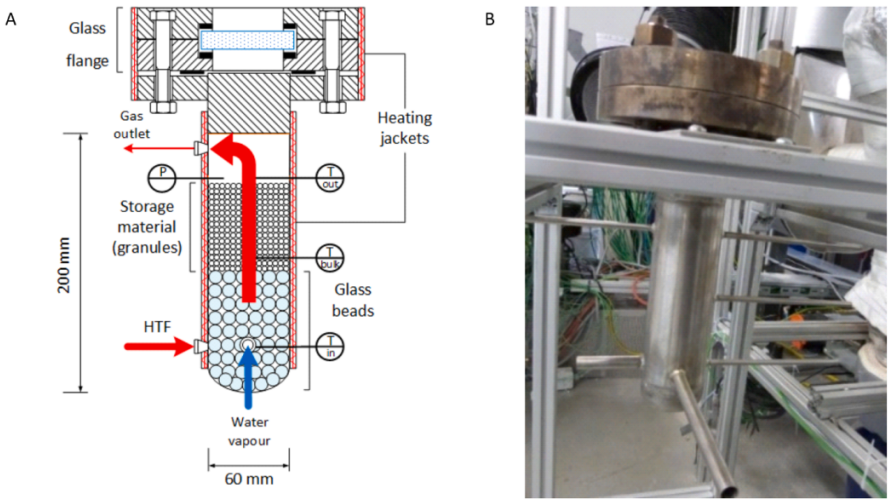

Fig. 1. A: Diagram of the visualization reaction chamber. B:Image of the setup without insulation during assembly.

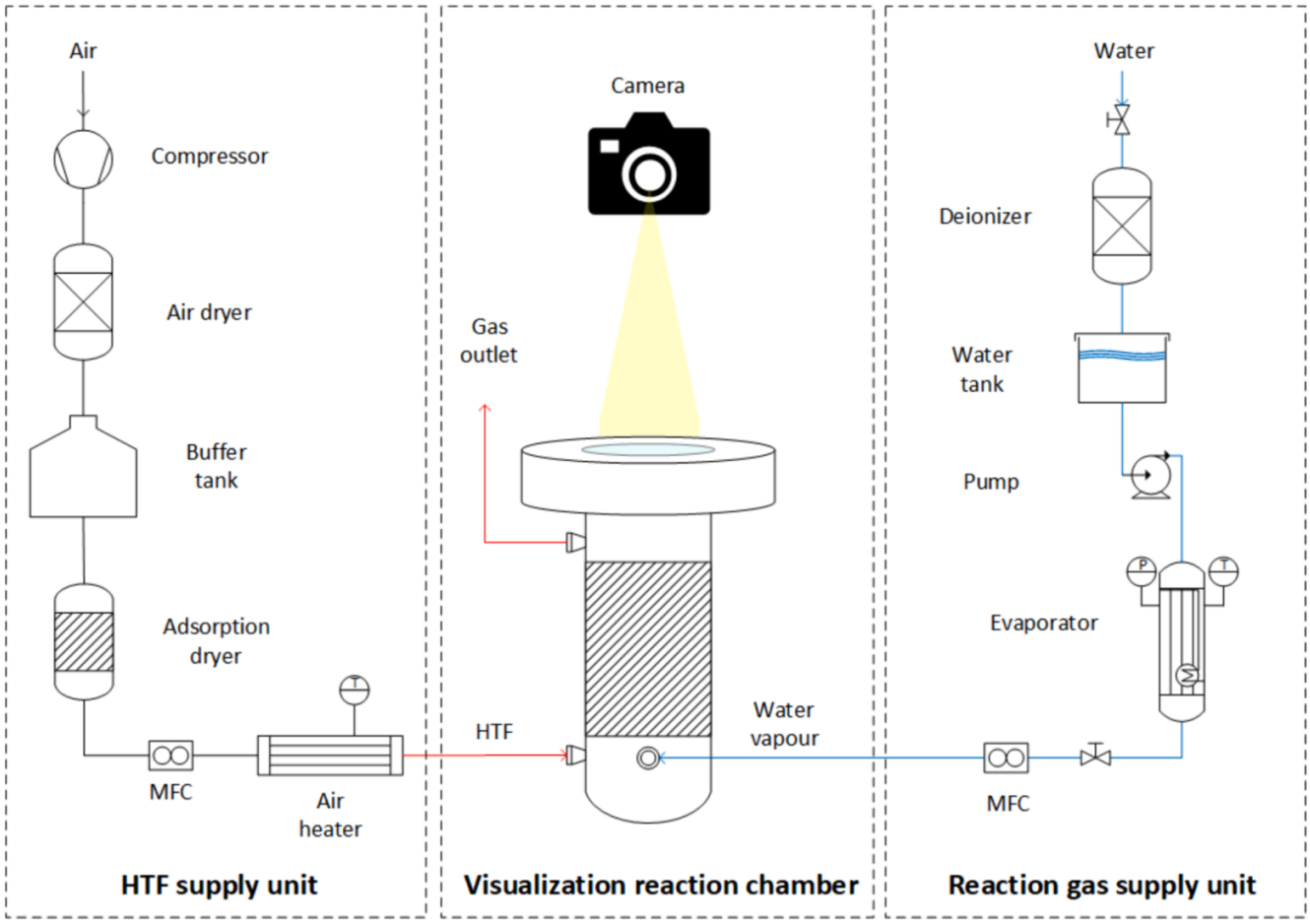

Fig. 2. The schematic diagram of the test bench.

40 wt% and granules with a diameter between 1.6 and 2 mm were chosen for the experiments (bulk density: 1085 kg/m^3). See Fig. 3 (C).

Experimental procedure

Equilibrium temperature and determination of parameters for hydration and dehydration

In order to select the parameters for the dehydration and hydration of this thermochemical reaction system in use, it is necessary to

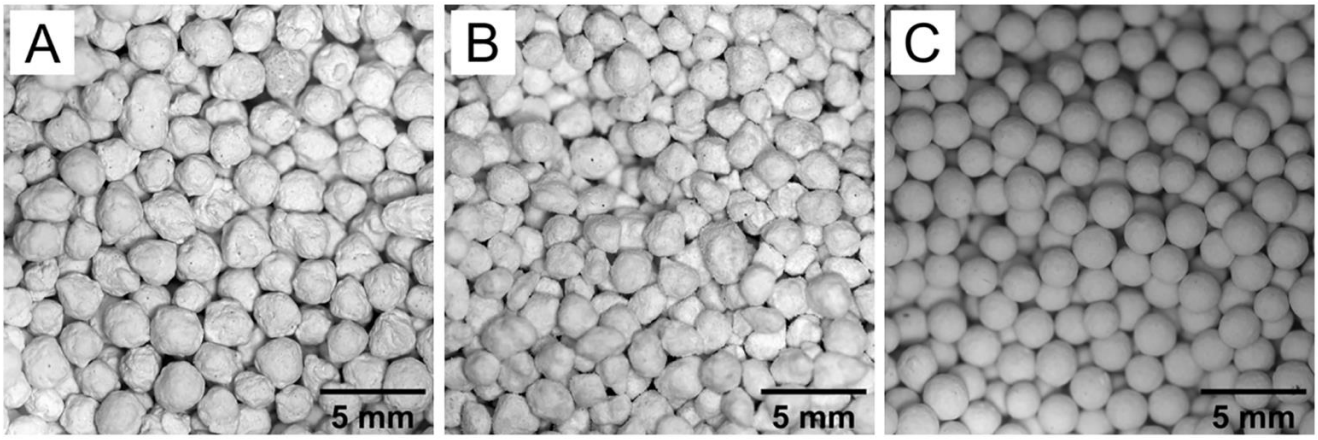

Fig. 3. Granulated $Ca(OH)_2$ samples used in the experiments. A: uncoated $Ca(OH)_2$ granules (reference material). B: $Ca(OH)_2$ granules coated with nanostructured Al_2O_3. C: $Ca(OH)_2/CaCO_3$ composites.

understand the relationship between the water vapor pressure and equilibrium temperature. Here, the water vapor pressure dictates the corresponding reaction temperature in the system. Fig. 4 shows the theoretical values of temperature at different pressure values for $Ca(OH)_2/CaO$ [37].

The pressure–temperature equilibrium of the $Ca(OH)_2/CaO$ reaction system has been investigated by several authors. For this work, we use the equation proposed by Samms et al. [9]:

$$\ln\left(\frac{p_{H_2O}[Pa]}{10^5}\right) = -\frac{11375}{T[K]} + 14.574 \tag{1}$$

The partial pressure of water vapor in the gas stream mixture (p_{H_2O}) is calculated by Eq. (2), where the molar flow of air ($\dot{n}_{air}$) and water vapor ($\dot{n}_{H_2O}$) are determined by Eq. (3) and (4):

$$p_{H_2O} = \frac{\dot{n}_{H_2O}}{\dot{n}_{air} + \dot{n}_{H_2O}} * 101.325\, kPa \tag{2}$$

$$\dot{n}_{H_2O} = \frac{\dot{m}_{H_2O}}{M_{H_2O}} \tag{3}$$

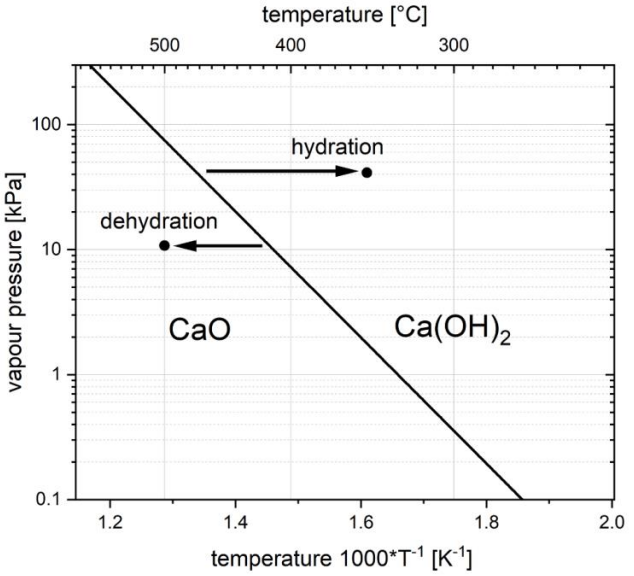

Fig. 4. Equilibrium line for the Ca(OH)2/CaO reaction system based on the values of Barin [37].

$$\dot{n}_{air} = \frac{\dot{m}_{air}}{M_{air}} \tag{4}$$

where $\dot{m}$ is the mass flow and M the molar mass.

Therefore, the experimental parameters for the dehydration consider high air inlet temperature (T_{in}) to ensure the dehydration of the samples even though a very small partial pressure of water vapor is expected since most of it is removed by the air dryer. For hydration, T_{in} is set below the equilibrium temperature that corresponds to the calculated partial pressure of the steam supplied (Eq.2) (compare with Fig. 4).

Three batches, each of 0.1 L of the storage granules are filled separately in the chamber. Each batch is subject of 20 thermochemical cycles (dehydration and hydration) under the experimental parameters described in Table 1.

Dehydration

First, the samples are filled up in the chamber until the level right below the thermocouple T_{out} (see Fig. 1). After that, in order to preheat the samples, the air volume flow ($\dot{V}$) is set to 1 Nm^3/h and the air inlet temperature to 350 °C ($T_{HTF,\,start}$). At the same time, the heating cords in the chamber and sight flange are set to 350 °C. Once the temperatures are stable, the air inlet and heating cord temperatures are increased to 500 °C. In principle, the dehydration begins when the temperature measured in the bulk of granules is higher than the equilibrium temperature. The endothermal reaction causes a decrease in the rising slope of the bulk (T_{bulk}) and outlet temperature (T_{out}). The charging phase is considered complete when the slope of both bulk and outlet temperatures rise again.

Hydration

The dehydrated samples contained in the reaction chamber are preheated by means of air volume flow set at 1 Nm^3/h, air inlet temperature and heating cords set at 350 °C. At the reaction gas unit, water vapor is prepared and the mass flow ($\dot{m}_{H_2O}$) is set at 0.6 kg/h at the MFC. In order to start the hydration, the valve that connects the evaporator and MFC is opened and the water vapor streams to the reaction chamber.

Table 1
Experimental parameters for dehydration and hydration for air inlet temperature during the preheating stage ($T_{HTF,start}$), air volume flow ($\dot{V}$), set air inlet temperature ($T_{HTF,set}$) and water vapor mass flow ($\dot{m}_{H_2O}$).

Setting	$T_{HTF,start}$ [°C]	$\dot{V}$ [Nm^3/h]	$T_{HTF,set}$ [°C]	$\dot{m}_{H_2O}$ [Kg/h]
Dehydration	350	1	500	0
Hydration	350	1	350	0.6

The steam and the air mix in the lower region of the chamber and then stream through the bulk of granules to hydrate the CaO contained in the samples. This causes an exothermal reaction that rises the temperature of the bulk (T_{bulk}). This effect is also visible in the outlet temperature (T_{out}) and the reaction is complete when the measured temperature at both bulk and outlet fall again.

Conversion

In order to determine the degree of conversion, a sample is taken from the bulk of granules before cycling and after the 10th and 20th rehydration. The samples are subject of thermogravimetric analysis (TGA) in a simultaneous thermal analyzer (Netzsch STA 449 F3 Jupiter). In the furnace of this device, the sample is heated up to 850 °C and under volume flows of nitrogen as protective and purge gases. The experiments last 2 h and the degree of rehydration ($X_{hy}(\%)$) is calculated as follows:

$$X_{hy}(\%) = \frac{mH_2O_{measured}}{mH_2O_{stoich}} * 100(\%) \quad (5)$$

where $mH_2O_{measured}$ is the total mass of water dehydrated during the thermal analysis and mH_2O_{stoich} is the stochiometric mass of water of the reactive material present in the sample.

Phase composition, morphology and texture

While the samples overall storage density can be assessed by determination of the degree of conversion, the phase composition can give important insights on side reactions occurring in the coated samples under the hydrothermal conditions accompanying thermochemical cycling. In order to identify individual crystalline phases, X-ray diffraction (XRD) followed by Rietveld-analysis on the measured diffraction patterns are performed. Measurements are made in reflection mode on powdered samples prepared in circular holders of 80 mm diameter in a scan range from 10 to 75 °2Θ with a linear detector and Cu K_α-radiation using a Panalytical ẊPert Pro PW 3040/60 powder diffractometer. For phase quantification an external standard reference (ZnO, NIST standard reference) is used. The morphology and texture of the samples is probed by scanning electron microscopy (SEM) using a FEI Quanta FEG 250 microscope equipped with a large field detector for secondary ion (SE) imaging in low-vacuum mode in a pressure range from 90-110 Pa.

Structural integrity

The state of the granules in the bulk of samples is qualitatively assessed by means of high-resolution images obtained from a digital camera (Canon EOS 77D) equipped with macro lens (Canon EF 100 mm f/2.8L Macro IS USM). The camera is placed right above the viewport of the sight flange (see Fig. 2). The images of the top of the bulk are taken before and after every experiment in the 20-cycle series.

In order to quantify the degree of deterioration of the granules over the cycles, the particle size distribution of the samples is determined by sieve analysis before the first and after the 20th cycle. To this end, a tower of sieves with pore sizes of $\geq$ 0.5 mm, $\geq$ 1 mm, $\geq$ 1.25 mm, $\geq$ 1.6 mm and $\geq$ 2 mm was used. After shaking the tower manually for around 5 min, the content of each sieve is separately weighed.

Mechanical stability

The mechanical stability of the granules is tested by dynamometry. For each batch, a sample of 50 individual granules are withdrawn from the bulk at three different points in the experimental series: before the thermochemical cycling, after the 10th cycle and after the 20th cycle. A force gauge attached to a manually operated test stand (PCE-DFG N 500, max. capacity: 500 N, resolution 0.1 N) is used to perform the compression tests. The mechanical stability of each sample is calculated from the mean value of the individual measurements whereas the standard deviation represents the uncertainty.

Results and discussion

Set into operation

Reference experiments with uncoated $Ca(OH)_2$ granules

A batch consisting of 123 g of reference $Ca(OH)_2$ granules were subject of a 20-fold thermochemical cycling in the visualization reaction chamber. The experiments were used to test the operation settings for the dehydration and hydration. The results are used as baseline to compare with the other two samples: $Ca(OH)_2$ granules coated with Al_2O_3 and $Ca(OH)_2/CaCO_3$ composites.

Dehydration. Fig. 5 (A) displays a reference dehydration experiment with reference granules. The dehydration starts approximately at minute 10 when the rising slope of the bulk of granules (T_{bulk}) decreases. This indicates that the endothermal reaction takes place in the zone of the thermocouple. At minute 20, the slope of the temperature rises at a fast rate again indicating that most of the reactive material in this zone of the bulk has dehydrated.

The outlet temperature profile (T_{out}) reveals that the fall in the rising slope occurs at minute 15 (5 min later than for T_{bulk}) and a plateau extends for around 45 min. Furthermore, the temperature of the plateau is around 25 K lower for T_{bulk} due to the thermal losses in the upper part of the setup. At minute 60, the temperature increases again indicating the completion of the reaction.

The largest difference between T_{bulk} and Tout occurs between minute 40 and 60 which can be explained by the high amount of energy that is taken up to drive the dehydration of the $Ca(OH)_2$. Once most of the material is dehydrated, more thermal energy is available at T_{out} and therefore the temperature rises. The experiment proceeds for 30 min longer to make sure that the whole storage material has reacted. Furthermore, the heat losses in the upper section of the chamber causes the lower rate of reaction of the respective zone in the bulk.

Hydration. Fig. 5 (B) displays the temperature trends of the hydration reference experiment. Here, the temperature of the bulk (T_{bulk}) increases rapidly as a consequence of the exothermal reaction of the CaO in the granules. The temperature rises up to 455 °C, which is very close to the equilibrium temperature given by the water vapor partial pressure supplied (see section 2.3). The release of heat lasts approximately 10 min when the temperature returns to initial values indicating that most of the reactive material close to the thermocouple has hydrated.

The effect of the exothermal reaction at the outlet temperature (T_{out}) displays a different trend. In this case, the measured temperature rises up to 415 °C and stays fairly stable until minute 25 approximately. At minute 45, the temperature decreases to initial values which indicates that most of the material in the chamber has rehydrated.

Similar to the dehydration experiment, the temperature measured at the outlet thermocouple resulted around 40 K lower due to unavoidable heat losses in the upper section of the reaction chamber.

It is relevant to mention the effect of the steam temperature over the inlet temperature as it decreases significantly once the water vapor streams in the chamber. In addition, a tooth-shaped variation is observed in the three temperature profiles. This can be explained by the oscillating volume flow of water vapor in the reaction chamber caused by the mass flow controller (MFC). Despite the limitations of this device, the oscillation in the T_{out} is small, ranging between 2 and 7 K.

The thermogravimetric analysis (TGA) over the samples taken after both dehydration and rehydration revealed that full conversion was achieved using the parameters given in Table 1.

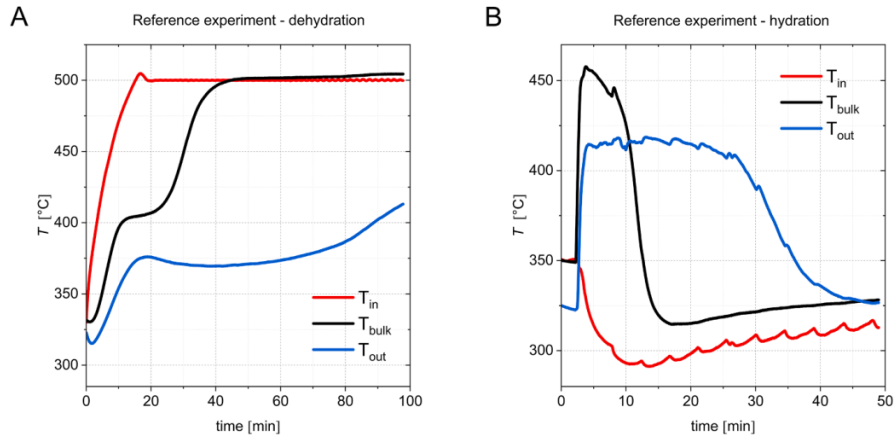

Fig. 5. Temperature profiles of dehydration (A) and hydration (B) experiments with reference granules.

Cycling stability

Fig. 6 displays the degree of hydration referred to pure $Ca(OH)_2$ mass after cycle 10 and cycle 20 for the reference, coated and composite granules. The thermogravimetric analysis (TGA) of the samples reveals that for the reference granules the rehydration remained stable along the entire experimental series with values that account for 92 % and 89 % for cycles 10 and 20 respectively. Similarly, the rehydration of the $Ca(OH)_2/CaCO_3$ composites display stable values over the cycles: 91 % after the 10th hydration and 89 % after the 20th hydration. Thereby, at the end of the 20 cycles, the energy density is slightly reduced by 11 % (from 261 kWh/m^3 to 233 kWh/m^3) for the reference granules and by 12 % (from 178 kWh/m^3 to 156 kWh/m^3) for the composites. Conversely, the rehydration of the coated granules resulted lower: 65 % after the 10th cycle and 54 % after the last rehydration of the series. In this case, the energy density decreased from 247 kWh/m^3 for the uncycled granules to 135 kWh/m^3 (-45 %) after 20 cycles In order to further understand the reason behind the lower conversion of this sample, a more detailed analysis of its phase composition along with the morphology and texture of the cycled coated granules is carried out (see section 3.2.1).

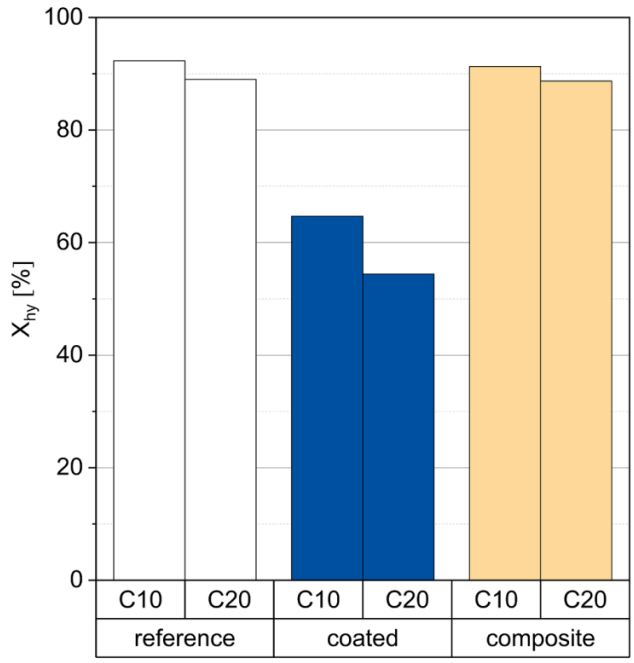

Fig. 6. Conversion achieved after 10th (C10) and 20th (C20) rehydration for the reference granules (reference), coated with Al_2O_3 (coated) and $Ca(OH)_2/CaCO_3$ composites (composite).

Phase composition, morphology and texture of the coated granules

Fig. 7 depicts the diffraction patterns recorded for the reference and coated powdered samples before cycling and after 10 and 20 reaction cycles. Common to all patterns is the presence of an amorphous hump in the background, indicating for small, X-ray amorphous particles. In case of the reference samples (Fig. 7 (A)), main reflexes stem from crystalline $Ca(OH)_2$, while minor reflexes are assigned to $CaCO_3$ (calcite). A minor amount of calcite is already present in the reference starting material, indicating a partly recarbonization after precipitation, drying and granulation of the $Ca(OH)_2$ starting material during its manufacturing process. After 10 and 20 cycles of conversion the main reflexes of $Ca(OH)_2$ show a slight broadening which is assigned to a decrease of crystallite size as a consequence of the breakage of initial crystals associated with repeated recrystallization accompanying charging and discharging.

Similar observations are also made for the samples coated with nanostructured Al_2O_3. However, in this case additional reflexes of calcium-aluminate phases, namely katoite ($Ca_3Al_2(OH)_{12}$) and mayenite ($Ca_{12}Al1_4O_{33}$) are detected after 10 and 20 reaction cycles (Fig. 7 (B)). The identified calcium-aluminates are side products formed by chemical reaction of CaO and nanostructured, hence reactive, Al_2O_3 on the interface of the storage material core and the coating layer under hydrothermal conditions. It is probable that the newly formed phases during thermochemical cycling provide an increased mechanical stability of the coating layer and hence hinder a structural disintegration of the storage material core. Since one of the formed side products contains water of constitution (katoite) and the other does not (mayenite), it is of interest to examine in detail whether the side products take part in the de- and rehydration reactions in future investigations.

By comparing the phase composition quantified by Rietveld-analysis depicted in Fig. 8, it is found that for the reference granules the amount of amorphous material has increased after the 10th reaction cycle from 6 wt% to 13 wt% as a result of the breakup of crystals during recrystallization processes into smaller, X-ray amorphous particles. After 20 cycles, however, the amount of the amorphous phase has not increased, which leads to the assumption that up from a certain size the strain induced in the lattice is not sufficient for further breakage.

A similar observation is made for the coated samples. However, in this case the initial amount of amorphous material in the uncycled granules is higher due to the additional share of nanostructured Al_2O_3 (10 wt%). After 10 and 20 de- and rehydrations, part of the nanostructured material reacts with the storage material forming the identified, crystalline calcium-aluminates. Their amount is up to around 4 wt

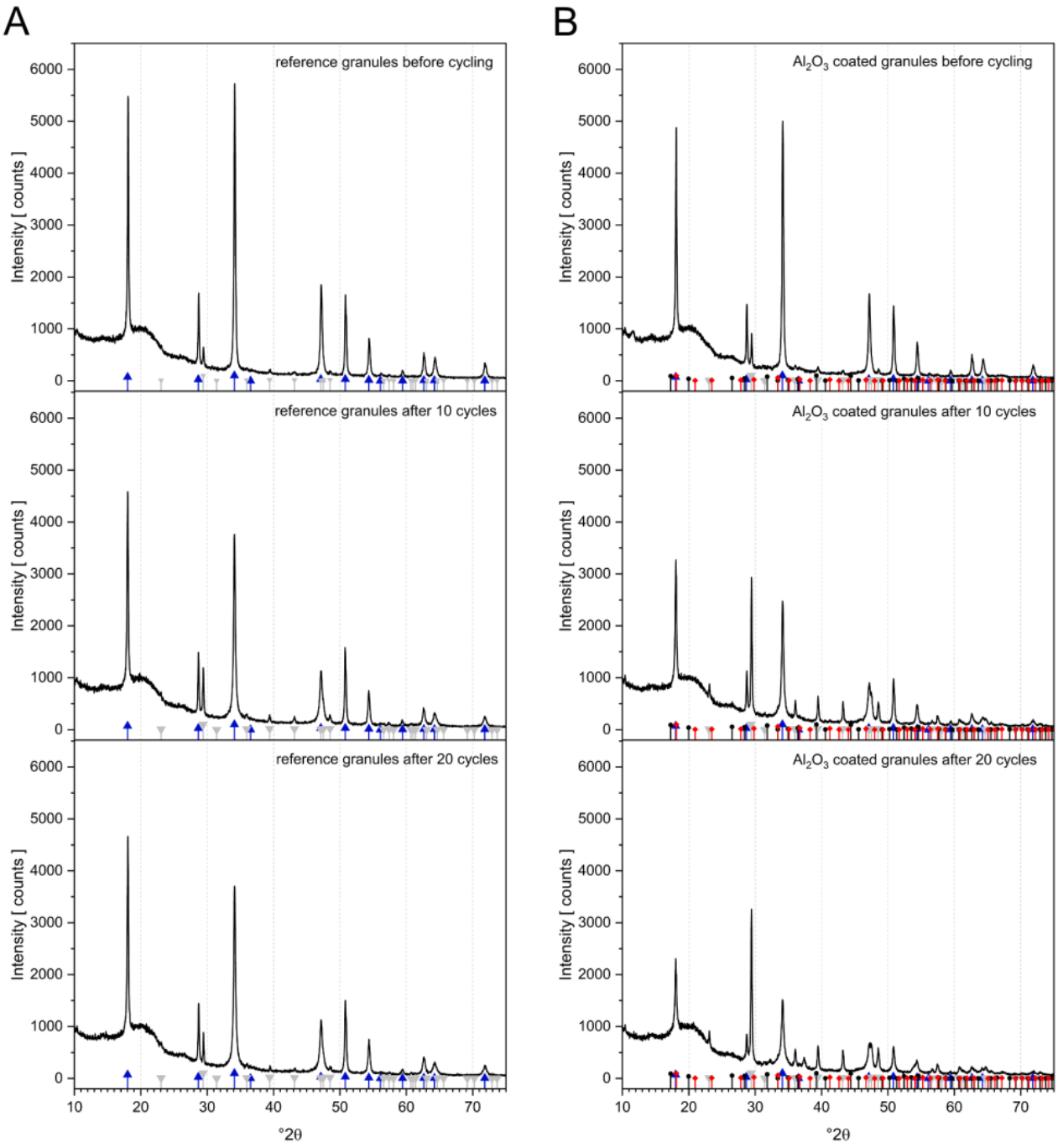

Fig. 7. X-ray diffractograms of reference $Ca(OH)_2$ granules (A) and of the granules coated with nanostructured Al_2O_3 (B) before cycling,after 10 thermochemical cycles and after 20 thermochemical cycles. Anchor lines indicate identified phases. Blue: $Ca(OH)_2$; light grey: $CaCO_3$ (calcite); black: katoite ($Ca_3Al_2(OH)_{12}$); red: mayenite ($Ca_{12}Al_{14}O_{33}$). (For interpretation of the references to colour in this figure legend, the reader is referred to the web version of this article.)

% after 10 reaction cycles and increases to in sum 18 wt% after the 20th rehydration.

Fig. 9 and Fig. 10 display the SEM-micrographs taken of reference granules and granules coated with nanostructured Al_2O_3 respectively. The images were taken before cycling, after 10 and 20 reaction cycles. In Fig. 10 (B) and (C), it can be seen that after 10 and 20 cycles, cracks on the granules appear as a result of the volume change of the crystals during de- and rehydration and associated stress induced on the microstructure of the overall granule. However, the complete structural disintegration observed for most reference granules (Fig. 9 (B) and (C)) does not occur due to the stabilizing effect of the formed calcium-aluminate layer. By comparing the surface of reference granules (Fig. 9 (D), (E) and (F)) with the coated granules after 10 and 20 cycles (Fig. 10 (E) and (F)), the formation of a layer partly containing visible crystalline products can be detected. This result matches with the results of X-ray diffraction where katoite and mayenite were identified as crystalline side products.

In summary, during the thermal cycling of the coated granules, new phases are formed from the interaction between the $Ca(OH)_2$ in the sample and the Al_2O_3 nanostructured particles. This is in accordance with the results of a previous study from our research group where it was found that such phases form a continuous layer on the surface of the

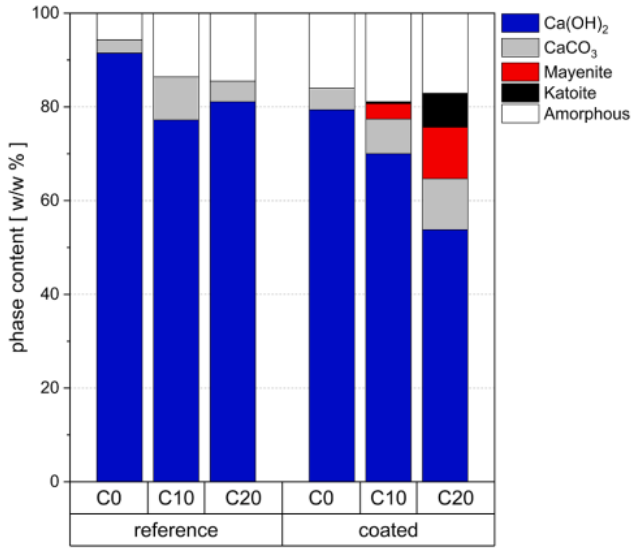

Fig. 8. Phase composition of the reference granules and of the granules coated with nanostructured Al_2O_3before cycling (C0), after 10 (C10) and 20 (C20) cycles of de- and rehydration.

coated granules. The layer is responsible for the enhancement of the mechanical stability of the granule and it was found that it did not display a major reduction in the storage density of the samples [35]. Furthermore, the temperatures at which the phases hydrate and dehydrate are within the range of the operating temperatures set for the charge and discharge experiments in this work [26,27,38,39]. Nevertheless, the extent at which the new phases convert and therefore contribute to the overall energy density of the coated granules needs to be further investigated.

Structural integrity

Fig. 11 shows the top of the bulk of granules of the three samples at different moments along their respective experimental series. Before the samples are subject of thermochemical cycling, the granules appear complete and the surfaces have a smooth appearance. The images taken after the 10th hydration reveal that an important number of reference granules have lost their initial structural integrity. After the 20th cycle, the number of the intact granules is hardly observed. The deterioration of the original structure of the coated granules is also observed along the experimental series. However, after the 10th cycle it appears that a larger number of granules maintained their shape, although cracks are visible on their surfaces. The image taken after the 20th hydration shows that most of the coated granules broke into pieces. Conversely, all the Ca $(OH)_2/CaCO_3$ composites appear intact after 10 thermochemical cycles. Moreover, even after 20 cycles in the reaction chamber, very few granules have fallen apart or display cracks. The images of the three samples also reveal that the volume that the granules occupy grows progressively with the number of cycles since the thermocouple that is visible before cycling is partly and completely covered after the 10th and 20th cycle respectively.

A more detailed track of the state of the granules along the entire experimental series is available in video as supplementary material. Here, a change in the volume of the bulk of granules is visible after each cycle. The granules reduce their volume during dehydration whereas it grows during hydration. This leads to mechanical stress and later to structural deterioration of the granules. From the comparison of the images, a qualitative analysis can be made. For example, after the 3rd dehydration for reference granules cracks start to appear whereas a number of coated granules break into smaller pieces. The composite granules, however, result unharmed. After 11 cycles, the original shape of most reference granules is lost and smaller pieces in the form of shells are visible whilst the coated granules show a similar process of deterioration, however, to a lesser extent since a far larger number of whole granules are observed. In contrast, most composite granules keep their original structure, only a few start to exhibit cracks on their surface.

Although this method helps to analyze the process of decay of the structure of the granules, it takes into consideration only the visible part of the bulk. Therefore, a quantifiable measurement over the entire batch is necessary.

In order to further understand how the structural integrity of the granules change over the cycles, the particle size distribution of each batch was analyzed after the experimental series (Fig. 12). For the reference granules, 60.5 % of the mass broke into smaller pieces (particle size < 1.60 mm) whereas 7.7 % was found in the form of agglomerated lumps (particle size > 2.0 mm). This is in agreement with the results of Funayama et al. [40] who documented agglomerations of

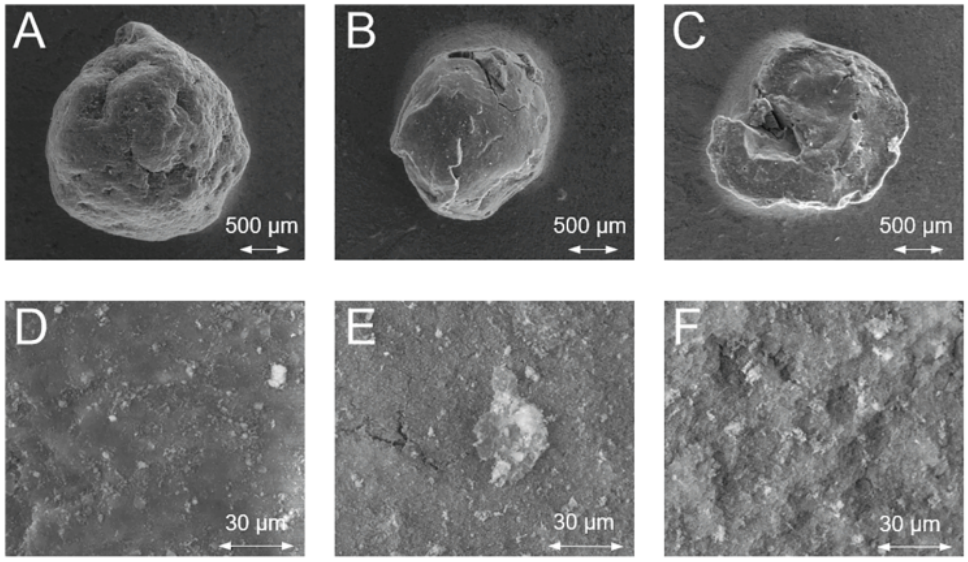

Fig. 9. Top row: $Ca(OH)_2$ reference granules before cycling (A), after 10 cycles (B) and after 20 cycles (C) 100-fold magnification. Bottom row: enlarged view on the surface of the corresponding granules before cycling (D), after 10 cycles (E) and after 20 cycles (F) taken at 2500-fold magnification.

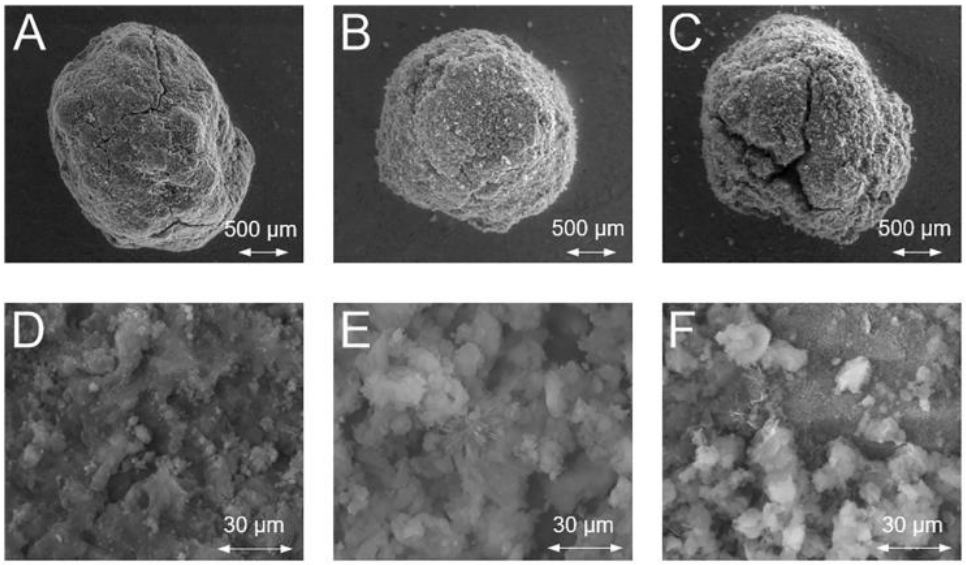

Fig. 10. Top row: $Ca(OH)_2$ granules coated with Al_2O_3 before cycling (A), after 10 cycles (B) and after 20 cycles (C) 100-fold magnification. Bottom row: enlarged view on the surface of the corresponding granules before cycling (D), after 10 cycles (E) and after 20 cycles (F) taken at 2500-fold magnification.

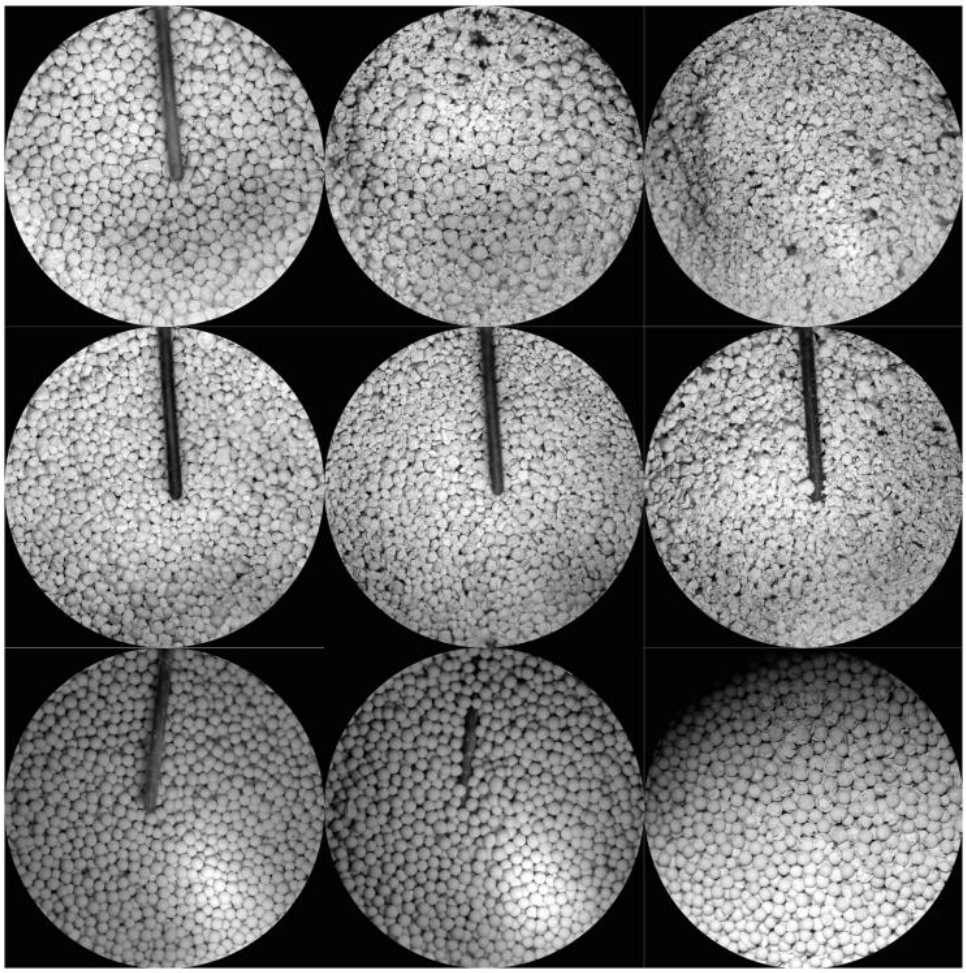

Fig. 11. Structural integrity of the three batches of granules along the 20-cycle experimental series: before cycling, after cycle 10 and after cycle 20.

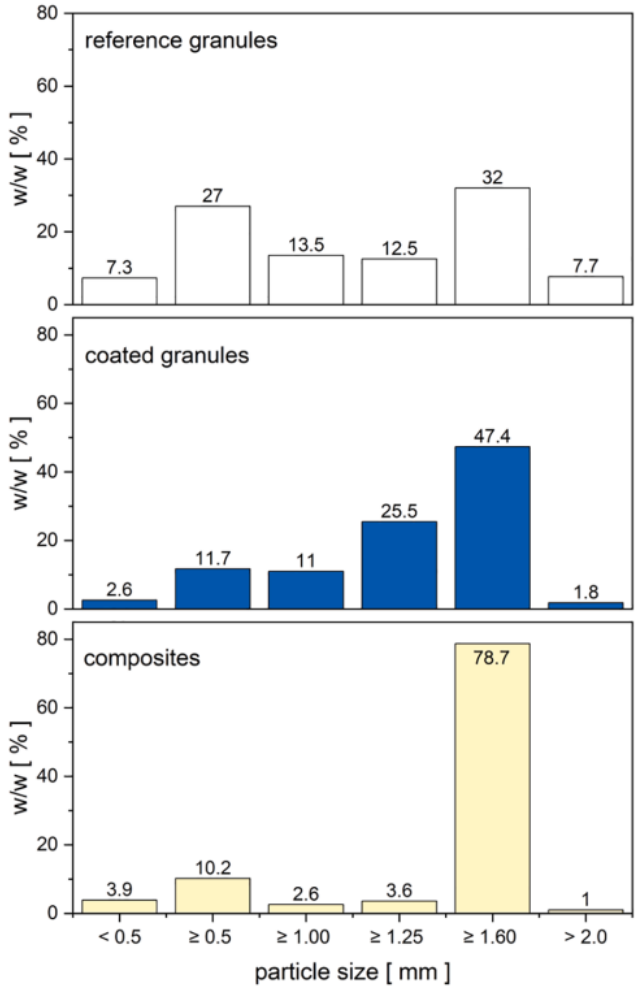

Fig. 12. Particle size distribution after 20-fold thermochemical cycles (original granule diameter: 1.6–2.0 mm).

$Ca(OH)_2$ pellets after thermal cycling.

As for the coated granules, only 2.6 % of the mass corresponds to fines (particle size < 0.5 mm). This is almost one third of the share of fines for the reference granules (7.3 %) and 30 % less than for the composites. In addition, the share of particles larger than 2 mm amounts to 1.8 %, which indicates a significantly lower degree of agglomeration when it is compared to the reference granules.

Regarding the composites, the results are in good agreement with the images taken after 20 cycles since 78.7 % of the mass of granules correspond to the original diameter size (≥1.60 mm) which is by far the largest share among the 3 samples. This could be explained by the volume change alleviation effect of the significantly lower reactive share content in this sample (40 wt% $Ca(OH)_2$). Thus, the the mechanical stress over the composite structure is less severe during hydration and dehydration. Furthermore, the share of agglomerates (>2 mm) accounts for 1 %, which is slightly lower than for coated granules. In contrast, the amount of fines found for composites is 50 % higher than for the granules coated with Al_2O_3.

To sum up, the process of decay in the structure of granules is delayed in the coated granules and composites. This is confirmed by the quantitative analysis as significantly lower quantities of fines and agglomerates were found after the 20-fold thermochemical cycling. On the one hand, the $Ca(OH)_2$ /$CaCO_3$ composites show the best results in maintaining the original structural integrity which also persists over the cycles. On the other hand, the Al_2O_3 coating performs best to prevent the formation of fines since the coated granules display 50 % less fine particles than the composites and 65 % less than the reference granules.

Mechanical stability

Fig. 13 depicts the mechanical stability of each of the three samples before cycling, after cycle 10 and after cycle 20. In general, the average mechanical strength of the three samples falls progressively with the number of cycles. In the case of the reference and coated granules, a sharp decrease is observed. For instance, after 10 cycles the C.S of reference and coated granules fell by 65 % and 46 % respectively. This trend is in agreement with other investigations on $Ca(OH)_2$ based granules [23,34]. In general, the change in dimensions of the granules during thermal cycling results in severe decrease of mechanical strength [22,34]. Although the $Ca(OH)_2$/$CaCO_3$ composites display a similar trend, the composites perform better than for the other two samples. Similar to the results of Gollsch et al. [23], the $CaCO_3$ in the samples increases the mechanical strength. It is interesting to observe that even after 20 cycles, the composites display higher mechanical stability than the other two samples at the 10th cycle. Nevertheless, the large standard deviations found are an indication of the inhomogeinity of the granules and challenges the comparison [23].

In summary, the positive effect on the mechanical strength given by both alumina coating and the share of $CaCO_3$ in the composites has been proved. Although the enhancement of the mechanical stability decreases with the number of cycles, it displays higher values than the reference granules. For the coated granules, although their original structure decays and they turn into smaller pieces, most of them do not ultimately become fine particles or agglomerates (compare with Fig. 12). This leads to the hypothesis that the Al_2O_3 additive is able to enhance the stability of the pieces produced after brittle. Future work will further investigate this and whether the particle stabilization persists over a larger number of cycles.

Conclusions and outlook

This work presents the real-time observation and analysis of the behavior of $Ca(OH)_2$-based granules under reaction conditions in a specifically designed visualization reaction chamber. The performance of two different samples of stabilized granules were compared along 20 thermochemical cycles in terms of cycling stability, structural integrity and mechanical stability. The first batch corresponds to $Ca(OH)_2$ granules coated with Al_2O_3 nanostructured particles whereas the second is comprised of $Ca(OH)_2$/$CaCO_3$ composites. Uncoated $Ca(OH)_2$ granules were used as reference material to compare the performance of the two modifications.

The results obtained demonstrate that the setup developed was operational as it allows for the rapid cycling of the samples. Furthermore, the in-situ and continuous visualization of the bulk of granules during dehydration and hydration under technical conditions was achieved for the first time. Thus, the qualitative assessment and comparison

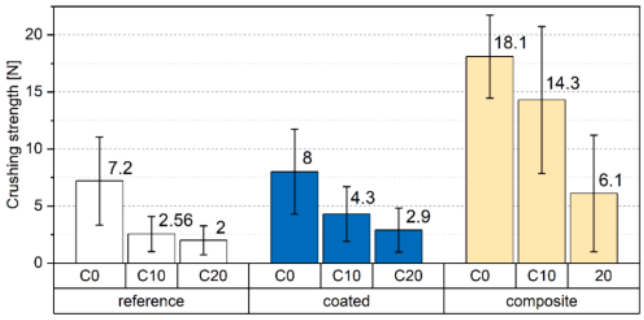

Fig. 13. Crushing strength (C.S) values and standard deviations for the three samples before cycling (C0), after cycle 10 (C10) and after cycle 20 (C20).

of the bulk of granules (e.g. crack formation, collapse of the granule structure) over the cycles was realized.

On the material side, the structural integrity and mechanical stability of the coated granules and composites resulted enhanced along the experimental series. Furthermore, the amount of fines and agglomerates were not significant. This finding suggests that both samples are capable of moving by gravity assistance after multiple cycling and could therefore be considered for the design of moving bed reactors.

The coated granules have been proved to react with the $Ca(OH)_2$ during the thermochemical cycling and form two phases: mayenite and katoite. They are responsible for the enhanced mechanical stability of the granule although their formation leads to a lower content of $Ca(OH)_2$. Nevertheless, both phases dehydrate/hydrate within the operating parameters used for the charge and discharge of $Ca(OH)_2$/CaO system. Yet, the contribution to the overall energy density of this modification needs to be further investigated.

For the $Ca(OH)_2/CaCO_3$ composites the extent of rehydration remains stable. Thus, the energy density results unaffected by the thermochemical cycling. Nevertheless, it is the lowest among the three samples due to the higher content of $CaCO_3$.

In summary, both coated granules and composites feature the enhancement of the mechanical properties and at the same time improve the bulk behavior. The Al_2O_3 coating prevents the formation of fines and agglomerates whereas the use of $CaCO_3$ at 60 wt% in the composites proved the highest mechanical strength although it displays the lowest energy density.

In view of the positive results obtained in terms of stabilization of granules, a combination of both modification approaches seems to be reasonable to investigate. Thus, composites with a higher content of $Ca(OH)_2$ and coated with alumina can be synthesized. Although a higher content of $Ca(OH)_2$ results in more mechanical stress over the granule structure, this could be compensated by the Al_2O_3 coating.

Finally, this work produced relevant results for the design of a reactor concept that detaches power and capacity. For instance, the use of stabilized larger-sized particles enables the heat transfer by means of direct gas flow. Thereby, the reactor could be designed to operate at low gas velocities to avoid the fluidization of the bed and yet achieve a high heat transfer coefficient due to the large heat transfer area of the particles. Thus, the formation of fine particles is minimized whilst high-power densities could potentially be achieved. Furthermore, as the agglomeration is avoided, the pressure drop along the bed is reduced which allows for the consideration of a larger reactive bulk of granules. Finally, the bulk density of the coated granules is about two times higher than powder $Ca(OH)_2$. This is an advantage when volumetric storage density is considered and of high relevance for the application in large storage capacities. Currently, a new pilot plant designed under these considerations and for the storage granules is set into operation in order to validate the functionality of the material under real application conditions.

CRediT authorship contribution statement

Aldo Cosquillo Mejia: Writing – review & editing, Writing – original draft, Visualization, Software, Investigation, Formal analysis, Data curation, Conceptualization. **Sandra Afflerbach:** Writing – original draft, Visualization, Methodology, Investigation, Formal analysis. **Marc Linder:** Writing – review & editing, Resources, Funding acquisition. **Matthias Schmidt:** Writing – review & editing, Supervision, Project administration, Methodology, Investigation, Funding acquisition, Formal analysis, Conceptualization.

Declaration of competing interest

The authors declare that they have no known competing financial interests or personal relationships that could have appeared to influence the work reported in this paper.

Data availability

Data will be made available on request.

Acknowledgements

This work was partially funded by the European Funds for Regional Development (EFRE Program) in the frame of the I-TESS project —Project-ID EFRE-0801821 and the Deutsche Forschungsgemeinschaft (DFG, German Research Foundation)—Project-ID 279064222—in the frame of the SFB 1244.

The authors thank Hannes Neckermann for the experimental work carried out in the laboratory of DLR- Cologne and also thank Andreas Weigl for the technical support during the setting into operation of the visualization reaction chamber. Special thanks to the company Rheinkalk GmbH, Lhoist group for providing the granular raw material.

Appendix A. Supplementary data

Supplementary data to this article can be found online at https://doi.org/10.1016/j.ecmx.2024.100656.

References

[1] Xu J, Wang R, Li Y. A review of available technologies for seasonal thermal energy storage. Sol Energy 2014;103:610–38.
[2] Schaube F, Koch LK, Wörner A, Müller-Steinhagen HM. A thermodynamic and kinetic study of the de- and rehydration of Ca(OH)2 at high H2O partial pressures for thermo-chemical heat storage. Thermochim Acta 2012;538:9–20.
[3] F. Schaube, A. Wörner, and R. Tamme, "High Temperature Thermochemical Heat Storage for Concentrated Solar Power Using Gas–Solid Reactions," *Journal of Solar Energy Engineering*, vol. 133, no. 3, 2011, doi: 10.1115/1.4004245.
[4] Rosemary JK, Bauerle GL, Springer TH. Solar Energy Storage Using Reversible Hydration-Dehydration of CaO-Ca(OH)2. J Energy 1979;3:321–2.
[5] K. Wang, T. Yan, R. K. Li, and W. G. Pan, "A review for Ca(OH)2/CaO thermochemical energy storage systems," *Journal of Energy Storage*, vol. 50, p. 104612, 06/01 2022, doi: 10.1016/j.est.2022.104612.
[6] Schmidt M, Linder M. A Novel Thermochemical Long Term Storage Concept: Balance of Renewable Electricity and Heat Demand in Buildings. In *Frontiers in Energy Research*. 2020.
[7] Fisch MN, Guigas M, Dalenbäck J-O. A REVIEW OF LARGE-SCALE SOLAR HEATING SYSTEMS IN EUROPE. Sol Energy 1998;63:355–66.
[8] T. Hanein, M. Simoni, C. L. Woo, J. L. Provis, and H. Kinoshita, "Decarbonisation of calcium carbonate at atmospheric temperatures and pressures, with simultaneous CO2 capture, through production of sodium carbonate," *Energy & Environmental Science*, 10.1039/D1EE02637B vol. 14, no. 12, pp. 6595-6604, 2021, doi: 10.1039/D1EE02637B.
[9] Samms JAC, Evans BE. Thermal dissociation of Ca(OH)2 at elevated pressures. J Appl Chem 1968;18(1):5–8. https://doi.org/10.1002/jctb.5010180102.
[10] Criado YA, Alonso M, Abanades JC. Kinetics of the CaO/Ca(OH)2 Hydration/Dehydration Reaction for Thermochemical Energy Storage Applications. Ind Eng Chem Res 2014;53:12594–601.
[11] Lin S, Wang Y, Suzuki Y. High-Temperature CaO Hydration/Ca(OH)2 Decomposition over a Multitude of Cycles. Energy Fuel 2009/06/18 2009,;23(6): 2855–61. https://doi.org/10.1021/ef801088x.
[12] Schmidt M, Gutiérrez A, Linder M. Thermochemical energy storage with CaO/Ca(OH)2 Experimental investigation of the thermal capability at low vapor pressures in a lab scale reactor. Appl Energy 2017;188:672–81.
[13] Schaube F, Kohzer A, Schütz J, Wörner A, Müller-Steinhagen HM. De- and rehydration of Ca(OH)2 in a reactor with direct heat transfer for thermo-chemical heat storage. Part A: Experimental results. Chem Eng Res Des 2013;91:856–64.
[14] Roßkopf C, et al. Investigations of nano coated calcium hydroxide cycled in a thermochemical heat storage. Energ Conver Manage 2015;97:94–102.
[15] Schmidt M, Szczukowski C, Roßkopf C, Linder M, Wörner A. Experimental results of a 10 kW high temperature thermochemical storage reactor based on calcium hydroxide. Appl Therm Eng 2014;62:553–9.
[16] Yan J, Zhao C. Experimental study of CaO/Ca(OH)2 in a fixed-bed reactor for thermochemical heat storage. Appl Energy 2016;175:277–84.
[17] K. Risthaus, M. Linder, and M. Schmidt, "Experimental investigation of a novel mechanically fluidized bed reactor for thermochemical energy storage with calcium hydroxide/calcium oxide," *Applied Energy*, vol. 315, no. 118976, 2022, doi: 10.1016/j.apenergy.2022.118976.
[18] Xia BQ, Zhao CY, Yan J, Khosa AA. Development of granular thermochemical heat storage composite based on calcium oxide. Renew Energy 2020;147:969–78.
[19] Ogura H, Miyazaki M, Matsuda H, Hasatani M, Yanadori M, Hiramatsu M. Experimental Study on Heat Transfer Enhancement of the Solid Reactant Particle Bed in a Chemical Heat Pump Using Ca(OH)2/CaO Reaction. Kagaku Kogaku Ronbunshu 1991;17(5):916–23. https://doi.org/10.1252/kakoronbunshu.17.916.

[20] M. Schmidt, M. Gollsch, F. Giger, M. Grün, and M. Linder, "Development of a Moving Bed Pilot Plant for Thermochemical Energy Storage with CaO/Ca(OH)2," 2016.
[21] Cosquillo Mejia A, Afflerbach S, Linder M, Schmidt M. Experimental analysis of encapsulated CaO/Ca(OH)2 granules as thermochemical storage in a novel moving bed reactor. Appl Therm Eng 2020;169:114961.
[22] Afflerbach S, Kappes M, Gipperich A, Trettin R, Krumm W. Semipermeable encapsulation of calcium hydroxide for thermochemical heat storage solutions. Sol Energy 2017;148:1–11.
[23] Gollsch M, Afflerbach S, Drexler M, Linder M. Structural integrity of calcium hydroxide granule bulks for thermochemical energy storage. Sol Energy 2020;208:873–83.
[24] Angerer M, et al. Design of a MW-scale thermo-chemical energy storage reactor. Energy Rep 2018.
[25] Rougé S, Criado YA, Soriano O, Abanades JC. Continuous CaO/Ca(OH)2 Fluidized Bed Reactor for Energy Storage: First Experimental Results and Reactor Model Validation. Ind Eng Chem Res 2017;56:844–52.
[26] Fujii I, Ishino M, Akiyama S, Murthy MS, Rajanandam KS. Behavior of Ca(OH)2/CaO pellet under dehydration and hydration. Sol Energy 1994;53:329–41.
[27] Sakellariou KG, Karagiannakis G, Criado YA, Konstandopoulos AG. Calcium oxide based materials for thermochemical heat storage in concentrated solar power plants. Sol Energy 2015;122:215–30.
[28] Criado YA, Alonso M, Abanades JC. Enhancement of a CaO/Ca(OH)2 based material for thermochemical energy storage. Sol Energy 2016/10/01/ 2016,;135:800–9. https://doi.org/10.1016/j.solener.2016.06.056.
[29] Sakellariou KG, Criado YA, Tsongidis NI, Karagiannakis G, Konstandopoulos AG. Multi-cyclic evaluation of composite CaO-based structured bodies for thermochemical heat storage via the CaO/Ca(OH)2 reaction scheme. Sol Energy 2017/04/01/ 2017,;146:65–78. https://doi.org/10.1016/j.solener.2017.02.013.
[30] Criado YA, Alonso M, Abanades JC. Composite Material for Thermochemical Energy Storage Using CaO/Ca(OH)2. Ind Eng Chem Res 2015;54(38):9314–27. https://doi.org/10.1021/acs.iecr.5b02688.
[31] Kariya J, Ryu J, Kato Y. Development of thermal storage material using vermiculite and calcium hydroxide. Appl Therm Eng 2016/02/05/ 2016,;94:186–92. https://doi.org/10.1016/j.applthermaleng.2015.10.090.
[32] Funayama S, Schmidt M, Mochizuki K, Linder M, Takasu H, Kato Y. Calcium hydroxide and porous silicon-impregnated silicon carbide-based composites for thermochemical energy storage. Appl Therm Eng 2023/02/05/ 2023,;220:119675. https://doi.org/10.1016/j.applthermaleng.2022.119675.
[33] Valverde-Pizarro CM, et al. Coating of Ca(OH)2 /#^{3}-Al2O3 pellets with mesoporous Al2O3 and its application in thermochemical heat storage for CSP plants. Renew Energy 2020;162:587–95.
[34] A. Jashari, S. Afflerbach, K. Afflerbach, and W. Krumm, "Structural stabilization of granular Ca(OH)2 by coating with nanostructured additives for thermochemical cycling in a fixed reaction bed," *Energy Conversion and Management: X*, vol. 18, p. 100367, 2023/04/01/ 2023, doi: https://doi.org/10.1016/j.ecmx.2023.100367.
[35] Cosquillo Mejia A, Afflerbach S, Linder M, Schmidt M. Development of a Moving Bed Reactor for Thermochemical Heat Storage Based on Granulated Ca(OH)2. Processes 2022;10(9):1680.
[36] B. W. Lucke, S. Afflerbach, and W. Krumm, "Optimization of the Coating Process of a Ca(OH)2-Based Thermochemical Energy Storage Material," *Chemie Ingenieur Technik*, vol. n/a, no. n/a, doi: https://doi.org/10.1002/cite.202300081.
[37] I. Barin, "Thermochemical Data of Pure Substances," 1995, pp. 416-523.
[38] A. Zaki, A. Faik, A. Gutierrez, M. Schmidt, D. Bielsa, and M. Linder, "Investigation of Ca12Al14O33 Mayenite for hydration/dehydration thermochemical energy storage," *Journal of Energy Storage*, 07/14 2020, doi: 10.1016/j.est.2020.101647.
[39] A. A. Lima Pacheco, T. R. Santos Nobre, M. Hark Maciel, C. V. Santilli, A. C. Vieira Coelho, and S. Cirelli Angulo, "Rehydration of katoite as a layered double hydroxide: an in situ study," *RILEM Technical Letters*, vol. 6, no. 0, pp. 8-16, 03/16 2021, doi: 10.21809/rilemtechlett.2021.130.
[40] Funayama S, Takasu H, Zamengo M, Kariya J, Kim ST, Kato Y. Performance of thermochemical energy storage of a packed bed of calcium hydroxide pellets. Energy Storage 2019;1(2):e40.

Glossary

Symbols

T: Temperature (K)
$\dot{V}$: Volumetric flow (Nm^3/h)
$\dot{m}$: mass flow (kg/h)
p_{H_2O}: Water vapor partial pressure (Pa)
$\dot{n}$: Molar flow (mol/h)
M: Molar mass (kg/mol)
X_{hy}: Rehydration degree (%)
m: Mass (Kg)

Abbreviations

TA: Thermal Analyzer
HTF: Heat transfer fluid
MFC: Mass flow controller
TGA: Thermogravimetric analysis
XRD: X-ray diffraction
SEM: Scanning electron microscopy
SE: Secondary ion
C.S: Crushing strength

Paper II: Preliminary tests in an indirectly heated reactor

Applied Thermal Engineering 169 (2020) 114961

Contents lists available at ScienceDirect

Applied Thermal Engineering

journal homepage: www.elsevier.com/locate/apthermeng

Experimental analysis of encapsulated CaO/$Ca(OH)_2$ granules as thermochemical storage in a novel moving bed reactor

Aldo Cosquillo Mejia[a,*], Sandra Afflerbach[b], Marc Linder[c], Matthias Schmidt[a]

[a] German Aerospace Center – DLR e.V., Institute of Engineering Thermodynamics, Linder Höhe, 51147 Köln, Germany
[b] University of Siegen, Institute for Building and Materials Chemistry, Paul-Bonatz-Str. 9-11, 57076 Siegen, Germany
[c] German Aerospace Center – DLR e.V., Institute of Engineering Thermodynamics, Pfaffenwaldring 38-40, 70569 Stuttgart, Germany

HIGHLIGHTS

- Development and demonstration of a novel moving bed reactor concept.
- Encapsulation of $Ca(OH)_2$ with ceramic shell and Al_2O_3 nanostructured particles.
- Experimental investigation of encapsulated materials in a lab scale reactor.
- Enhancement of stability of $Ca(OH)_2$ granules along multiple thermochemical cycles.
- Encapsulated granules investigated under application-oriented operating conditions.

ARTICLE INFO

Keywords:
Moving bed reactor
Calcium oxide
Calcium hydroxide
Thermochemical energy storage
Encapsulation
Nanostructured particles

ABSTRACT

The advantages of $Ca(OH)_2$ such as low cost and high energy density make it a promising material for thermal energy storage. However, the development of cost efficient large scale storage systems remains challenging. One reason is that the low thermal conductivity and cohesiveness of the powder bulk material impede the reliable operation of moving bed reactors. One approach to address these drawbacks is the macro encapsulation of pre-granulated storage material.

In this work, a newly moving bed reactor was developed and the performance of two encapsulated storage materials was investigated in lab scale and under application relevant boundary conditions. The two tested material samples were ceramic encapsulated CaO granules (sample 5D1F) and $Ca(OH)_2$ granules coated with Al_2O_3 nanostructured particles (sample Al_2O_3). The reaction performance, cycling stability and ability to flow were experimentally examined and the operation of the moving bed reactor was successfully demonstrated. It was found that both encapsulated materials retained their shape after sixfold cycling. After the experiment series, the sample 5D1F flowed freely out of the reactor while the sample Al_2O_3 clogged the reactor tubes due to the volume expansion during hydration. Further, the experiments revealed that the reaction performance of the sample 5D1F is reduced, while the performance of the sample Al_2O_3 is comparable to unmodified $Ca(OH)_2$ granules. Overall, this study shows that encapsulated granules are stable under operation in larger reactors and the granules further facilitate the reactor design and operation. Additionally, the volumetric energy density of compacted granules is higher compared to the loose powder bulk. In particular, the encapsulation with Al_2O_3 nanostructured particles showed promising performance for the cost efficient development of a scalable thermochemical energy storage system and therefore needs to be further investigated.

Abbreviations: CSP, concentrated solar power; TGA, thermogravimetric analysis; TA, thermal analyser; MFC, mass flow controller; HTF, heat transfer fluid; SEM, scanning electron microscopy; $m_{H_2O\ stoich.}$, stoichiometric mass of water; wt. %, weight percent; X_{tot}, conversion; Ref., reference sample; P1, P2, pressure sensor 1 and 2; TCS, thermochemical storage; F, filling level; T1,T2, temperature sensor 1 and 2; T, temperature; p, pressure; $\dot{V}$, volumetric flow rate; m, mass; Nm^3, normal cubic meter; MW_{th}/MWh_{th}, thermal power/thermal energy

* Corresponding author.
E-mail address: aldo.cosquillo@dlr.de (A. Cosquillo Mejia).

https://doi.org/10.1016/j.applthermaleng.2020.114961
Received 5 September 2019; Received in revised form 13 January 2020; Accepted 15 January 2020
Available online 16 January 2020

1. Introduction

Nowadays, the expansion of the capacity of the renewable energy sources is challenging as their integration within the power systems is complex due to their intermittent nature [1,2]. Consequently, it is necessary to complement the systems with energy storage technologies [3]. The gas-solid reaction of calcium hydroxide to calcium oxide and water vapour is of particular interest for thermochemical storage (TCS) purposes:

$$Ca(OH)_2 + 104.4\ kJ/mol \rightleftharpoons CaO + H_2O$$

The storage of thermal energy is particularly advantageous for Concentrated Solar Power (CSP) plants as it increases their flexibility [4]. The integration of a TCS based on $CaO/Ca(OH)_2$ in a molten salt CSP plant was thermodynamically evaluated in a recent study. In the concept, a first TCS reactor operates at low water vapour pressures (10 kPa) and supplies thermal energy for the preheater and the steam generator. A second high pressure (450 kPa) TCS reactor provides heat to the superheater and reheater. The heat of condensation of the exhaust steam of the low pressure turbine is used for the discharge reaction in the low pressure reactor. For the high pressure reactor, the generation of steam is driven by the condensation enthalpy of steam which is extracted from the turbine. The efficiency of the storage system under this operation mode accounts for 87% [5]. Similar integration concepts were investigated by Pelay et al. [6]. The decarbonation reaction of $CaCO_3$ is also investigated as TCS in a CSP. The reaction offers a remarkably higher energy density [7–9] and the operating temperature of the carbonation/calcination reaction (800–900 °C) is much higher compared to the hydration/dehydration reaction of the $CaO/Ca(OH)_2$ storage system (400–600 °C). Bayon et al. recently summarised different thermochemical reactions, their application for CSP plants and evaluated the systems techno-economically [10].

The reaction can also be used for the recovery of waste heat in order to enhance the energy efficiency of industrial processes [11]. The operation was proved successful under low vapour pressures ranging from 1.4 kPa and 20 kPa which allows the incorporation of low temperature waste heat to produce the required discharge steam [12].

The thermochemical storage system also features fast kinetics and was proved to be reversible and stable over a large number of cycles [13]. Furthermore, the raw material is not toxic, inexpensive and the reaction has a high enthalpy of reaction [14,15]. For this reason, a significant number of investigations have been conducted at lab- and pilot-scale. Thermogravimetric analysis (TGA) was carried out intensively using very small samples in the order of milligrams [14–17] whereas for larger masses of storage material different reactor concepts were developed. Currently, the most investigated concepts are fixed bed reactors, fluidised bed reactors and moving bed reactors.

Several studies have been conducted on fixed bed reactors [12,13,18,19]. This concept has the main disadvantage of discontinuous operation and therefore requires the use of large heat exchangers for large storage capacities. As a consequence, the costs of this type of reactors rise with increasing storage capacity and thus outweigh the low cost feature of the storage material [20].

In order to decouple the expensive heat exchange surface from the storage capacity and to allow continuous operation, the fluidised and moving bed reactor concepts are currently under investigation. Regarding the first, Pardo et al. [21] carried out the $Ca(OH)_2/CaO$ reaction in a batch bubbling fluidised bed reactor with a mix of 30% $Ca(OH)_2$ and 70% Al_2O_3 (easy-to-fluidise particles) whereas Criado et al. [22] and Rouge et al. [23] used CaO particles previously calcined at very high temperatures. These works demonstrated the feasibility of this reactor concept. Angerer et al. [20] presented a design for a MW-scale reactor using pure commercial CaO calcined under moderate conditions and with higher reactivity. This design was technically proven in preliminary experimental tests and a 10 kW pilot scale reactor is currently being commissioned.

In a moving bed reactor, the storage material moves through the heat exchanger while it reacts, thus allowing continuous operation. Although this concept overcomes one of the main drawbacks of fixed bed reactors by decoupling power and capacity, in practice the raw material has unfavourable properties like the tendency to agglomerate and a low thermal conductivity [24]. Furthermore, the powder is fine and cohesive which results in poor ability to flow [25]. Consequently, to improve the flowability and to stabilise the particle size of the storage material [26], different modifications have been tested.

One of the modification approaches is to use additives to decrease the Van der Waals forces between the $Ca(OH)_2$ particles and therefore reduce their cohesiveness. The investigation of Roßkopf et al. [27] showed that the use of SiO_2 nanostructured particles actually prevents the agglomeration of the material. However, the reactivity is reduced due to the formation of unreactive side products. Following the same line of investigation, Schmidt el al. [25] tested the effect of adding Al_2O_3 to the powder material in a moving bed reactor. The flowability of the powder material was improved for cold conditions but under reaction conditions the effect decreased and the free flow of the powder through the reactor could not be achieved.

Another approach is to shape the material in the form of granules or pellets. Yet in general, the granules based on CaO powder fall apart into smaller particles as soon as the hydration reaction is performed. To stabilise the granules, Fuji et al. [28] investigated the behaviour of doped $Ca(OH)_2$ spheres and pellets under reaction conditions. Although the addition of aluminium salts contributed to some extent to maintain the original shape, this effect was lost after cycling. Sakellariou et al. [29] used kaolinite as binder in spherical structured formulations with limestone. The mechanical integrity of the pellets resulted enhanced under this formulation although the reactivity was reduced to 50%. Despite the efforts, granules which are satisfactorily stable under thermochemical operation in moving bed reactors have not been reported yet.

Recently, new modified materials, under the approach of encapsulating larger granules of $Ca(OH)_2$, have been developed by Afflerbach et al. [26]. The group tested granules encapsulated with a ceramic shell. The results after a 10-cycle experiment series in a TA instrument showed that the structural integrity of the granules remained and 100% conversion of the reactive material was achieved. In another modification approach, small amounts of Al_2O_3 nanostructured particles were mixed with granules of $Ca(OH)_2$. It was discovered that the structural integrity of the modified granules was comparable to the granules encapsulated in ceramic shell, but with clearly reduced manufacturing complexity and higher conversion. Nevertheless, an experimental investigation of these two novel encapsulated storage materials in larger scale and under operation in a moving bed reactor is still missing.

The aim of this work is therefore to investigate the performance of the novel encapsulated materials under application oriented operating conditions and to demonstrate the feasibility of the moving bed concept. In order to test the materials, a novel moving bed reactor for encapsulated storage materials in laboratory scale has been developed and set into operation. Two batches of both materials were manufactured in kg-scale and cycled in the reactor. Several hydration and dehydration experiments were conducted to analyse the cycling stability as well as the reaction performance of the materials. The flowability through the reactor and the structural integrity of the granules were investigated after the thermochemical cycling. This study therefore presents the first investigation of encapsulated $Ca(OH)_2$ granules in a laboratory scale moving bed and reveals important information on the performance of the newly developed storage materials and the reactor concept. Based on the experimental results of this study, conclusions regarding further improvements for the material development as well as the design of moving bed reactors are derived.

2. Experimental setup

2.1. Reactor type

In an indirectly heated moving bed, the thermochemical storage material is physically separated from the heat transfer fluid (HTF). This offers the advantage that the side of the heat exchanger, where the material is hosted, can independently be optimised to ensure its flow. Since the material is only moving through the heat exchanger by gravity, mechanical stress on the particles is minimised. Additionally, the reaction gas, heat transfer fluid and material flow rate can all be adjusted independently allowing for the most flexible operation possibilities for this reactor concept. One major drawback of the concept is that the heat transfer is extremely limited by the low thermal conductivity of the storage material. As a consequence, only small distances between the reacting particles and the heat exchange surface can be tolerated. Due to the advantages of lower stress on the storage granules and the operation flexibility, an indirectly heated moving bed concept was chosen for the reactor development.

2.2. Development of a lab-scale moving bed reactor

As a general concept, a tube bundle heat exchanger was chosen. The main idea was that a well-known cost efficient heat exchanger design could be adapted to serve as thermochemical storage reactor. Fig. 1 shows the proposed concept. The storage material flows inside the tubes, assisted only by gravity. Thermal energy is delivered or taken up by the heat transfer fluid which flows on the shell side of the heat exchanger directed by baffle plates. These plates ensure a high velocity of the air flow in order to obtain a good heat transfer coefficient between the gas flow and the tube surface. A counter current flow was chosen where the unreacted cold material enters the tubes from the top and the hot incoming air enters the reactor at the bottom. The tube diameter had to be optimised between a very small diameter, which would increase the overall heat transfer coefficient to the storage material, and a sufficiently large diameter that ensures the flow. Experimental pretesting revealed that with a diameter of 18 mm, the granules with diameter between 1 and 3 mm flowed through the tubes in cold conditions.

The length of the tube defines the heat exchange area and the residence time of the reacting material in the tube. Based on an available numerical model [25], simulations were performed in order to determine the tube length and diameter. The final design resulted in 22 tubes, with 18 mm diameter and 330 mm length, which account for a total heat exchange area of 0.41 m^2 and a total volume for the storage material of 1.85 L. With the available heat exchange area and HTF flow rate of 20 Nm^3/h with a temperature difference between the air inlet and outlet of 200 K, a thermal power of 1 kW could be reached. The reactor is designed to operate at pressures between 10 and 150 kPa and a maximum temperature of 550 °C (key parameters are summarised in Table 1).

Table 1
Technical features of the moving bed reactor.

Heat exchanger type	Indirect, tube bundle
Tube diameter	18 mm
Tube length	330 mm
Number of tubes	22
Volume	1.85 L
Heat exchange area	0.41 m^2
Thermal power	1 kW
Construction material	Stainless steel 1.4571

2.3. Test bench

The test bench consists of the moving bed system, the reaction gas unit and the heat transfer fluid (HTF) supply unit (Fig. 2).

The feeding tank, with a volume of 20 L for the storage material, is located at the top of the moving bed system. The tank contains unreacted storage material and is attached to a pneumatically controlled flap. The adjustable opening angles of the flaps control the mass flow of the unreacted/reacted material respectively. By opening the upper flap, the storage material can flow down to fill the 22 tubes of the reactor. Below the upper flap, a double jacket cylinder is located where the inner cylinder contains a fine steel mesh with a pore size of 2 μm. The cylinder is connected to the reaction gas unit and the fine mesh allows the water vapour to stream in and out of the reactor. The cylinder volume stays free of storage material, thus the gas can equally distribute all over the reactor tubes. Once all the tubes are filled with material, the hydration/dehydration process can start. As soon as the material in the lower part of the tube bundle has reacted completely, the lower flap is opened to allow the material to flow down to the reception tank. Simultaneously, the upper flap is opened again to fill the void left in the tubes with unreacted material. By controlling the mass flow in and out of the reactor, the system can be operated as continuous moving bed, quasi continuous moving bed or fixed bed, allowing the

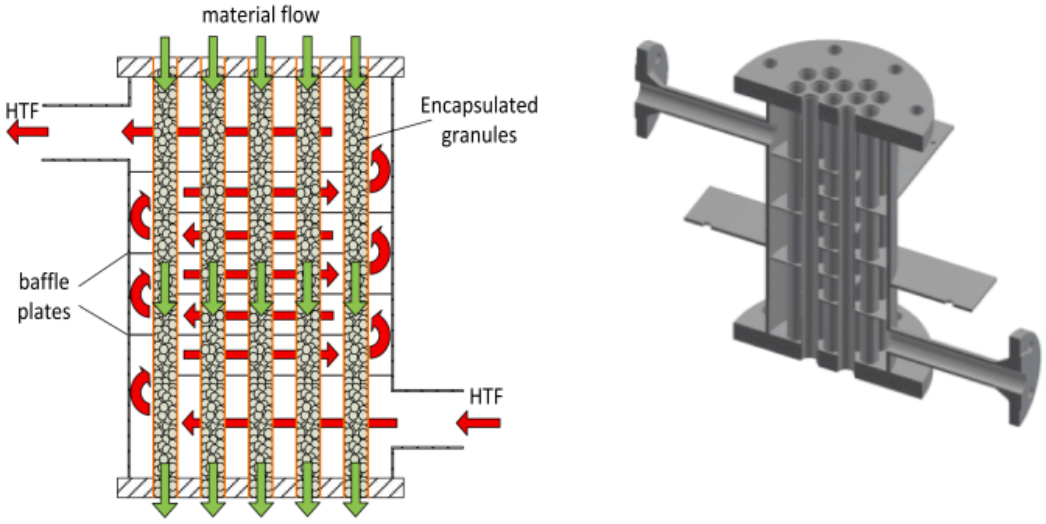

Fig. 1. Left: Schematic representation of the flow of the HTF on the shell side (red arrows) and the storage material in the tubes of the reactor (green arrows). Right: 3D image of the tube-bundle reactor. (For interpretation of the references to colour in this figure legend, the reader is referred to the web version of this article.)

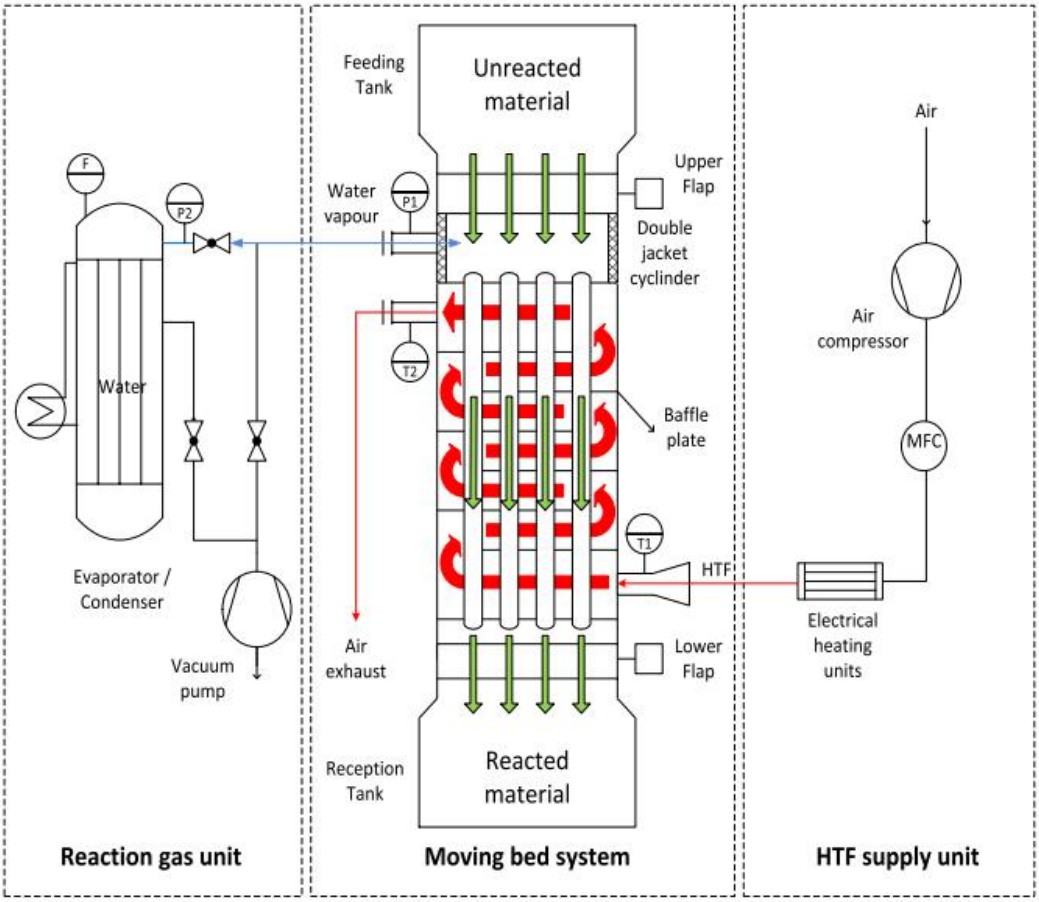

Fig. 2. Schematics of the moving bed reactor integrated in the test bench.

investigation of such operation modes.

The reaction gas unit is composed by the evaporator/condenser which is equipped with a filling level measurement sensor (Vegaflex 65, ± 2mm). The evaporator/condenser supplies water vapour at different pressures and depending on the direction of the reaction occurring in the reactor, the vapour is either taken up or released from the storage material. This causes a pressure change in the system, followed by compensation through further evaporation or condensation of water in the reaction gas unit. Consequently, the volume of the liquid water changes, which is measured by the filling level measurement sensor (1 mm accounts for 0.013 kg H_2O). Thus, the degree of the conversion is calculated as follows:

$$X_{tot} = \frac{m_{H_2O\ evaporated/condensed}}{m_{H_2O\ stoich.}} = \frac{|Filling\ level_{start} - Filling\ level_{end}| * 0.013\ [kg]}{m_{H_2O\ stoich.}\ [kg]}$$

The expression in the numerator refers to the actual mass of water evaporated or condensed in the evaporator/condenser. The term in the denominator corresponds to the stoichiometric mass of water of the reactive material present in the reactor.

The error of the measurement sensor in the filling level corresponds to 0.026 kg H_2O. Therefore, the % conversion error is calculated as follows:

$$\%\ error = \pm \frac{0.026\ [kg]}{m_{H_2O\ stoich.}\ [kg]}\%$$

2.4. Material

2.4.1. Reference material – $Ca(OH)_2$ granules

As reference material, commercially available granulated $Ca(OH)_2$ (Sorbacal® H90) was supplied by Rheinkalk GmbH. The product contains 92.9 wt% $Ca(OH)_2$ and granules with diameter between 1 and 4 mm were used in the experiments (Fig. 3).

Fig. 3. Reference material – $Ca(OH)_2$ granules.

2.4.2. $Ca(OH)_2$ granules encapsulated with a ceramic shell - sample 5D1F

For the production of the ceramic encapsulated storage material, granulated $Ca(OH)_2$ was taken as starting material and put into a mixer (Eirich, type R02/E). Under co-current flow, liquid paraffin was added as adhesion promoting agent before the powdered ceramic precursor was admixed. The coating process was finished when the ceramic precursor covered the entire surface of the granulated $Ca(OH)_2$ templates. To achieve the mechanical stability and water vapour permeability, the coated material was sintered in a second step. Thereby, organic constituents within the precursor are decomposed, leaving an open porous network within the shell through which water vapour can be transported during the charging and discharging of the inner storage material core. The entire process was described in detail by Afflerbach et al. [26]. However, in the present work the ceramic precursor was admixed with 5%(w/w) of SiO_2 in form of diatomaceous earth and 1% (w/w) of Na_2CO_3 as flux agent in order to increase the mechanical stability of the ceramic shell. The final encapsulated granules contain 39 wt% CaO.

2.4.3. $Ca(OH)_2$ granules encapsulated with a nanostructured particle shell - sample Al_2O_3

In order to probe the functionality of a thinner capsule, $Ca(OH)_2$ granules were coated with nanostructured Al_2O_3. As in case of the production of the previous material, the granules were put into a mixer (Eirich, type R02/E) where water as adhesion promoting agent was added under co-current flow. Subsequently, Al_2O_3 was added to the granules up to the point that all surfaces were thoroughly covered and no fines of the additives aggregated separately within the mixing container. In case of this sample, no further processing of the material was performed. The content of $Ca(OH)_2$ for this modification variant accounts for 90 wt%.

2.5. Experimental procedure

To carry out the experiments, the 22 tubes of the reactor were filled with the samples which remained in the tubes during the experiments (e.g. the reactor was used as fixed bed).

2.5.1. Dehydration procedure

Initially the reactor is filled with storage material and then it is evacuated in order to ensure a pure water vapour atmosphere during the experiments. After setting the volumetric flow at 20 Nm/h, the HTF temperature is set to 350 °C to preheat the calcium hydroxide material in the reactor. At the condenser side, a water vapour pressure of 10 kPa is adjusted. Once the preheating temperature is stable, the valve that separates the condenser and the reactor is opened, thus the pressure in the whole system equalises. Then the air inlet temperature is increased to 540 °C. The dehydration starts when the reaction bed exceeds the equilibrium temperature (405 °C at 10 kPa). The water vapour released from the endothermic reaction is collected in the condenser. The reaction proceeds until all the $Ca(OH)_2$ is dehydrated indicated by no more water volume change in the condenser.

2.5.2. Hydration procedure

The calcium oxide samples present in the reactor are pre-heated at 540 °C. Meanwhile, water vapour pressure at 100 kPa is prepared separately in the evaporator. When the valve that connects the evaporator and the reactor is opened, the water vapour pressure equalises in both sections. In order to start the reaction, the temperature has to decrease below the equilibrium temperature (505 °C at 100 kPa). Therefore, the air inlet temperature is set to 350 °C and the heat released by the exothermal process is taken up by the HTF. As the calcium oxide in the reaction bed absorbs water vapour, additional volume needs to be evaporated in the reaction gas unit to compensate the pressure loss and thus maintain the pressure set.

The operation settings used in the experiments of the present work are presented in Table 2.

Table 2
Operation settings for hydration and dehydration experiments.

Experiment	$T_{air,initial}$/ °C	$\dot{V}$ / $\frac{N.m}{h}$	$T_{air,inlet}$/ °C	$p_{cond./evap}$/ kPa
Dehydration	350	20	540	10
Hydration	540	20	350	100

2.6. Morphological investigation

The morphology of the probed samples was investigated comparatively before and after cycling by scanning electron microscopy (SEM). Therefore, a FEI Quanta FEG 250 microscope was utilised. All scans were taken in low vacuum mode at pressures between 90 and 110 Pa. For high resolution imaging, a large field detector operated in secondary electron mode was chosen.

3. Experimental results

The aim of this work is to demonstrate the functionality of the newly developed moving bed reactor and to analyse the performance of different encapsulated storage materials at laboratory scale. Therefore, first the reactor operation was tested with unmodified $Ca(OH)_2$ granules. In the second step, the performance of the newly developed storage granules was analysed. Two batches of the manufactured granules were cycled 6 times (hydration and dehydration) in the reactor. Based on the experiments, the reaction performance, cycling stability and the flowability of the granules were assessed. Additionally, the structural integrity, in particular the stability of the shell around the granules after the thermochemical cycling, was investigated.

3.1. Reference experiment with pure $Ca(OH)_2$ granules

Two experiments using the reference material were performed to verify the operation of the reactor and the operation parameters selected for the hydration and dehydration procedure. The results obtained also serve as a baseline to compare with the experiments with the modified materials.

3.1.1. Dehydration

Fig. 4 depicts the temperature and conversion trend for the dehydration experiment. Once the preheating temperature and pressure are steady, the experiment starts by increasing the air inlet temperature to 540 °C (at min. 3). At minute 30 as the air outlet temperature exceeds 440 °C, the slope of the temperature trend, (blue line) decreases significantly. Simultaneously, the slope of the conversion trend becomes steeper indicating a high rate of reaction. Therefore, the drop in the temperature trend is a consequence of the endothermal reaction that proceeds in the reactor. The storage material takes up significant amount of the thermal energy from the HTF, thus the temperature difference between air inlet and outlet increases. The dehydration reaction proceeds in the following period. At minute 160, all profiles become steady again which indicates that the reaction is complete.

3.1.2. Hydration

Fig. 5 shows the temperature and conversion trends for the hydration procedure. At minute 3, water vapour is supplied to the reactor and simultaneously the air inlet temperature is reduced to 350 °C. It can be observed that at minute 10 the slope of the falling air outlet temperature significantly declines compared to the period between minute 3 and 10. The reason for this is that the temperature in the reactor falls below the reaction equilibrium temperature of 505 °C that is defined by the vapour pressure of 100 kPa. Consequently, the exothermal reaction of calcium oxide with the water vapour starts and thermal energy is

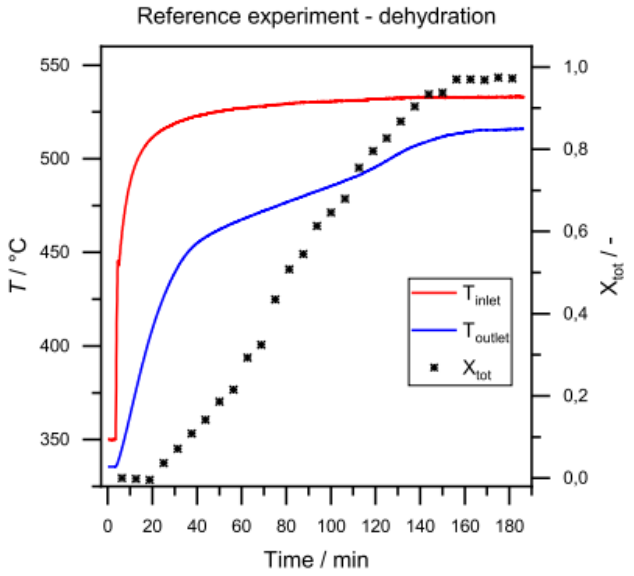

Fig. 4. Temperature and conversion trends during the dehydration experiment using reference material.

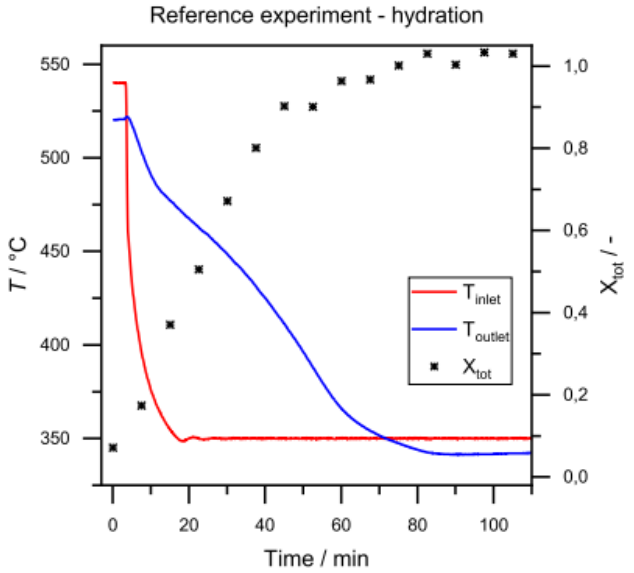

Fig. 5. Temperature and conversion trends during the hydration experiment for the reference material.

released. The heat released by the storage material is taken up from the air flow thus reducing the temperature drop rate. Accordingly, the conversion trend confirms that the exothermic reaction takes place. The reaction proceeds until minute 80 when full conversion is reached. After that point, no more material reacts. Consequently, both conversion and outlet temperature trends stabilise.

In the reference experiments full conversion was reached for the pure $Ca(OH)_2$ material for both the dehydration and hydration procedure. The results confirm the successful operation of the reactor and that the chosen operating parameters for reaction gas pressure and temperature allow complete conversion.

3.2. Analysis of modified encapsulated granules

As mentioned in the material section, $Ca(OH)_2$ granules encapsulated with a gas permeable shell have been developed by two different methods. The first are granules encapsulated with a ceramic

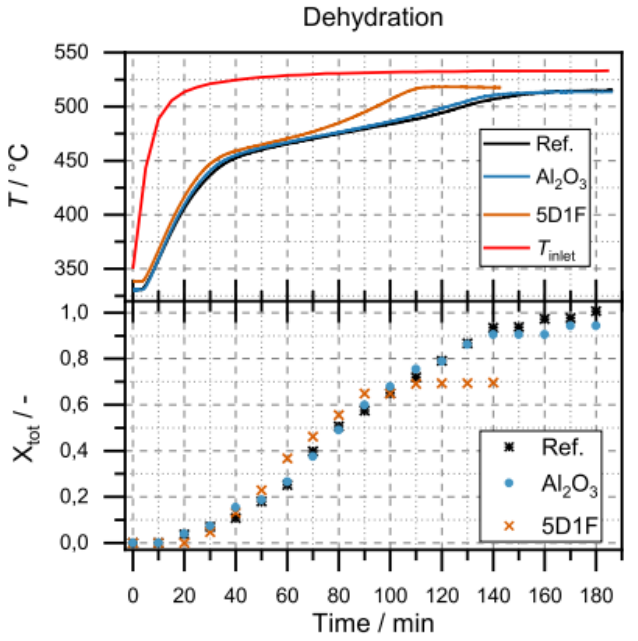

Fig 6. Temperature and conversion trends for both encapsulated materials and reference material during dehydration.

shell (sample 5D1F) and the second batch are granules coated with Al_2O_3 nanostructured particles (sample Al_2O_3). Both newly developed materials have so far only been investigated as single granules in a TGA device. The behaviour of the granules as larger bulk in a laboratory moving bed reactor is still unclear. Therefore, the materials were manufactured in kg scale and the reactor tubes were filled with 2.232 kg of the sample 5D1F and 1.584 kg of the sample Al_2O_3 respectively. The two batches were cycled 6 times under fixed bed conditions. The dehydration and subsequent hydration experiments were performed according to the procedure described in Section 2.5.

3.2.1. Dehydration

Fig. 6 shows the temperature and conversion trends for both encapsulated materials as well as the unmodified reference material (presented in Section 2.4). At the beginning of every experiment the whole set up was preheated to 350 °C and at minute 3 the air inlet temperature was increased to 540 °C in order to initiate the dehydration reaction. In all cases the start of the reaction can be observed after around 30 min indicated by the measured increase of conversion. Simultaneously, the slope of the air outlet temperature trends decreases which reflects the absorption of thermal energy by the endothermal reaction. The reaction proceeds in the following period which is indicated by a very slow increase in the outlet temperature slope. With the ongoing reaction more material has completely reacted, thus the absorption of thermal energy due to the endothermal reaction diminishes. As a consequence, the air outlet temperature increases faster again. The change in the slope of the outlet temperature trend can be observed after 80 min for the sample 5D1F and after 110 min for the sample Al_2O_3. Accordingly, for the sample 5D1F after 100 min, no additional water release due to the dehydration of the material is measured and the air temperatures become constant again. The reaction is over at this point even though the total conversion of the sample 5D1F was 70%. For the sample Al_2O_3, temperature and conversion become constant after 140 min and a total conversion of 94% was determined.

The energy taken up during dehydration is calculated based on the conversion achieved, which accounts for 0.315 kWh for the sample 5D1F and 0.525 kWh for the sample Al_2O_3. To determine the energy density of both materials, the volume of the 22 tubes of the reactor

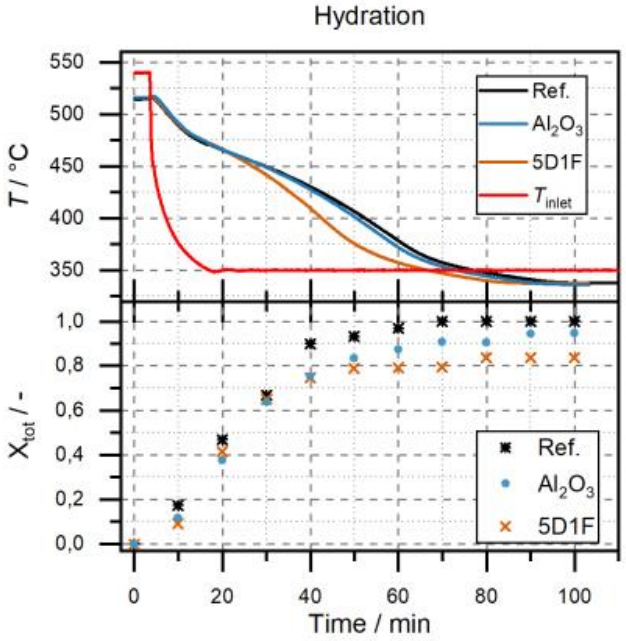

Fig 7. Temperature and conversion trends for both encapsulated materials and reference material during hydration.

(1.85 L) was taken into account. Thus, 170.5 kWh/m^3 correspond to the sample 5D1F and 284 kWh/m^3 to the sample Al_2O_3.

3.2.2. Hydration

After every dehydration experiment, the hydration procedure was performed according to the method described in Section 2.5 with both batches of the encapsulated granules. Fig. 7 shows temperature and conversion trends for the hydration procedure. The reactor was pre-heated to 540 °C and water vapour at 100 kPa was introduced into the reactor at minute 3. In order to start the hydration reaction, the HTF inlet temperature is simultaneously set to 350 °C. For all cases, when the temperature in the reactor drops below the equilibrium temperature of the reaction (505 °C), the exothermic reaction starts (at around minute 10). The release of heat is visible as the decrease of the outlet temperature slows down. This indicates that the energy freed by the reaction is taken up by the HTF. Accordingly, a continuous increase of conversion is also measured. For the sample 5D1F no more conversion is measured after minute 50 while for the sample Al_2O_3 the conversion trend becomes steady after minute 70. In total, for the sample 5D1F only a conversion of 83.7% was measured. For the sample Al_2O_3 a total conversion of 94% was reached. The incomplete conversion of the sample 5D1F can also be observed at the outlet temperature trend. From minute 30, the outlet temperature of the sample 5D1F experiment decreases faster than the temperature of the sample Al_2O_3 because less energy is released by the reaction.

The energy released from the hydration of the sample 5D1F resulted in 0.377 kWh whereas for the Al_2O_3 sample it was 0.525 kWh. The thermal power obtained accounts for 0.328 kW for the sample 5D1F and 0.444 kW for the sample Al_2O_3.

3.2.3. Flowability and structural integrity

For the reference material the ability to flow was tested after the hydration reaction. It was found that the unmodified granules formed agglomerations that clogged the tubes and prevented the flow. After dehydration, the flow was achieved after a short initial poking of the granules in the tubes. The visual inspection of the material withdrawn revealed that some granules broke into small particles or powder; other maintained their shape but had significant cracks that would most likely lead to fractures in the subsequent cycles.

Regarding the encapsulated granules, after the last thermochemical cycle the batches were released out of the reactor by opening the lower flap. All 5D1F granules flowed instantaneously and freely out of the tubes, as it can be seen in Fig. 8 left. In contrast, none of the granules of the sample Al_2O_3 flowed out of the tubes after opening the reactor. The granules stuck partially together and formed larger agglomerates which clogged the tubes completely (compare Fig. 8 right). Nevertheless, again by poking, it was possible to loosen the agglomerates easily and the granules flowed out freely. After withdrawing the granules, their structural integrity was analysed.

Fig. 9a shows the state of the sample 5D1F before and after the experiment series. The comparison reveals that for some granules the ceramic shell had visible cracks or was partly lost. Nevertheless, the majority of the granules were intact and maintained their overall shape. For the sample Al_2O_3 no cracks or loss of the very thin shell layer was visible (compare Fig. 9b). Furthermore, almost all the granules maintained their shape.

3.2.4. Cycling stability

It already became obvious in the analysis of the dehydration experiment (compare Fig. 6) that for the sample 5D1F full conversion was not reached. Nevertheless, it was also observed that the conversion values remained constant for the last 30 min of the experiment. It can be concluded that no further dehydration was possible under the applied experimental conditions. Fig. 10 displays the conversion values obtained for all 6 cycles of the experiment series with the sample 5D1F. It can be seen that complete dehydration was never reached and the obtained values vary between 56% and 74%. The reached conversion

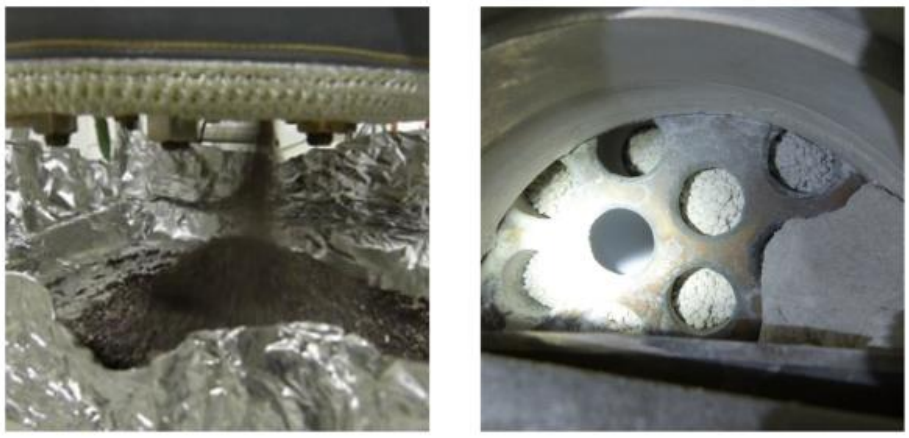

Fig. 8. Left: 5D1F granules flowing out of the reactor. Right: Al_2O_3 granules stuck in the tubes of the reactor.

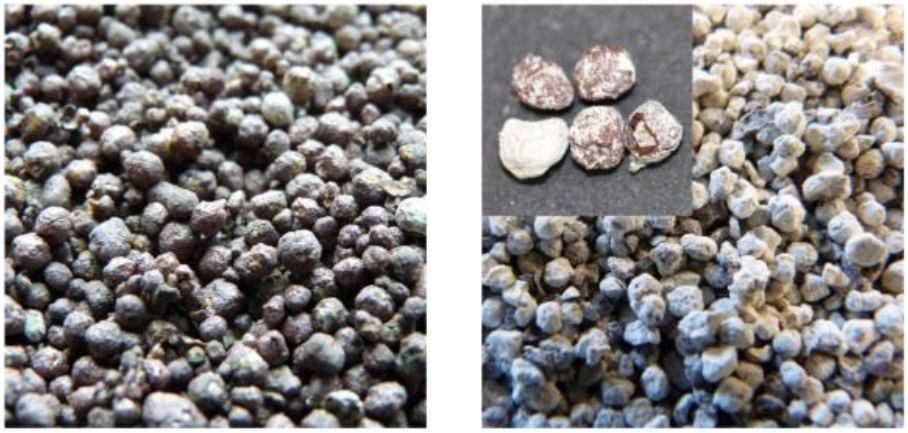

Fig. 9a. State of the sample 5D1F before (left) and after (right) the experiment series.

during hydration is slightly higher in most cases but in general in accordance to the conversion reached in the corresponding dehydration cycle. The higher conversion values measured during hydration can be explained by the experimental procedure carried out. Before every hydration experiment the reactor was preheated under continuous vacuuming for approximately one hour. During that time, the very low pressure and pre-heating temperatures of 550 °C allowed additional dehydration which was not measured. As a consequence, in the following experiment there is more mass of CaO available for hydration and thus the conversion values for hydration are slightly higher.

In general, the incomplete conversion of the sample 5D1F was unexpected because previous investigations in the TGA showed the possibility of complete conversion of the reactive core of the encapsulated granule. Additionally, the reference experiment proved that full conversion during dehydration is possible in the reactor under the applied operating conditions (compare Fig. 4). The reason for the incomplete dehydration will be further explained in Section 3.3.

In contrast, the dehydration procedure for the sample Al_2O_3 can be considered complete. Fig. 11 shows the reached values which are between 94% and 100%. The hydration values are in general in good accordance with the dehydration values of the corresponding cycle. Some variations in the total conversion can be observed for each cycle, which can be attributed to measurement deviations. It is of particular importance that no trend of degradation can be observed with increasing number of cycles. Hence, the shell layer does not influence the reactivity of the storage material over cycling. Furthermore, this observation also leads to the conclusion that there is no continuous increase of thermochemically inert side products formed between the core and the coating material during cycling.

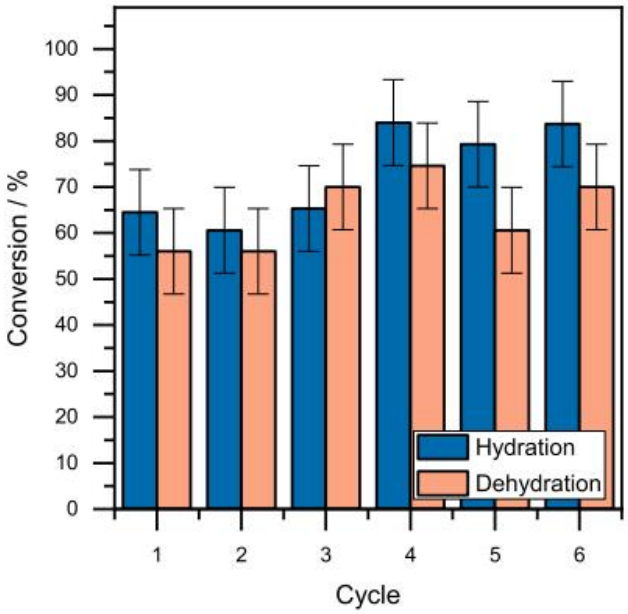

Fig. 10. Conversion results over the 6-cycle experiment series with the sample 5D1F.

The high level of uncertainty (9.3% for the sample 5D1F and 7.5% for the sample Al_2O_3) is the result of the resolution of the filling level sensor and the relatively small mass of the samples. Furthermore,

Fig. 9b. State of the sample Al_2O_3 before (left) and after (right) the experiment series.

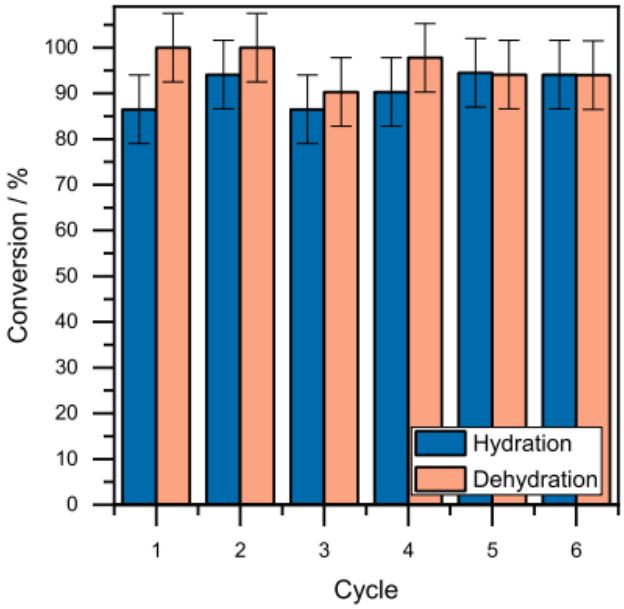

Fig. 11. Conversion results over the 6-cycle experiment series with the sample Al_2O_3.

determining accurate absolute conversion values was not the sole purpose of this study but also observing how the material reacts in larger scale and process boundary conditions. Therefore, the uncertainty can be regarded as acceptable. Detailed conversion measurement of both modified samples using TGA is currently under investigation.

3.2.5. Morphological investigation

In order to examine changes in structure and texture of the samples 5D1F and Al_2O_3, SEM-images were taken on the respective materials before and after sixfold cycling in the reactor. For the sample 5D1F it is observed that before cycling the ceramic shell thoroughly covers the surface of the storage material shell and is free from cracks or abrasions. At higher magnifications, the porosity of the ceramic surface becomes visible. The rather rough surface is entirely permeated by pores in the size range of about 5 µm to 20 µm (Fig. 12, top).

Furthermore, after thermochemical cycling, a majority of the particles is still covered by the ceramic shell. However, on a number of surfaces small cracks have formed. The majority of pores now appear to be enlarged in the size range between 40 µm and 60 µm (Fig. 12, bottom).

In case of the sample Al_2O_3, it is observable that the surface of the storage material granules is only partly covered by the nanostructured additive. The layer of the additive is of inhomogeneous thickness in a range between 30 µm and 80 µm. Before thermochemical cycling, the roughness and the loose cohesion of the additive layer on the surface of the $Ca(OH)_2$ granules is clearly observable (Fig. 13, top).

After sixfold cycling within the reactor the surface of the sample appears rather smooth, pointing to a densification of the additive on the surfaces under the experimental conditions during de- and rehydration. Although the additive is still not covering the granules surfaces homogeneously and some narrow cracks have formed, the particles are not fragmented. This observation indicates that also a thin layer of a suitable additive is capable of improving the overall particles cohesion despite the significant changes in molar volume during de- and rehydration (Fig. 13, bottom).

3.3. Discussion

The experiments with the reference material demonstrated the functionality of the reactor and served as a benchmark to compare the performance of the encapsulated materials. For the sample 5D1F, it was observed that the dehydration was incomplete under the applied operating conditions in the reactor. A reason for this might be that the ceramic shell causes a mass transport resistance. During the dehydration procedure, the reaction gas needs to flow out of the inner core through fine porous channels of the surrounding ceramic shell. If the system is operated at low vapour pressures, the pressure drop caused by the ceramic shell increases. As a consequence, the equilibrium temperature of the reaction increases and the temperature of the heat transfer fluid is not sufficient any more to drive the dehydration reaction.

In order to examine this hypothesis, an additional test was performed where the material was dehydrated for nine hours at 540 °C and under continuous operation of the vacuum pump. Thus, the dehydration time was extended and the water vapour pressure was reduced. Both measures would in principle lead to an increased conversion. In the next step, hydration was performed under the same conditions as before (350 °C and 100 kPa H_2O pressure). The results show that full conversion was reached after 80 min and the conversion and temperature trends obtained resulted very similar to the one of the reference material. Therefore, the reactive core of the sample 5D1F could completely dehydrate. However, the experiments conducted in this work revealed that the sample 5D1F has a reduced performance during dehydration compared to the sample Al_2O_3 and the reference material under the same operating conditions. From an application perspective this is disadvantageous since higher dehydration temperatures or longer charging procedures are required.

Regarding the flowability, the sample 5D1F showed good performance since the granules flowed out freely. It is clear that the ceramic shells of these granules are thick and thus provide certain mechanical stability. Furthermore, the outer diameter of the granules does not change during the hydration reaction which helps to maintain the flowability even after several cycles. However, an additional drawback of the sample 5D1F is that the manufacturing process is rather complex and demands several steps [26].

In contrast, the sample Al_2O_3 showed a reaction performance comparable to the reference $Ca(OH)_2$ for both dehydration and hydration. The experiments therefore proved that the coating with the very thin shell has no negative impact on the mass transport to and from the reactive core. The rate of reaction, the heat release and the degree of conversion are similar to the reference material (compare Fig. 7). Furthermore, the experiments revealed that the coating and the shape of the granules remain stable under reaction conditions in a laboratory reactor. The energy density (284 kWh/m^3) is only slightly lower, compared to the reference unmodified granules (315.4 kWh/m^3) since only 10 wt% is unreactive nanostructured particles. However, it is higher than the bulk $Ca(OH)_2$ material (184,2 kWh/m^3) [27]. In conclusion, the higher volumetric energy density leads to smaller required storage volumes. The granules can facilitate the reactor design and thus decrease investment costs. On the other hand, the costs for the storage material are clearly higher than for unmodified $Ca(OH)_2$. Therefore, a techno-economic evaluation must be conducted to determine whether the costs of modifying the storage material compensate the higher costs of the reactor.

As for the reached thermal power (0.444 kW), the value is below the nominal thermal power (1 kW) and responds to the limitations of the heat exchanger. However, in this work, the design of the heat exchanger primarily intends to enable the flow of the encapsulated granules. The improvement of the reactor's power density will be subject of further developments.

Additionally advantageous of this material is that the manufacturing process is very simple since only basic granules, nanostructured particles and binder need to be mixed. However, one drawback of the material is that granules swell and then stick together forming larger agglomerates which lead to clogged tubes in the

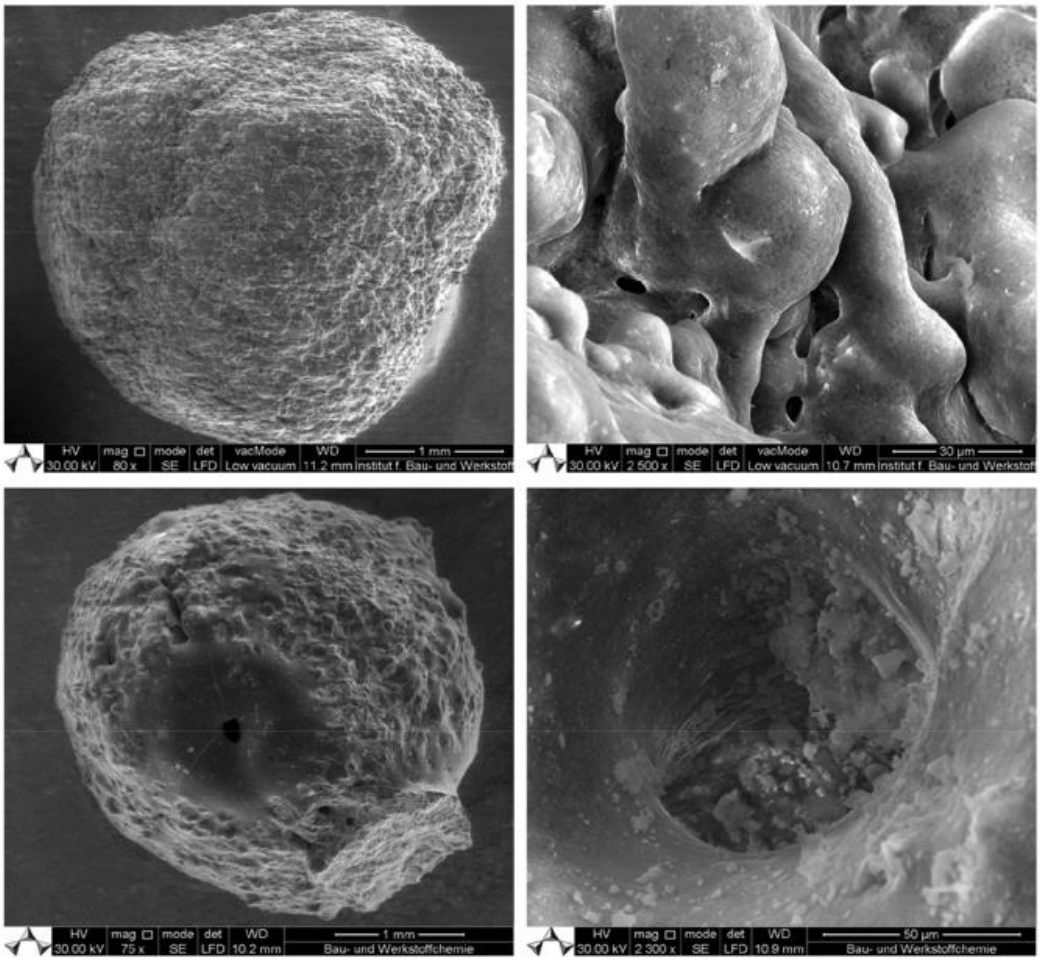

Fig. 12. Scanning electron micrographs of a granule of sample 5D1F before thermochemical cycling at 80-fold (top, left) and 2500-fold magnification (top, right) and after sixfold cycling in the reactor at 75-fold magnification (bottom, left) and 2300-fold magnification (bottom, right).

presented set up.

By scanning electron microscopy performed on the modified samples before and after cycling, it could be shown that it is possible to stabilise the storage material core persistently in size and shape. However, in the case of the ceramic encapsulated material it was found that the texture of pores changes significantly. Whereas the surface of the particles of the sample 5D1F is permeated by a rather large number of smaller pores before cycling, the pores appeared larger in size but fewer in number after cycling. This finding may also give an explanation for the reduced performance during thermochemical cycling. The coating of the sample Al_2O_3 was covering the surface only inhomogenously, before and after cycling. Although a densification of the coating layer after cycling was found, still a comparatively larger surface of the storage material remained uncovered and therefore enabled a good reaction performance of the material. Thereby, the granules mostly retained their initial shape.

4. Conclusions and outlook

The experimental results of encapsulated $CaO/Ca(OH)_2$ granules, which were cycled in an indirectly heated moving bed reactor, are presented in this work. The two modified material samples were ceramic encapsulated CaO granules (sample 5D1F) and $Ca(OH)_2$ granules coated with Al_2O_3 nanostructured particles (sample Al_2O_3). Six cycles (hydration and dehydration) were carried out to analyse the reaction performance, structural integrity, conversion and ability to flow of the two materials.

Based on the performed experiments, a novel developed moving bed reactor concept was demonstrated for the first time. For both modified storage materials the charging and discharging reaction was successfully carried out. The granules encapsulated with the ceramic shell (sample 5D1F) flowed freely out of the heat exchanger tubes even after several charging and discharging cycles. The shape of the granules was maintained while for some granules the ceramic shell was partially cracked or lost. Even though the ceramic shell material showed good flowability after cycling, a reduced reaction performance and incomplete conversion under the operating conditions in the reactor was determined. The effect can be attributed to a mass transport resistance caused by the ceramic shell at low pressure operation and is currently under further investigation. Additional drawbacks of the ceramic shell material are the complex manufacturing process as well as a significantly reduced energy density due to the relatively thick unreactive shell.

In comparison, the sample Al_2O_3 showed a reaction performance and energy density comparable to basic unmodified $Ca(OH)_2$ granules. In contrast to unmodified $Ca(OH)_2$ granules, which in general fell apart into smaller particles after only one thermochemical cycle, the granules of the sample Al_2O_3 maintained their spherical shape after several cycles. This study therefore proves that the very thin coating layer is preserved under operation in a moving bed reactor and positively affects the stability of the granules, while it only has a negligible effect on the reaction performance. In addition, the manufacturing process of the material is easy and inexpensive. Nevertheless, the volume of the granules also expanded during the hydration procedure causing

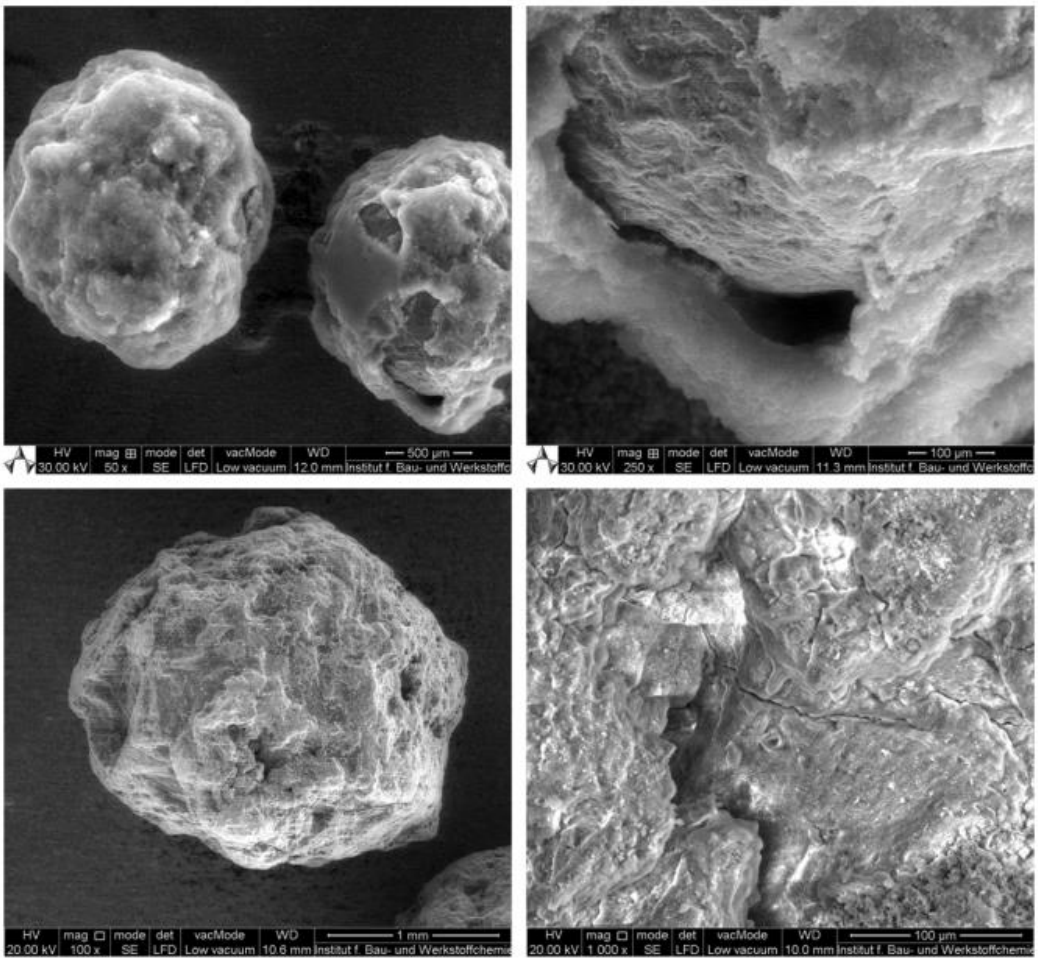

Fig. 13. Scanning electron micrographs of two granules of sample Al_2O_3 before thermochemical cycling at 50-fold (top, left) and 250-fold magnification (top, right) and of a granule after sixfold thermochemical cycling in the reactor at 100-fold (bottom, left) and 1000-fold magnification (bottom, right).

clogging in the heat exchanger tubes in the presented reactor. Thus, a free flow of the granules through the reactor after hydration was not achieved yet. Currently, detailed characterisation of the modified granules is ongoing. The outcome will serve as input for the manufacture of new modifications based on Al_2O_3 nanostructured particles that aim to limit the volume change during the cycles. One approach could be to produce coated granules with a much smaller diameter. Furthermore, the results will also be used to design a new customised reactor, which compensates the volume expansion of the granules and thus enables their flow.

Declaration of Competing Interest

The authors declare that they have no known competing financial interests or personal relationships that could have appeared to influence the work reported in this paper.

Acknowledgement

This work has been partially funded by the German Federal Ministry for Economic Affairs and Energy (BMWi) in the frame of the BERTI project (03ESP112A).

Appendix A. Supplementary material

Supplementary data to this article can be found online at https://doi.org/10.1016/j.applthermaleng.2020.114961.

References

[1] B. Steffen, C. Weber, Efficient storage capacity in power systems with thermal and renewable generation, Energy Econ. 36 (2013) 556–567, https://doi.org/10.1016/j.eneco.2012.11.007.
[2] L. Hirth, I. Ziegenhagen, Balancing power and variable renewables: three links, Renew. Sustain. Energy Rev. 50 (2015) 1035–1051, https://doi.org/10.1016/j.rser.2015.04.180.
[3] H. Zhang, J. Baeyens, G. Cáceres, J. Degrève, Y. Lv, Thermal energy storage: recent developments and practical aspects, Prog. Energy Combust. Sci. 53 (2016) 1–40, https://doi.org/10.1016/j.pecs.2015.10.003.
[4] P. Pardo, A. Deydier, Z. Anxionnaz-Minvielle, S. Rougé, M. Cabassud, P. Cognet, A review on high temperature thermochemical heat energy storage, Renew. Sustain. Energy Rev. 32 (2014) 591–610, https://doi.org/10.1016/j.rser.2013.12.014.
[5] M. Schmidt, M. Linder, Power generation based on the $Ca(OH)_2$/CaO thermochemical storage system – Experimental investigation of discharge operation modes in lab scale and corresponding conceptual process design, Appl. Energy 203 (2017) 594–607, https://doi.org/10.1016/j.apenergy.2017.06.063.
[6] U. Pelay, L. Luo, Y. Fan, D. Stitou, C. Castelain, Integration of a thermochemical energy storage system in a Rankine cycle driven by concentrating solar power: Energy and exergy analyses, Energy 167 (2019) 498–510, https://doi.org/10.1016/j.energy.2018.10.163.
[7] S.E.B. Edwards, V. Materic, Calcium looping in solar power generation plants, Sol. Energy 86 (2012) 2494–2503, https://doi.org/10.1016/j.solener.2012.05.019.
[8] A. Alovisio, R. Chacartegui, C. Ortiz, J.M. Valverde, V. Verda, Optimizing the CSP-calcium looping integration for thermochemical energy storage, Energy Convers. Manage. 136 (2017) 85–98, https://doi.org/10.1016/j.enconman.2016.12.093.
[9] R. Chacartegui, A. Alovisio, C. Ortiz, J.M. Valverde, V. Verda, J.A. Becerra, Thermochemical energy storage of concentrated solar power by integration of the calcium looping process and a CO_2 power cycle, Appl. Energy 173 (2016) 589–605, https://doi.org/10.1016/j.apenergy.2016.04.053.
[10] A. Bayon, R. Bader, M. Jafarian, L. Fedunik-Hofman, Y. Sun, J. Hinkley, et al., Techno-economic assessment of solid–gas thermochemical energy storage systems for solar thermal power applications, Energy 149 (2018) 473–484, https://doi.org/

10.1016/j.energy.2017.11.084.
[11] A. Shkatulov, Y. Aristov, Modification of magnesium and calcium hydroxides with salts: an efficient way to advanced materials for storage of middle-temperature heat, Energy 85 (2015) 667–676, https://doi.org/10.1016/j.energy.2015.04.004.
[12] M. Schmidt, A. Gutierrez, M. Linder, Thermochemical energy storage with CaO/Ca$(OH)_2$ – experimental investigation of the thermal capability at low vapor pressures in a lab scale reactor, Appl. Energy 188 (2017) 672–681, https://doi.org/10.1016/j.apenergy.2016.11.023.
[13] F. Schaube, A. Kohzer, J. Schütz, A. Wörner, H. Müller-Steinhagen, De- and rehydration of Ca(OH)2 in a reactor with direct heat transfer for thermo-chemical heat storage Part A: Experimental results, Chem. Eng. Res. Des. 91 (2013) 856–864, https://doi.org/10.1016/j.cherd.2012.09.020.
[14] Y.A. Criado, M. Alonso, J.C. Abanades, Kinetics of the CaO/Ca$(OH)_2$ hydration/dehydration reaction for thermochemical energy storage applications, Industr. Eng. Chem. Res. 53 (2014) 12594–12601, https://doi.org/10.1021/ie404246p.
[15] H.F. Schaube, L. Koch, A. Wörner, Müller-Steinhagen, A thermodynamic and kinetic study of the de- and rehydration of Ca(OH)2 at high H2O partial pressures for thermo-chemical heat storage, Thermochim. Acta 538 (2012) 9–20, https://doi.org/10.1016/j.tca.2012.03.003.
[16] J.K. Rosemary, G.L. Bauerle, T.H. Springer, Solar energy storage using reversible hydration-dehydration of CaO-Ca$(OH)_2$, J. Energy 3 (1979) 321–322, https://doi.org/10.2514/3.62440.
[17] Y.A. Criado, M. Alonso, J.C. Abanades, Enhancement of a CaO/Ca$(OH)_2$ based material for thermochemical energy storage, Sol. Energy 135 (2016) 800–809, https://doi.org/10.1016/j.solener.2016.06.056.
[18] Matthias A. Schmidt, Christian Szczukowski, Christian Roßkopf, Marc Linder, Wörner, Experimental results of a 10 kW high temperature thermochemical storage reactor based on calcium hydroxide, Appl. Therm. Eng. 62 (2014) 553–559, https://doi.org/10.1016/j.applthermaleng.2013.09.020.
[19] J. Yan, C.Y. Zhao, Experimental study of CaO/Ca$(OH)_2$ in a fixed-bed reactor for thermochemical heat storage, Appl. Energy 175 (2016) 277–284, https://doi.org/10.1016/j.apenergy.2016.05.038.
[20] M. Angerer, M. Becker, S. Härzschel, K. Kröper, S. Gleis, A. Vandersickel, et al., Design of a MW-scale thermo-chemical energy storage reactor, Energy Rep. 4 (2018) 507–519, https://doi.org/10.1016/j.egyr.2018.07.005.
[21] P. Pardo, Z. Anxionnaz-Minvielle, S. Rougé, P. Cognet, M. Cabassud, Ca$(OH)_2$/CaO reversible reaction in a fluidized bed reactor for thermochemical heat storage, Sol. Energy 107 (2014) 605–616, https://doi.org/10.1016/j.solener.2014.06.010.
[22] Y.A. Criado, A. Huille, S. Rougé, J.C. Abanades, Experimental investigation and model validation of a CaO/Ca$(OH)_2$ fluidized bed reactor for thermochemical energy storage applications, Chem. Eng. J. 313 (2017) 1194–1205, https://doi.org/10.1016/j.cej.2016.11.010.
[23] S. Rougé, Y.A. Criado, O. Soriano, J.C. Abanades, Continuous CaO/Ca$(OH)_2$ fluidized bed reactor for energy storage: first experimental results and reactor model validation, Ind. Eng. Chem. Res. 56 (2017) 844–852, https://doi.org/10.1021/acs.iecr.6b04105.
[24] C. Roßkopf, M. Haas, A. Faik, M. Linder, A. Wörner, Improving powder bed properties for thermochemical storage by adding nanoparticles, Energy Convers. Manage. 86 (2014) 93–98, https://doi.org/10.1016/j.enconman.2014.05.017.
[25] M. Schmidt, M. Gollsch, F. Giger, M. Grün, M. Linder, Development of a moving bed pilot plant for thermochemical energy storage with CaO/Ca(OH)2, 2016, doi:10.1063/1.4949139.
[26] S. Afflerbach, M. Kappes, A. Gipperich, R. Trettin, W. Krumm, Semipermeable encapsulation of calcium hydroxide for thermochemical heat storage solutions, Sol. Energy 148 (2017) 1–11, https://doi.org/10.1016/j.solener.2017.03.074.
[27] C. Roßkopf, S. Afflerbach, M. Schmidt, B. Görtz, T. Kowald, M. Linder, et al., Investigations of nano coated calcium hydroxide cycled in a thermochemical heat storage, Energy Convers. Manage. 97 (2015) 94–102, https://doi.org/10.1016/j.enconman.2015.03.034.
[28] I. Fujii, M. Ishino, S. Akiyama, M.S. Murthy, K.S. Rajanandam, Behavior of Ca$(OH)_2$/CaO pellet under dehydration and hydration, Sol. Energy 53 (1994) 329–341, https://doi.org/10.1016/0038-092x(94)90036-1.
[29] K.G. Sakellariou, Y.A. Criado, N.I. Tsongidis, G. Karagiannakis, A.G. Konstandopoulos, Multi-cyclic evaluation of composite CaO-based structured bodies for thermochemical heat storage via the CaO/Ca$(OH)_2$ reaction scheme, Sol. Energy 146 (2017) 65–78, https://doi.org/10.1016/j.solener.2017.02.013.

Paper III: Development of a lab-scale reactor

processes

MDPI

Article

Development of a Moving Bed Reactor for Thermochemical Heat Storage Based on Granulated $Ca(OH)_2$

Aldo Cosquillo Mejia [1,*], Sandra Afflerbach [2], Marc Linder [3] and Matthias Schmidt [1]

[1] German Aerospace Center—DLR e.V., Institute of Engineering Thermodynamics, Linder Höhe, 51147 Cologne, Germany
[2] Chair for Environmental and Process Engineering, University of Siegen, Paul-Bonatz-Str. 9–11, 57076 Siegen, Germany
[3] German Aerospace Center—DLR e.V., Institute of Engineering Thermodynamics, Pfaffenwaldring 38–40, 70569 Stuttgart, Germany
* Correspondence: aldo.cosquillo@dlr.de

Abstract: Calcium hydroxide is promising for thermal energy storage due to its low cost and high energy density. Nevertheless, the powdered material is cohesive and has low thermal conductivity which is a major challenge for the operation of moving bed reactors. One approach to facilitate the movement of the reaction bed is the stabilisation of the particles through the coating of $Ca(OH)_2$ granules with Al_2O_3 particles. In this work, a newly designed reactor concept was specifically developed for testing coated $Ca(OH)_2$ granules. The design allows for the movement of the reaction bed by gravity assistance and direct heating of the particles by a counter current gas flow. The operation was successfully demonstrated and proved to achieve high heat transfer between gas and granules. Furthermore, the movement of the reaction bed was achieved after the discharging phase. Two batches of uncoated and coated $Ca(OH)_2$ granules were subject of 10 thermochemical cycles in this reactor. The cycling stability, structural integrity, mechanical stability, morphology and phase composition of the granules were analysed. Full conversion of both samples was demonstrated for the entire experimental series. It was found that the alumina coating enhances the mechanical stability of the granules under reaction conditions.

Keywords: reactive moving bed; calcium hydroxide; nanocoated particle stabilization; thermochemical storage

Citation: Cosquillo Mejia, A.; Afflerbach, S.; Linder, M.; Schmidt, M. Development of a Moving Bed Reactor for Thermochemical Heat Storage Based on Granulated $Ca(OH)_2$. *Processes* **2022**, *10*, 1680. https://doi.org/10.3390/pr10091680

Academic Editor: Andrea Petrella

Received: 19 July 2022
Accepted: 19 August 2022
Published: 24 August 2022

1. Introduction

A major challenge for the transition to a zero-emission energy system is the intermittent availability of the renewable energy sources [1] (e.g., solar and wind power). In order to match the supply and demand, energy storage solutions can be implemented [2]. The thermochemical storage system based on the gas-solid reaction: $CaO + H_2O \rightleftharpoons Ca(OH)_2 + 104$ kJ/mol is considered promising due to the number of advantages it features such as high energy density, non-toxicity, multiple cyclability [3], general availability and low cost [4]. The applications of this storage system have been analysed for concentrated solar power (CSP) plants, conventional power plants and waste heat recovery [5,6]. It is also free of heat losses during the time of storage and therefore suitable for seasonal long-term storage. For all these reasons, multiple studies have been carried out to characterise the reaction, determine the thermodynamic equilibrium and reaction enthalpy [6–8].

This storage system has been tested in different reactors concepts. For example, fixed bed reactors were demonstrated in several investigations [5,9–14] and served successfully for the thermodynamic characterisation of the reaction process in technical scale. However, as in this concept the storage material is attached to the reactor, large heat exchange surfaces are necessary for large storage capacities in industrial-scale applications which increases the cost of the storage. One challenge currently addressed is therefore the development of a suitable concept that separates the storage material from the heat exchanger. The

investigated approaches to achieve this are fluidised bed and moving bed reactor concepts. However, the raw powder material possesses disadvantageous inherent properties such as cohesiveness, low thermal conductivity and a tendency to agglomerate. For this reason, the realisation of a moving bed based on raw powder material that is solely assisted by gravity seems difficult. One approach to improve the bulk properties was the addition of SiO_2 nano particles to coat the surface of the particles of the storage material [10,15,16]. The flowability of the material was improved and the free flow in a moving bed reactor could be demonstrated. However, the enhanced flowability effect was lost after some thermochemical cycling of the material [17].

A different approach is to stabilise larger particles of the storage material to enable the operation of fluidised bed reactors. First investigations were successfully carried out with this concept [16,18,19] but the stability of the granules is not yet reported for a larger number of cycles. Thermal and mechanical stress on the particles is very high in a fluidised bed. Thus, it remains challenging for larger particles to retain the stability during cycling. Therefore, other works on the material development concentrate on the stabilisation of the storage material particles and flowability of the bulk. For instance, pellets of storage material doped with Zn, Cu and Al salts showed enhanced structural stability. However, this effect lasted only up to 2 thermochemical cycles [20,21]. Criado et al. tested sodium silicate as a binder for CaO. Although the mechanical strength of the composites was enhanced, it required a specific step to synthesise the binding framework and the incomplete hydration of the storage material [22]. Sakellariou et al. [23] also obtained improved mechanical stability by manufacturing CaO-based composites using kaolinite as binder. However, the hydration capacity of the CaO in the mix resulted reduced (40–50% of the theoretical value). An encapsulation approach using oxide ceramic material was tested by Afflerbach et al. [24]. After a 10-cycle experimental series in a thermal analyser, it was found that the stability of the samples was retained. The capsules were tested in a lab-scale reactor [25,26] and the flowability of the bulk was reported even after 6 reaction cycles [27]. The drawback of the this modification is the significantly reduced energy density (200 kWh/m^3) compared to pure $Ca(OH)_2$ granules (340 kWh/m^3).

Recently, another approach of coating $Ca(OH)_2$ granules with a small amount of nano additives have been proposed and tested in TG (thermogravimetric) devices [28,29]. A previous work from our research group conducted a 6-fold thermochemical cycling using $Ca(OH)_2$ granules coated with alumina in a moving bed reactor [27]. The results showed that the coating layer has a positive effect on the structural integrity of the granules without compromising their performance and with minimal impact on the energy density. Furthermore, the manufacturing process is simpler when compared to the encapsulation method. Despite these promising outcomes on the material development side, the movement of the bulk through the heat exchanger of the reactor could not be achieved due to the specific reactor design.

To summarise, the stabilisation of $Ca(OH)_2$ granules in a range of 0.5 to 3 mm, would in general facilitate the reactor design and allow for novel concepts and heat exchange mechanisms. Recent investigations with nanocoated granules showed evidence that the coating enhances the stability of the granules and at least prolongs their stability over several reaction cycles. The granules could also facilitate the operation of a fluidised bed reactor but the mechanical stress over the material in this concept is extremely high and thus favours its fast decomposition into powder.

This paper therefore addresses the question of the development of a reactor concept suitable for the operation with $Ca(OH)_2$ granules taking into account conflicting design criteria. On the one hand, the mechanical stress on the granules should be minimised. On the other hand, the heat transfer into the granules should be maximised in order to allow a scalable concept with a competitive power density. The design additionally aims to compensate the growth and shrinkage of the granules and therefore enables the gravity assisted free flow of the material bulk under reaction conditions.

The aim of this work is therefore to demonstrate the operation of a newly-developed moving bed reactor designed for granulated $Ca(OH)_2$. Two batches of $Ca(OH)_2$ granules were manufactured in kg-scale and cycled in the reactor. A number of dehydration and hydration experiments were carried out to prove the functionality of the setup in terms of thermal power output, energy released and thermal efficiency. The heat and mass transfer of the reactor is characterised for the thermal charging and discharging procedure. The ability of the granules to flow out of the reactor by gravity assistance is tested at the end of the experimental series. For the storage granules, the cycling stability, structural integrity and mechanical stability are analysed as well as the phase composition and morphology. This study presents the first operational data of nanocoated $Ca(OH)_2$-based granules in a directly heated moving bed reactor at kW scale. The conclusions derived from this work will contribute to the development of the storage material based on $Ca(OH)_2$ and to the achievement of a cost-efficient reactor for this storage system.

2. Materials and Methods

2.1. Reactor Development

In addition to the basic functions to supply and remove heat and reaction gas during dehydration and rehydration of the $Ca(OH)_2/CaO$, the reactor design needs to take into account specific techno-economic requirements. First, the reactor must allow for the continuous movement of the granules through the reaction zone whilst low mechanical stress on the material is guaranteed. Second, the natural volume expansion during the discharge process must be compensated to prevent the material from becoming stuck in the reactor. Third, high heat transfer is sought in order to reach high power density. In addition, a non-complex design has to be conceived to reach a cost-efficient reactor which could be upscaled to MW-range for industrial applications.

For the reactor development, 3 concepts were originally taken into consideration: moving bed, fluidised bed and rotary kilns. The investigations of $Ca(OH)_2$ as storage material in indirectly heated moving bed reactors showed two main disadvantages for this concept. First, the powder or granulated $Ca(OH)_2$ has low thermal conductivity which in turn leads to complex and expensive heat exchanger designs. Second, the material swells during hydration and therefore becomes stuck in the heat exchangers [17,27]. Fluidised beds display the high heat transfer coefficients, but the fluidisation also causes high mechanical stress on granules. Mechanically fluidised beds and rotary kilns also achieve high heat transfer coefficients [30,31]. Nevertheless, the mechanical assistance (e.g., rotating paddles) that enhances the heat and mass transfer within the bulk also contributes to the deterioration of the integrity of the granules. Moreover, the construction is complex since the rotating parts have to withstand relatively high temperatures.

Given the criteria to meet for the novel reactor design, a hybrid concept was chosen. The design incorporates the direct heating through a gas stream but at velocities that do not lead to the fluidisation of the bed. The direct contact between gas and solid still enables high heat transfer whilst the granules are not subject of severe attrition. In addition, since the reactor does not require a heat exchange structure, a wider radial pack is foreseen to prevent the bed from becoming stuck and therefore favour its movement.

Reactor Design

Considering the above-mentioned criteria, a reactor based on a standard steel pipe filled with the granules is designed (Figure 1). A countercurrent flow was chosen where the unreacted material enters from the top of the reactor. The hot air and water vapour enter from the bottom of the reactor and stream through the bulk of granules to the top. The main design parameter is the diameter of the pipe. On the one hand, a large diameter is required to keep the gas stream below the fluidisation velocity. On the other hand, the gas volume flow needs to be large in order to deliver enough thermal power to drive the reaction. In addition, the gas velocity should not be too low in order to ensure a sufficiently high heat transfer coefficient from gas to particle. The selected design therefore seeks to

balance these conflicting parameters by finding an operation window that allows high heat transfer coefficient at a gas velocity still below values that fluidise the reaction bed.

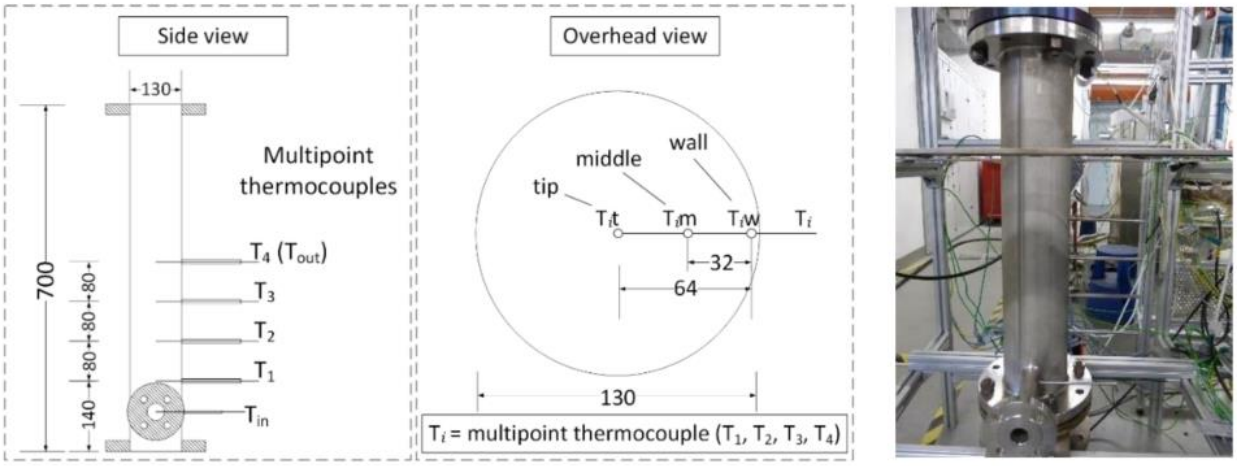

Figure 1. Left and **middle**: Side and overhead view of the reactor design, including the dimensions and the position of the multipoint thermocouples. **Right**: image of the actual reactor without insulation and connections.

The first criterion for the design is the temperature difference between the gas and the reaction equilibrium, which is assumed to range from 50 to 200 K. Based on this, for a nominal power of 1.2 kW (for 200 K temperature difference) a volume flow of 16 Nm^3/h is required. Hence, the operational power varies from 0.3 to 1.2 kW for temperature differences between 50 and 200 K, respectively. Based on a chosen nominal flow and a given particle diameter, the minimal fluidisation velocity (U_{mf}) can be calculated at the maximum inlet temperature of 550 °C and pressure of 1 bar (see Section 2.5, Equations (1)–(3)). This velocity corresponds to the maximum velocity of the reactor design and must not be exceeded.

In our case the diameter of the reactor was chosen to 0.130 m and consequently a volume flow of 45 Nm^3/h corresponds to a gas velocity in the reactor of 0.94 m/s, which is slightly below the minimal fluidisation velocity of 1 m/s. Hence, the maximum thermal power at which the reactor can be operated using this gas velocity and a 50 to 200 K temperature difference varies from 0.9 to 3.5 kW accordingly. In addition, the gas velocity affects the heat transfer coefficient (α) between gas and particles. The calculated values of α result in 140 and 248 W/m^2 K for volume flows of 16 (nominal) and 45 (maximum) Nm^3/h, respectively (see Section 2.6, Equations (4)–(12)).

The second criterion used is the size of the reaction bed. In the reactor pipe, a 0.24-m-high bed accounts for a 3-L volume of storage material which corresponds to 2.160 kg and an amount of energy of 0.78 kWh. Furthermore, the bed size determines the surface area of the granules available for the heat exchange with the gas. Bearing in mind that the granules have a small diameter of 2 mm, the surface area available for heat transfer amounts to 4.8 m^2. This area and the heat transfer coefficient at nominal conditions result in a specific power of 0.67 kW/K and a specific power density of 224 W/K L when the 3-litre storage material is considered. By comparing the specific power of the reactor to the nominal thermal power of the gas flow (0.3–1.2 kW), it is expected that the reactor can be operated with a small temperature difference between the reaction bed and the gas. Hence, the energy of the gas flow will be rapidly absorbed by the particles, the reaction zone will be small and progressively move upwards through the bed of granules. The reaction is therefore expected to be controlled by the gas volume flow and the inlet temperature of the gas. Finally, a homogeneous outlet temperature of the gas close to the equilibrium temperature of the reaction is foreseen to be reached. The design parameters are summarised in Table 1.

Table 1. Dimensions and technical features of the reactor.

Pipe diameter	0.13 m
Pipe length	0.70 m
Height of reaction bed	0.24 m
Volume of reaction bed	3 L
Mass of samples in reaction bed	2.160 kg
Surface area of granules	4.8 m^2
Nominal gas volume flow	16 Nm^3/h
Gas velocity at 550 °C inlet temperature and 1 bar	0.33 m/s
Fluidisation velocity at nominal operating parameters	1 m/s
Heat transfer coefficient at nominal conditions	140 W/ m^2 K
Thermal power at nominal gas flow	0.3–1.2 kW at 50–200 K difference
Thermal power at maximum gas flow	0.9–3.5 kW at 50–200 K difference
Construction material	Stainless steel 1.4571

2.2. Test Bench

The test bench consists of three main units: the reactor unit, the heat transfer fluid (HTF) supply unit and the reaction gas supply unit (Figure 2).

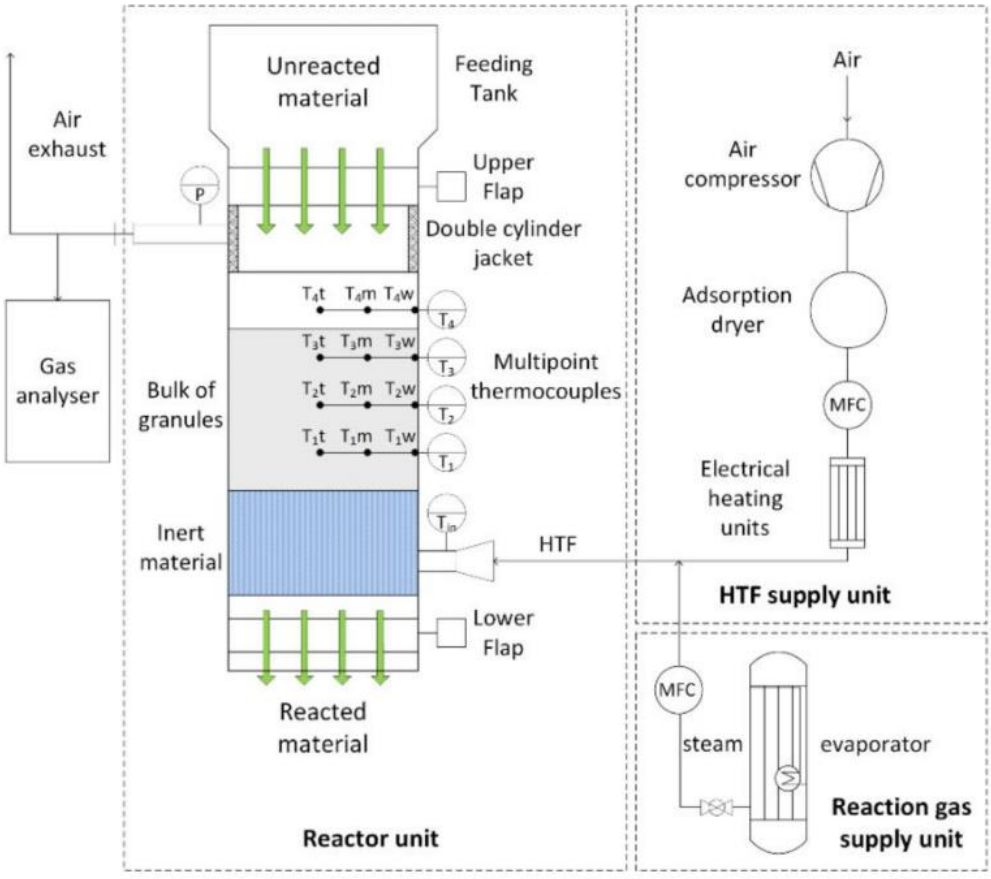

Figure 2. The schematic design of the test bench.

A feeding tank (20 L) is located at the top of the reactor unit and under it a controlled flap can adjust the mass flow of the granules into the reactor. A double cylinder jacket connects the upper flap and the reactor. The inner cylinder has a fine steel mesh wall (2 µm diameter) that allows the air and steam to leave the reactor and separates the gas from the solid material. The lower section of the reactor (100 mm high) is filled with 10-mm glass beads and then the samples are filled to make a 240-mm-high reaction bed (approximately

3 L). At the end of a reaction cycle the lower flap is opened and the material can flow out of the reactor.

Ambient air is used as heat transfer fluid (HTF) to supply heat to the reaction bed. The air is first compressed and then moisture and CO_2 are removed in an adsorption dryer. Once the air is dry and CO_2-free, the volumetric flow is set before the fluid is heated up in the electrical heaters. The heated air is then directed to the reactor. In the reaction gas supply unit, an evaporator is used to produce the steam that is later supplied to the reactor by means of a mass flow controller (MFC). A gas analyser is connected to the outlet pipe to monitor the content of water vapour present at the outlet of the reactor.

Four multipoint thermocouples (T_1, T_2, T_3 and T_4) are attached to the reactor at 4 different heights and one single thermocouple is attached at the inlet (T_{in}). Thus, the temperature at 13 different positions can be monitored (see Figure 1, left). Thus, the temperature distribution (axial and radial) throughout the reaction bed and the gas temperature right above it can be monitored.

2.3. Materials

2.3.1. Uncoated Granules

As reference material, commercially available granulated $Ca(OH)_2$ (Sorbacal® H90) was supplied by Rheinkalk GmbH. The product contains 92.9 wt.% Ca(OH)2 and granules with diameter between 1.6 and 2 mm were used in the experiments (Bulk density: 721 kg/m^3).

2.3.2. Coated Granules

Granulated $Ca(OH)_2$ (Sorbacal H90) was put into a mixer (Eirich, type R02/E) where water as adhesion promoting agent was added under co-current flow. Subsequently, nanostructured Al_2O_3 (AluC©, Evonik) was added to the granules up to the point that all surfaces were thoroughly covered, and no fines of the additives aggregated separately within the mixing container. In case of this sample, no further processing of the material was performed. The content of Al_2O_3 accounts for 10 wt.%. Coated granules with diameter between 1.6 and 2 mm were used in the experiments (Bulk density: 822 kg/m^3).

2.4. Experimental Procedure

In two measurement series, batches of 3 L of uncoated and coated granules are filled in the reactor. 10 cycles of dehydration and hydration are carried out with each batch which remained in the reactor for the whole series. Only after the last cycle the lower flap is opened to test the flowability of the storage material. The experimental parameters are given in Table 2.

Table 2. Parameters of temperature, volume and mass flow used in the experimental series.

Setting	$T_{HTF,\,start}$ /°C	$\dot{V}$/ $\frac{Nm3}{h}$	$T_{HTF,\ set}$/°C	$\dot{m}_{H_2O}$ /$\frac{kg}{h}$
Dehydration				
A	400	45	550	0
B	450	45	550	0
C	350	45	550	0
Hydration				
D	550	32	400	4
E	550	16	350	4

2.4.1. Dehydration

First, the upper flap is opened and the samples ($Ca(OH)_2$) contained in the feeding tank fill the reactor up until the level right above of the thermocouple T_3 (see Figure 2). In order to preheat the storage material in the reactor, the air volume flow is supplied and the preheating temperature (compare $T_{HTF,\,start}$ in Table 2) is set. Once the temperature is stable,

it is increased to the dehydration set temperature ($T_{HTF,\,set}$ in Table 2). The dehydration starts when the storage material temperature exceeds the equilibrium temperature, and an increase of water vapour is detected by the sensor located at the outlet pipe of the reactor. The dehydration is complete when the content of water vapour measured in the gas analyser decreases again and stays constant.

2.4.2. Hydration

The dehydrated samples (CaO) contained in the reactor are preheated with air volume flow at a starting temperature. In the reaction gas unit, water vapour is prepared in the evaporator and the MFC is set. The valve that connects the evaporator and MFC is opened and the water vapour mixes with the air volume flow before they stream into the reactor. At the same time, the temperature of the air flow is decreased to below the equilibrium temperature to start the hydration of the samples. Since the CaO present in the samples reacts with the water vapour supplied, the content of water vapour at the outlet sensor of the reactor decreases. When the value of the water content increases again and stabilises, the hydration is complete.

2.5. Determination of the Minimal Fluidisation Velocity

The minimal fluidisation velocity (U_{mf}) is calculated by the following expression [32]:

$$U_{mf} = \frac{Re_{mf}\mu}{\rho d_p} \tag{1}$$

where μ is the dynamic viscosity of the gas, ρ is the density of the gas and d_p the diameter of the particle. The term Re_{mf} refers to the Reynolds minimal fluidisation and is calculated as follows:

$$Re_{mf} = \left(33.3^2 + 0.33Ar\right)^{0.5} - 33.3 \tag{2}$$

where Ar corresponds to the Archimedes number and can be determined by the following expression:

$$Ar = \frac{g\rho\left(\rho_p - \rho\right){d_p}^3}{\mu^2} \tag{3}$$

ρ_p refers to the density of the particle, which accounts for 2313 kg/m^3 [24] and g to the gravitational acceleration: 9.81 m/s^2.

2.6. Determination of the Heat Transfer Coefficient

The heat transfer coefficient (α) can be represented by Equation (4) [33]:

$$\alpha = \frac{Nu\lambda}{d_p} \tag{4}$$

where λ is the thermal conductivity of the gas and Nu corresponds to the Nusselt number, which can be determined based on the factor f_a and the Nusselt number for sphere (Nu_{sphere}), in laminar (Nu_{lam}) and in turbulent flow (Nu_{turb}) (Equations (5)–(8)).

$$Nu = f_a\, Nu_{sphere} \tag{5}$$

$$Nu_{sphere} = 2 + \sqrt{Nu_{lam}^2 + Nu_{turb}^2} \tag{6}$$

$$Nu_{lam} = 0.664\,\sqrt{Re_\psi}\,\sqrt[3]{Pr} \tag{7}$$

$$Nu_{turb} = \frac{0.037 Re_\psi^{0.8}\, Pr}{1 * 2.44\, Re_\psi^{-0.1}\left(Pr^{\frac{2}{3}} - 1\right)} \tag{8}$$

The factor Re_ψ or Reynolds coefficient in the void fraction is calculated by means of the minimal fluidisation velocity (U_{mf}), the diameter of the granule (d_p), the kinematic viscosity of the gas (v) and the void fraction of the reactor (ψ) (Equation (9)):

$$Re_\psi = \frac{U_{mf}\, d_p}{\nu\, \psi} \tag{9}$$

The Prandtl number (Pr) is the quotient of the kinematic viscosity (ν) and thermal diffusivity (a) of the gas (Equation (10)):

$$Pr = \frac{\nu}{a} \tag{10}$$

The void fraction (ψ) can be obtained from the volume (V) of the reactor and the volume of all the granules in the bed (V_F) (Equation (11)). For the experiments in this work, ψ amounts to 0.625.

$$\psi = \frac{V - V_F}{V} \tag{11}$$

The factor f_a is calculated as follows:

$$f_a = 1 + 1.5\,(1 - \psi) \tag{12}$$

2.7. Determination of the Partial Pressure of Water Vapour and Equilibrium Temperature

The pressure of water vapour in the gas stream mixture is calculated by Equation (13):

$$p_{H_2O} = \frac{\dot{n}_{H_2O}}{\dot{n}_{air} + \dot{n}_{H_2O}} * 1.032\ bar \tag{13}$$

where $\dot{n}$ is the molar flow and is determined by Equations (14) and (15):

$$\dot{n}_{H_2O} = \frac{\dot{m}_{H_2O}}{M_{H_2O}} \tag{14}$$

$$\dot{n}_{air} = \frac{\dot{m}_{air}}{M_{air}} \tag{15}$$

where $\dot{m}$ is the mass flow and M the molar mass. Both mass flows (water vapour and air) are measured by mass flow controllers (MFC) in the set up (compare Figure 2). The equilibrium temperature used for analysis in this work is determined by the equation of Samms and Evans [34]:

$$\ln\left(p_{H_2O}[bar]\right) = -\frac{11375}{T\,[K]} + 14.574 \tag{16}$$

2.8. Cycling Stability

To determine the degree of conversion, after each experiment a sample of the storage material is taken and subject of thermogravimetric analysis (TGA). A simultaneous thermal analyser (Netzsch STA 449 F3 Jupiter) was used to carry out these measurements. In this device, the atmosphere inside the furnace is maintained inert by using volume flows of nitrogen as protective and purge gases. The sample was heated up to 850 °C and the experiments lasted 2 h. The extent of dehydration and rehydration in the test bench X_{dhy} and X_{hy}, respectively, is calculated by Equations (17) and (18):

$$X_{dhy}(\%) = \left(1 - \frac{mH_2O_{measured}}{mH_2O_{\ stoich}}\right) * 100\ (\%) \tag{17}$$

$$X_{hy}(\%) = \frac{mH_2O_{measured}}{mH_2O_{\ stoich}} * 100\ (\%) \quad (18)$$

where $mH_2O_{measured}$ is the total mass of water dehydrated during the thermal analysis and $mH_2O_{\ stoich}$ is the stochiometric mass of water of the reactive material present in the sample.

2.9. Structural Integrity

Initially, a defined range of diameters of the uncoated granules was selected as reference material and as raw material for the encapsulation process of the coated granules before it undergoes thermochemical cycling. This diameter range between 1.4 and 2 mm was prepared by sieving the initial granules with broader diameter distribution. After tenfold thermochemical cycling, the particle size distribution of the uncoated and coated material was tested by sieve analysis again. Therefore, sieves with the mesh sizes of ≥0.5 mm, ≥1 mm, ≥1.25 mm, ≥1.4 mm and ≥2 mm were used. The sieving duration, associated with a vibrant motion of the stacked sieves was each 5 min.

Additionally, images of granules taken after every experiment are used in order to qualitatively assess the degree of deterioration over the experimental series.

2.10. Mechanical Stability

The mechanical stability of the uncoated and coated granules was tested before and after tenfold thermochemical cycling by dynamometry. Therefore, a manually operated test stand equipped with a force gauge (SHIMPO, FGE-100X, max. capacity: 500 N, resolution 0.1 N) was used. All measurements were conducted with a flat-head measuring module mounted to the force gauge with the sample lying on a flat steel plate. For each sample, an amount of 25 individual granules were measured. The final mechanical stability of each sample was calculated as the mean value of the individual measurements whereas the respective standard deviation gives the uncertainty of stability. This uncertainty is thereby not only interpreted as statistic deviation from the mean, but also gives an idea about the variation of inhomogeneities within the sample's microstructure affecting the mechanical stability.

2.11. Flowability

After the last hydration of the series, the ability of the reaction bed to move through the reactor is tested. The lower pneumatic flap is opened to let the glass beads and the bulk of granules leave the reactor by the action of gravity.

2.12. Morphological Investigation and Determination of Phase Composition

The morphology and the surface texture of the samples were examined by scanning electron microscopy (FEI Quanta FEG 250). Thereby, the initial granules are compared to the granules after tenfold thermochemical cycling. All micrographs were taken in low vacuum mode at a pressure of 90—110 Pa using a large field detector for secondary electron imaging. The high resolution of the detector allows for a high-resolution imaging as needed for this purpose.

The crystalline phase composition of the materials was probed by X-ray powder diffraction (Panalytical X'Pert Pro PW 3040/60) in a scan range between 8° to 70° 2θ using Cu Kα-radiation. For phase quantification by Riteveld-refinement of the obtained pattern, ZnO (NIST standard reference) was used as external standard.

3. Results and Discussion

3.1. Reactor Operation

3.1.1. Thermal Cycling with Uncoated Granules

2.160 kg of the uncoated granules were subject of a 10-fold thermochemical cycling. The results are used as a baseline to analyse the reactor performance and operational behaviour according to the design considerations.

Figure 3 (left) shows a reference dehydration experiment with the uncoated samples. First, the air inlet temperature (T_{in}) is set at 350 °C and the volumetric flow at 45 Nm^3/h. Once the temperature is stable, the experiment starts by increasing the gas inlet temperature to 550 °C. The dehydration starts approximately at minute 25 when the rising slope of all the bulk temperatures start to decrease indicating that the endothermal reaction is occurring. At the same time, the measured water vapour content at the outlet starts to increase, confirming that dehydration takes place. After minute 68, the bulk temperatures increase faster again and the vapour content falls, indicating that a major part of the storage material is already dehydrated. The dehydration of the material proceeds until approximately minute 100, when the temperatures in the bulk reach their maximum and the content of water vapour returns to its initial values. At this point the dehydration procedure is considered finished.

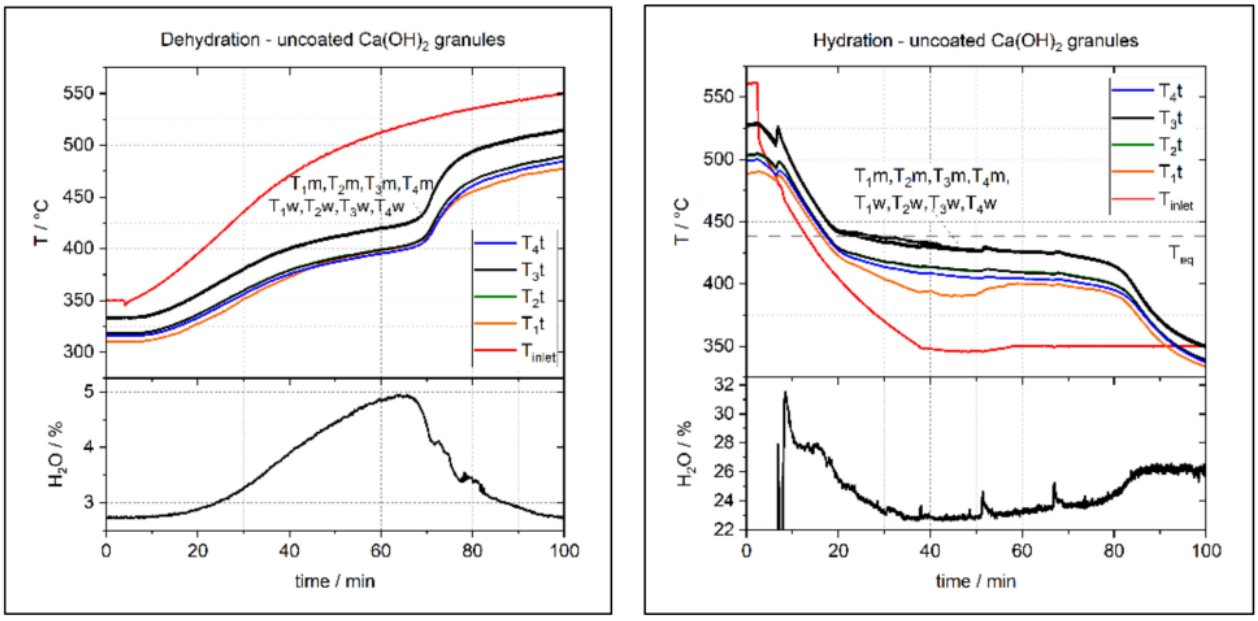

Figure 3. Temperature profiles and values of water vapour of reference experiments for dehydration (**left**) and hydration (**right**) for uncoated granules.

Bearing in mind that water vapour is not supplied during the charging process, the equilibrium temperature is actually below the air inlet temperature (350 °C) during the pre-heating stage. Therefore, it is likely that a portion of the bulk starts dehydrating but at a very slow rate. However, no significant release of water vapour is measured at this point. Therefore, even though dehydration might occur, it is not of technical relevance. As the experiment proceeds, the temperature of the storage material increases. Consequently, the reaction kinetics becomes faster and the rate at which water vapour is released rises as well. In general, a plateau in the temperatures of the bed appears when the heat influx is in equilibrium with the thermal energy absorbed to drive the endothermal reaction. Since the plateau observed is not completely flat, in our chosen operation mode the heat influx to the reaction bed is always higher than the energy taken up by the reaction.

The hydration shown in Figure 3 (right) follows subsequently after the dehydration. The air inlet temperature initially remains at 550 °C at a lower volumetric flow rate of 16 Nm^3/h. After initially reaching steady temperatures in the bulk, the gas inlet temperature is lowered to 350 °C and water vapour is additionally supplied to the gas stream at a 4 kg/h mass flow. The mixture of 16 Nm^3/h of air and 4 kg/h water vapour at a total pressure of 1 bar at the reactor inlet corresponds to a water vapour partial pressure of 0.24 bar (see Section 2.7). At around minute 20, the slope of the falling temperatures within the bulk significantly decreases, indicating that the exothermal reaction accelerates. The

temperature at which this effect starts, approximately 440 °C, corresponds to the calculated equilibrium temperature given by the partial pressure of water vapour present in the reactor (compare dotted line in Figure 3, right). Accordingly, the content of water vapour measured at the reactor outlet falls. At minute 80, the temperatures start to decrease again, which indicates that the heat release becomes smaller. This is again in accordance with the increase of water vapour measured. The reaction is complete at minute 100 when the bulk temperatures are below the inlet temperature because no more heat is released from the granules.

During the discharge, the heat release produced by the exothermal reaction leads to temperatures with a distinct plateau and with a slow but constant decrease in all measuring points, which lasts approximately 60 min (minute 20–minute 80). The bulk and outlet temperatures measured near the wall (Tw) and in the middle of the thermocouples show a plateau at 430 °C. Furthermore, a fairly constant difference to the gas inlet (350 °C) is observed between the minute 45 and 80. In the same region of the reactor, close to the wall (compare Tw and Tm), the measured temperatures of the bulk and the gas above it are the same, which indicates an excellent gas to particle heat transfer coefficient. It is observed, however, that the temperatures measured in the middle of the reactor (Tt) are 15–25 K lower.

3.1.2. Thermal Cycling with Coated Granules

In a second measurement series a 3.025-kg batch of coated granules was cycled 10 times in order to investigate the performance of the reactor concept with coated granules. The aim was also to cycle the novel granules under technical-scale reactor conditions. Samples of the granules were taken after each experiment and characterised in terms of cycling stability, structural integrity, mechanical stability and flowability. Morphological investigation is carried out by scanning electron microscopy after the 10 cycles. The results related to the characterisation of the properties of the granules are presented in Section 3.3.

Figure 4 (left) displays one dehydration experiment with coated granules. The storage material in the reactor is preheated to 350 °C and a volumetric air flow of 45 Nm^3/h. The experiment then starts by increasing the gas inlet temperature to 550 °C. At around minute 20, the rising slope of the temperatures in the reaction bed start decreasing and the water vapour content measured at the outlet of the reactor increases. This indicates that the dehydration of $Ca(OH)_2$ occurs in the reactor. Shortly after minute 60, the bulk temperatures increase faster again, and the vapour content falls. After 70 min, the vapour content reaches its initial value again which clearly indicates that the reaction is completed.

For the subsequent hydration procedure, presented in Figure 4 (right), the air volumetric flow is lowered to 16 Nm^3/h and the gas inlet temperature remains initially at 550 °C. After having constant temperatures in the bulk at the beginning, the procedure is started by lowering the gas inlet temperature from 530 °C to 350 °C. At the same time, water vapour is added to the gas stream at a mass flow rate of 4 kg/h. The conditions result again in a vapour partial pressure of 0.24 bar (see Section 2.7). At minute 20, the slope of the temperatures within the bulk changes and stay fairly stable at around 440 °C, which is in accordance with the calculated equilibrium temperature based on the partial pressure of water in the reactor (compare dotted line in Figure 4, right). The gas analyser, accordingly, detects the decrease of the water vapour content at the outlet. Both the temperature plateau and the measured water vapour content confirm that the release of heat and the uptake of H_2O in the CaO of the samples occurs. After the minute 90, the bulk temperatures are below the air inlet and the reaction is therefore complete. A reference hydration experiment is shown in Figure 4 (right).

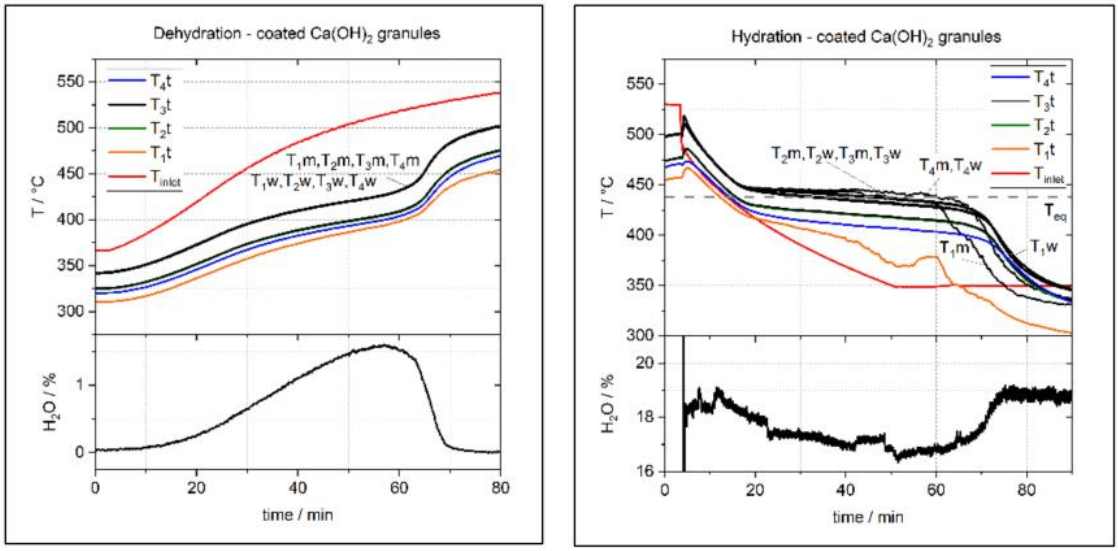

Figure 4. Temperature profiles and values of water vapour for dehydration (**left**) and hydration (**right**) for coated granules.

3.2. Thermodynamic Analysis of the Reactor Concept

3.2.1. Thermal Power and Energy Release

Figure 5 (left) displays the power and energy curve for dehydration of uncoated granules. Here, the maximum difference between the endothermal reaction temperature plateau and the gas inlet temperature allowing for the calculation of the maximum power required during dehydration. This value accounts for −1.76 kW and lies within the design considerations (compare Section 2: reactor design). The outlet temperature of the gas is equal to the temperatures in the bulk (see Figure 3, left) which indicates that the entire thermal capacity of the gas volume flow is used. This supports the hypothesis that due to the high heat transfer between gas and particle a small reaction zone is formed which moves through the bulk up to the top as the experiment proceeds. Furthermore, the process is controlled by the thermal capacity of the gas flow. Thus, a larger difference between gas and dehydration temperature could increase the thermal power. Alternatively, higher gas volume flows are capable of having the same effect. However, this would lead to undesired fluidisation of the bed in the current design. In terms of energy efficiency, the energy input is significantly larger than the energy required to dehydrate the mass of the reactive material due to the large amount of sensible heat necessary to heat up the reactor and thermal losses that cannot be avoided. The effect of the latter is visible in the last part of the energy curve which never reaches a steady value. Instead, it always displays a rising slope and accounts for −6510 kJ at the end of the experiment. Nevertheless, for a continuous system as the one proposed in this work such sensible heat losses are only relevant for the preheating phase of the first cycle.

For hydration, the maximum difference between the minimal gas inlet temperature and the equilibrium temperature of the exothermal reaction determines the maximum power obtained of 0.62 kW (see Figure 5, right) and is in the range foreseen in the reactor design (compare Section 2). Similar to dehydration, the temperatures measured in the bed and at the outlet are the same which is proof of very high heat transfer between gas and particle. This also leads to a small reaction zone within the bed that moves up through it. The hydration process can also be controlled by the thermal capacity of the gas flow. Thus, the power could be increased either by setting a lower gas inlet temperature or by adjusting a higher equilibrium temperature. The thermal energy released accounts for 2392 kJ at minute 90 and remains fairly stable until the end of the experiment. This is different from the dehydration experiments due to the higher thermal losses.

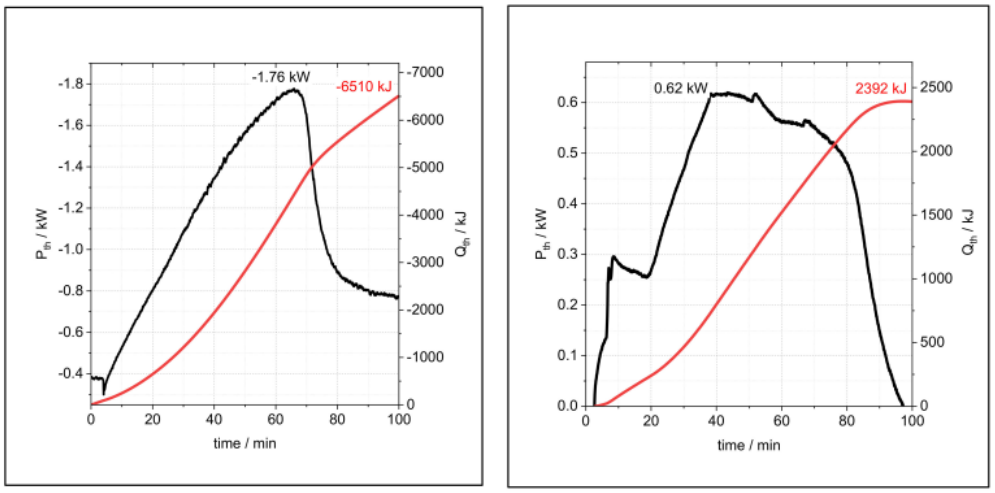

Figure 5. Power and energy curve for dehydration (**left**) and hydration (**right**) of uncoated granules.

To sum up, a successful operation of direct gas flow through a bed of granules was achieved. The design of the novel reactor concept presents a conflict in the use of high volume flows due to the undesired fluidisation of the bed of granules. Therefore, the main requirement for the maximum gas flow to reach high thermal power is that it remains below the minimal fluidisation velocity. Such volume flow and the difference between the gas inlet temperature and the endothermal/exothermal reaction equilibrium temperature defines the operational power. Finally, although the operation at higher pressures in principle allows for lower gas volume flows, it increases the complexity in the reactor design.

3.2.2. Gas Distribution within the Reaction Bed

Figure 6 depicts the temperature distribution for the dehydration of uncoated granules at minute 60. The data of the thermocouples located at the wall (Tw) and middle (Tm) in all the levels (T_1–T_4) shows a homogeneous axial distribution of the temperature. Conversely, in the center of the reactor the temperatures are approximately 25 K lower (compare Figure 1, left). Since this is observed in the dehydration and hydration experiments and for both materials, it is clear that the material has no influence on the gas distribution through the bulk. Instead, it is likely that the position of the inlet pipe in the reactor produces an uneven distribution of gas. To address this issue, a gas nozzle should be considered in the reactor designs.

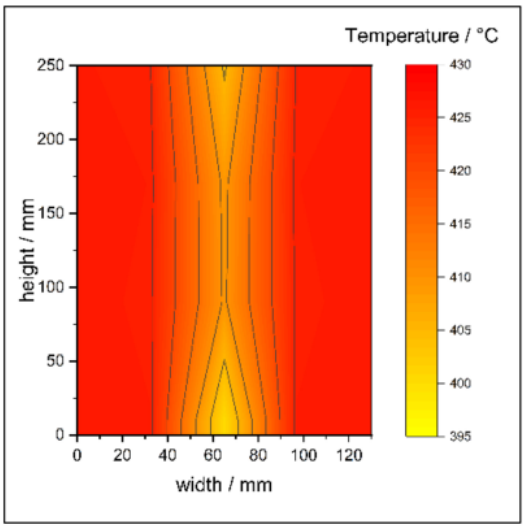

Figure 6. Side view of the temperature distribution in the reactor for the hydration of uncoated granules at minute 60.

3.3. Material Performance Analysis

After each thermal cycle, performed as described in the procedure section, a sample of granules was taken out of the reactor. The samples were characterized in several post analysis in order to assess the performance of the coating of the granules compared to uncoated granules. Cycling stability, structural integrity, mechanical stability, phase composition, morphology and flowability were analysed over the samples applying the respective methods explained in Section 2.

3.3.1. Cycling Stability

Figure 7 depicts the conversion achieved after every experiment carried out with uncoated and coated granules. As stated in Table 2, the values of the first cycle using uncoated granules correspond to the setting into operation experiments. Therefore, the data of dehydration and hydration in this cycle are not used for analysis. From cycle 2, the values found for rehydration of the uncoated granules are stable along the cycles and ranged between 92% and 97.5%. On the other hand, the dehydration varied from 77.5% to 92%. In general, the extent of dehydration was found lower than the following hydration in every cycle. This could be explained by the sampling method used which involves withdrawing a small amount of material and placing it in small jars for later TG analysis. Thus, the dehydrated samples probably rehydrated partially during the exposure to ambient air during the sampling and storage. Furthermore, since there is no clear degradation trend observable, these variations can be dedicated to the post processing of the small samples. In particular the conversion after dehydration in cycle 10 reaches almost 90% which can be assumed as technically full conversion. Additionally, the hydration conversion values are very stable over cycling, clearly indicating that previous dehydrations where also completed in the reactor.

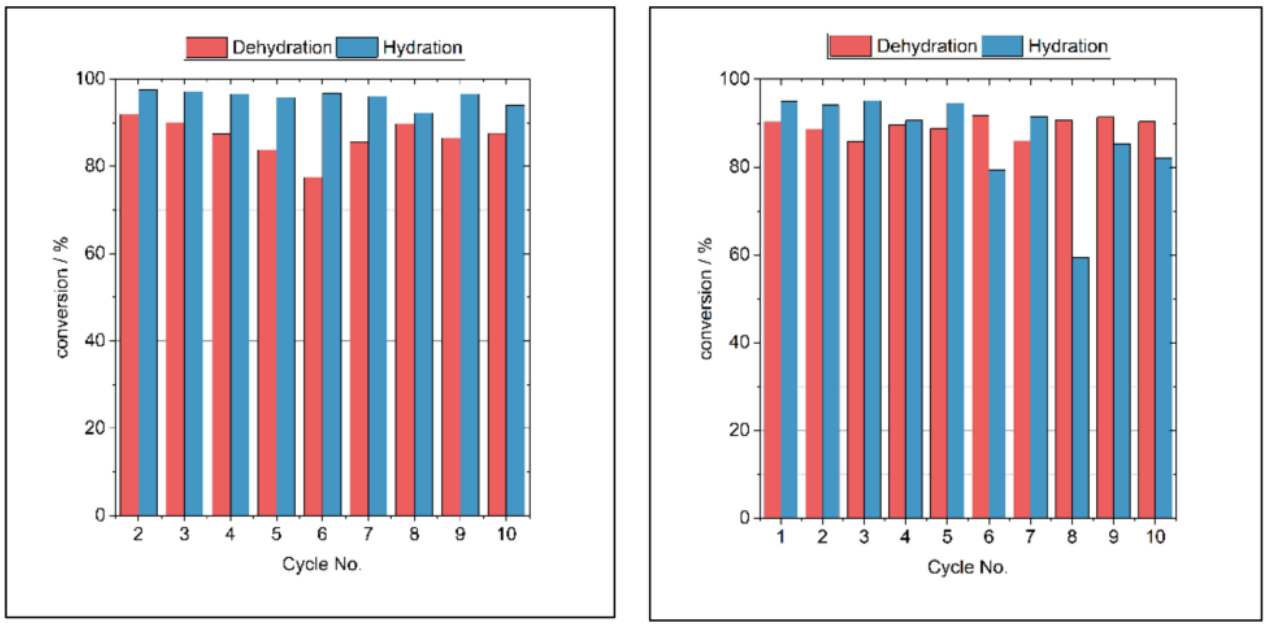

Figure 7. Conversion of uncoated granules (**left**) and coated granules (**right**) over the 10-fold thermochemical cycling.

Regarding the coated granules, it is observed that the dehydration reaches values similar to the reference uncoated material (around 90%). In addition, the conversion remains stable during the entire experimental series. On the other hand, the rehydration is stable until the 5th cycle with values that reach over 90%. After this, an oscillating behavior is observed with the lowest value in the 8th cycle (60%) and significantly higher values (over 80%) in the last two cycles of the series. This finding could suggest that the reactivity

of the coated granules is affected with the cycles due to a change in the composition. In order to further understand this, a more detailed analysis of the composition of the coated granules is described later in this work (see Section 3.3.4).

3.3.2. Structural Integrity

Figure 8 displays the state of the granules before and after the 10-fold cycling. Before the granules are cycled, they are compact, present a smooth surface and have a fairly homogeneous size distribution (see Figure 8, top left and top right). However, after 10 cycles, the signs of deterioration are clear since the granules display visible cracks or broke into smaller pieces (see Figure 8, bottom left and bottom right). Sieve analysis was carried out over the whole cycled batches and the results show that for both materials the largest share of the granules corresponds to broken pieces with a diameter between 0.5 and 1 mm (Figure 9). This finding leads to the question whether the broken pieces would further break with additional cycling, or a stable diameter size range has been achieved.

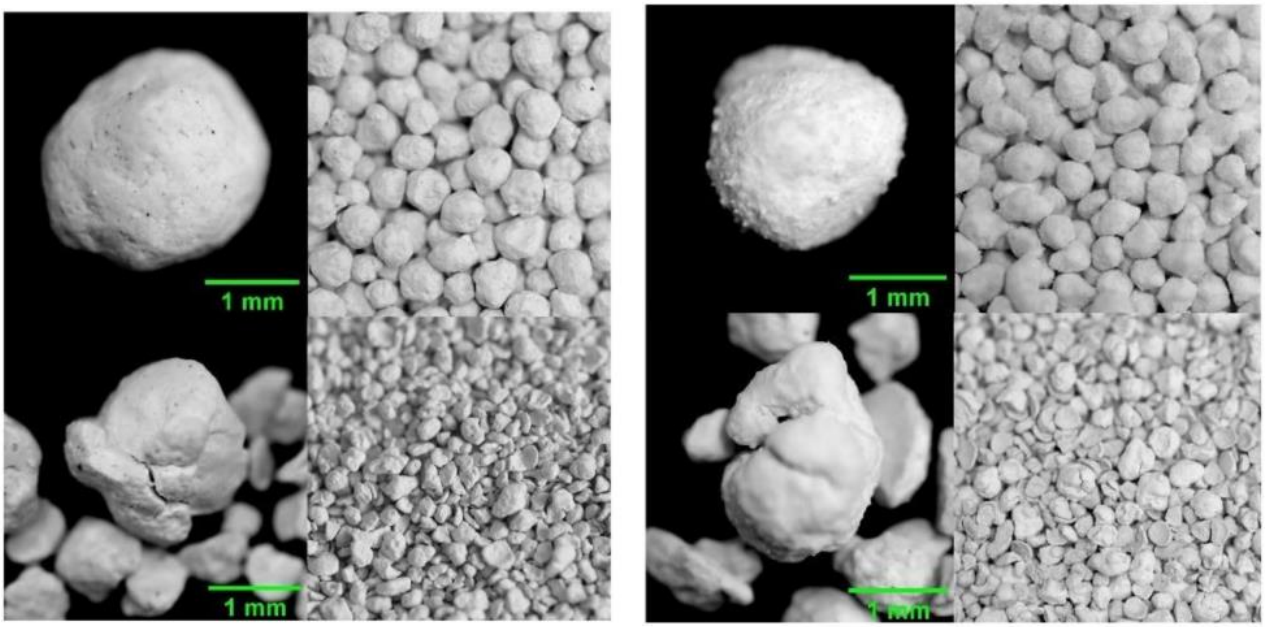

Figure 8. Images of uncoated and coated $Ca(OH)_2$ material as single granules and as bulk. **Left**: uncoated granules before (top) and after (bottom) the experimental series. **Right**: coated granules before (top) and after (bottom) the experimental series.

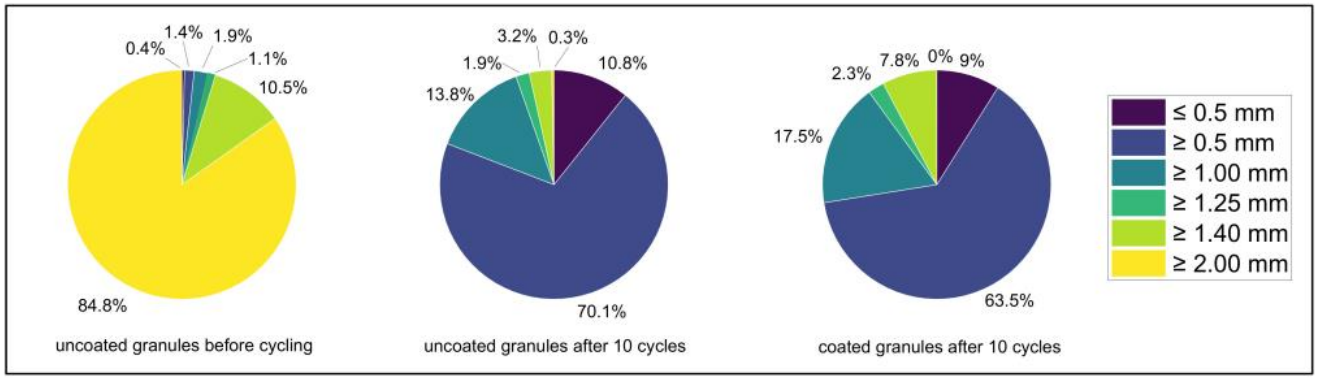

Figure 9. Sieve analysis performed on the selected particle size fraction of uncoated granules (**left**) and after tenfold thermochemical cycling of the uncoated (**middle**) as well as coated (**right**) granules.

In order to estimate the amount of fines generated during sieving, at first the granule diameter distribution of the selected particle size fraction of uncoated granules was determined. Thereby it was found that after sieving 95.3% of the granules are in the intended diameter range between 2 mm and 1.4 mm, while a fraction of 4.7% is of smaller diameter after the sieving due to abrasion occurring to the granules during the process. With this as a reference for the evaluation of the cycled samples, it was found that the uncoated and coated granules, undergo a significant deterioration during cycling. However, by coating the $Ca(OH)_2$ storage material with nanostructured Al_2O_3, the size fraction with diameters between 1 mm to 1.4 mm make a total fraction of around 28% while for the uncoated material only around 19% fall into this range. In addition, the amount of particles with diameters smaller than 1 mm is significantly reduced for the coated granules (Figure 9) This evidences the positive effect of the coating over the structure of the granules. Considering the fact that besides deterioration due to volumetric expansion and contraction, the intact granules decrease in mechanical stability during thermochemical cycling, the results indicate that the coated sample also has a higher resistance to abrasion forces occurring in the bulk during sieving.

3.3.3. Mechanical Stability

The mechanical stability of the uncoated granules as well as of the coated with nanostructured Al_2O_3 was examined after each of the ten dehydration and hydration reactions in the reactor. From the results, it can be shown that there is a strong discrepancy in the mechanical stability of the respective dehydrated and hydrated species. With regard to the uncoated storage material, it can be seen that the initial stability is of approximately 3 N and then it increases slightly in the next two cycles for the dehydrated species. A similar effect is observed for the hydrated form but with lower values of crushing strength. In fact, in the course of thermochemical cycling, the stability of the hydrated species slightly increases up to the fifth cycle. Furthermore, for both dehydrated and rehydrated uncoated granules, the mechanical stability decreases after the fifth cycle. In contrast, after the first dehydration the mechanical stability of the coated granules is three times higher than for the uncoated material and this difference increases even further after the first hydration. The mechanical stability of the coated granules also decreases in the course of thermochemical cycling by roughly 50% after ten completed de- and rehydration reactions. Nevertheless, it is significantly higher than for the uncoated granules (about three times) (Figure 10).

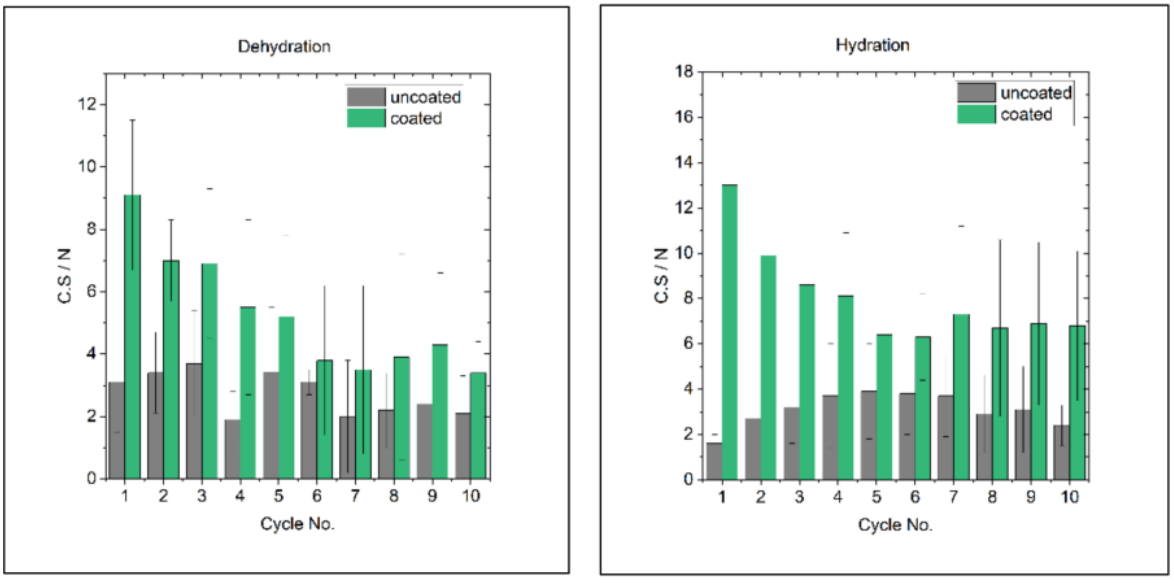

Figure 10. Mechanical strength of the uncoated and coated granules in the 10-cycle experiment series. **Left**: after dehydration. **Right**: after hydration.

3.3.4. Morphology and Phase Composition

In order to gain a detailed insight and further understanding in the observed particle size distribution and mechanical stability observed, the morphology and texture of the cycled samples were examined in comparison to the respective raw materials by scanning electron microscopy (SEM).

From the micrographs taken on the uncoated $Ca(OH)_2$ granules before and after ten reaction cycles, it can be seen from Figure 11 (top) that initially the granule surface appears rather smooth with some irregularities on the surface which might stem from the synthesis procedure, which is a built-up granulation process. For the examination after tenfold cycling, a visually intact granule was selected. The micrographs taken on this sample reveal numerous cracks on the granules surface throughout the entire surface (see Figure 11, bottom).

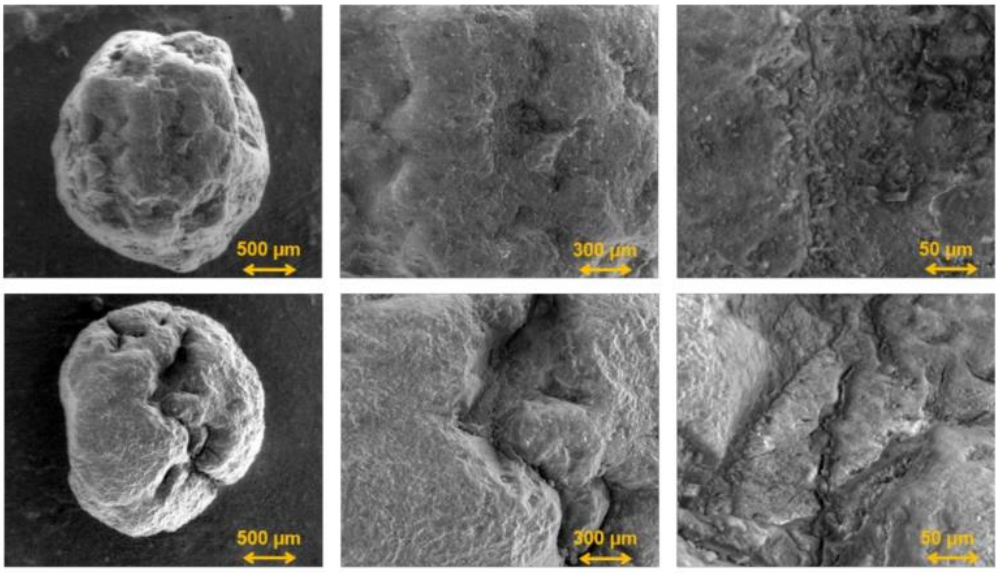

Figure 11. Scanning electron micrographs of the uncoated $Ca(OH)_2$ granule before (**top**) and after tenfold cycling (**bottom**), taken at 100-fold (**left**), 250-fold (**middle**) and 1.000-fold (**right**) magnification.

In contrast, the surface of the coated starting material reveals several cracks and is covered by a material rather rough in appearance, which is the nanostructured Al_2O_3 covering the entire granule (see Figure 12, top). After tenfold thermochemical cycles, no cracks on the granules surface are visible and the texture now appears to be rather smooth and dense, containing some larger pores as necessary for the transport of the gaseous reaction partner during charging and discharging (see Figure 12, bottom). This observation shows that the nanostructured additive forms a stabilising shell which enhances the structural integrity and mechanical stability of the granules during thermochemical cycling.

It is reasonable that the observed increased structural integrity and mechanical stability of the granulated $Ca(OH)_2$ coated with nanostructured Al_2O_3 is due to the formation of a stabilising shell during thermochemical cycling. The SEM-micrographs already revealed that there is a significant change in the texture of the respective sample before and after cycling. However, to explain the stabilising effect, it is necessary to learn about the phase composition of the shell during the course of thermochemical cycling. Therefore, the phase composition of the shell material was examined on the hydrated species by X-ray diffraction and quantified by subsequent Rietveld-analysis performed on the obtained patterns and compared to the initial phase composition of the uncycled uncoated granules as well as to the phase composition of the uncoated material during thermochemical cycling as reference.

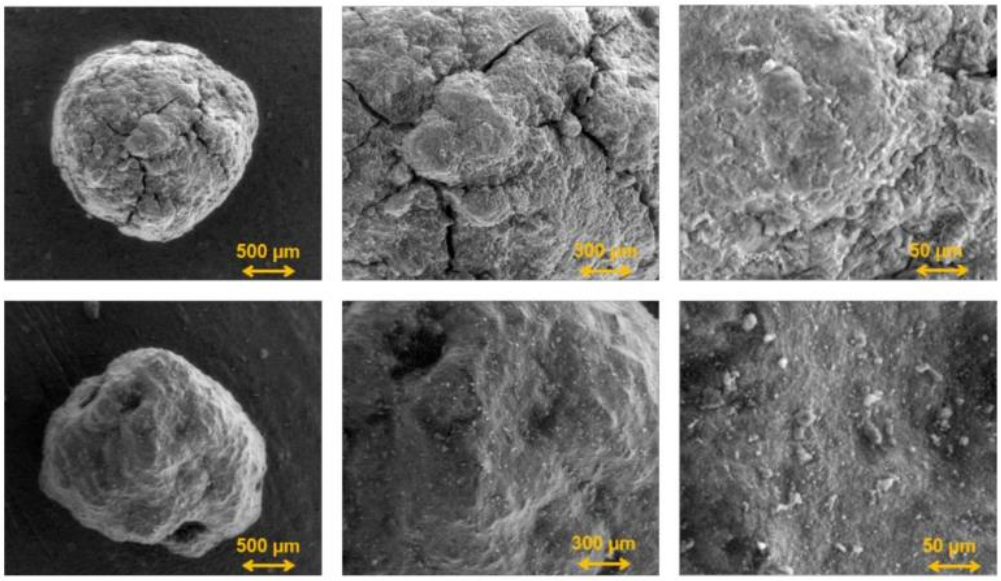

Figure 12. Scanning electron micrographs of the $Ca(OH)_2$ granule coated with nanostructured Al_2O_3 before (**top**) and after tenfold cycling (**bottom**), taken at 100-fold (**left**), 250-fold (**middle**) and 1.000-fold (**right**) magnification.

As can be seen from Figure 13 (left) the uncycled uncoated granules contain around 71% of crystalline $Ca(OH)_2$, 7% of $CaCO_3$ which most probable stems from the carbonation of the storage material during its contact with the ambient atmosphere and 22% of X-ray amorphous material. Due to the synthesis procedure of the $Ca(OH)_2$ by precipitation from solution, it is probable that the amorphous material predominantly contains nanoscaled $Ca(OH)_2$. The $Ca(OH)_2$ content of the bulk sample does not significantly change during thermochemical cycling. Except for the first hydration, where a small amount of CaO is detected. This observation can be explained by incomplete conversion after the completion of the previous dehydration reaction. A different situation is found for the granules coated with nanostructured Al_2O_3. In this case, the composition of the raw material is comparable to the uncoated material but from the first hydration reaction on, new phases can be identified. These phases are Katoite and Mayenite with the chemical composition $Ca_3Al_2(OH)_{12}$ and $Ca_{12}Al_{14}O_{33}$, respectively. The content of these phases varies during thermochemical cycling around a value of roughly 10% (w/w), with a predominant content of Katoite (Figure 13, right). It can be concluded, that these phases are formed as reaction products between the $Ca(OH)_2$ storage material and he nanostructured Al_2O_3 during the hydrothermal conditions associated with thermochemical cycling and that these phases are responsible for the observed enhanced mechanical stability by creating a largely contiguous structure on the granules surface. Interestingly, the $Ca(OH)_2$ content in this sample of coated granules varies to a larger extend during the individual hydration reactions than in the uncoated granules and the $CaCO_3$ content is slightly higher. It is conceivable, that these fluctuations are caused by the reaction between the stabilising shell and the storage material core. However, according to the results, the content of crystalline storage material $Ca(OH)_2$ after the final tenth dehydration is still in the same range of around 70% as in the starting (uncoated) material. Therefore, the results indicate that there is no major reduction in storage density due to coating by the nanostructured additive.

In summary, from the examination of the morphology and texture of the $Ca(OH)_2$ granules coated with nanostructured Al_2O_3, it has been found that upon thermochemical cycling the additive forms a largely contiguous layer covering the surface of the granules. By comparative evaluation with the determined phase composition, this layer was found to consist of calcium-aluminate compounds, namely Katoite and Mayenite, which provide the enhanced mechanical stability and increased structural integrity of this material. Thereby,

the stabilising effect caused by the formation of these compounds is initiated upon the first hydration reaction of the material, indicating that no further treatment may be necessary in order to achieve the desired effect.

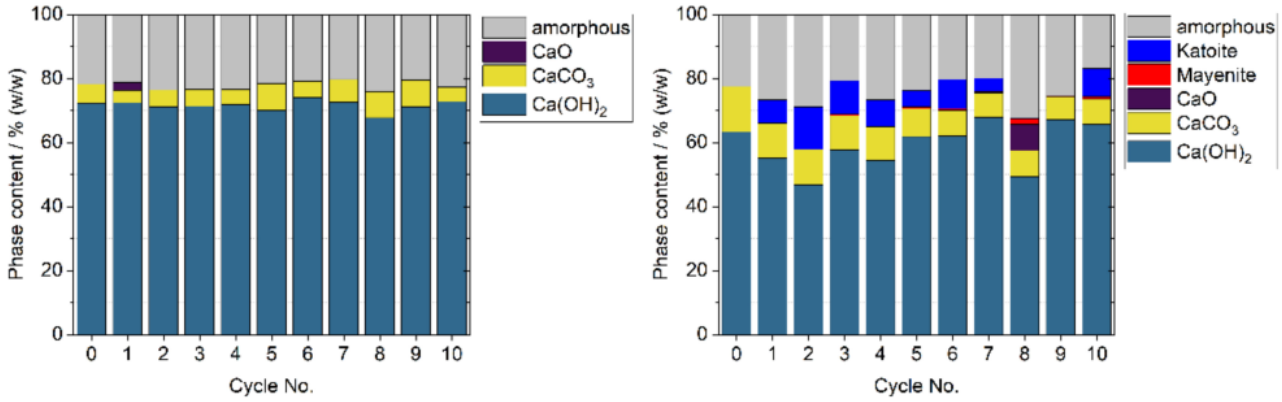

Figure 13. Phase composition of the uncoated (**left**) and coated (**right**) $Ca(OH)_2$ granules during thermochemical cycling, the uncycled material is indicated by cycle No. 0.

3.3.5. Flowability of the Bed of Granules

The moving bed feature of the reactor was tested after the last experiment with both materials. After cooling down the reactor, the lower flap was opened, and the entire reaction bed flowed out and was collected in a tray.

4. Conclusions and Outlook

This work presents a directly heated moving bed reactor, based on a new concept developed for $Ca(OH)_2$ granules as storage material. Two batches were used: $Ca(OH)_2$ granules and $Ca(OH)_2$ granules coated with Al_2O_3 nanostructured particles. The thermodynamic performance of the reactor was analysed based on the operation data obtained and reflected against our design considerations. Ten thermochemical cycles (dehydration and hydration) were carried out to analyse the cycling stability, structural integrity, mechanical stability and flowability of the storage granules.

The results obtained demonstrate that the reactor concept is operational. Overall, complete hydration and dehydration of the storage material was demonstrated. The operational data presented shows that the heat transfer between gas and particles was sufficiently high. The experimental data proves that all thermal energy contained in the gas flow was transferred to the particles during reaction. In both operation modes for dehydration and hydration, the process was controlled by the obtained temperature difference and the adjusted gas volume flow. The reaction zone in the bulk therefore had a small length and wanders as the reaction proceeds, from the bottom to the top of the bulk. The maximum thermal power obtained during the dehydration process at the maximal applied gas volume flow accounted for −1.76 kW. The operation of the reactor is capable of achieving even higher power densities. However, this potential is limited by the gas velocity in the reactor which must be maintained below the fluidisation velocity. If the fluidisation can be avoided, the high heat transfer coefficient and the large available surface of the 2 mm granules would enable to reach a specific power density of 300 W/K L.

One important conclusion dedicated to the reactor concept is that the particles freely flowed out of the reactor after 10 cycles. This observation leads to the conclusion that the hot gas stream in direct contact with the granules helps to prevent the agglomeration. Therefore, based on this concept, the gravity assisted movement of cycled particles in technical scale has been demonstrated for the first time [17,27].

With regard to the materials used, it was found that complete technical conversion was achieved. In addition, no degradation attributed to the directly heated reactor concept was observed. After the experimental series, the largest share of both materials broke

into smaller pieces which range in the size of 0.5–1 mm. Nevertheless, for the coated granules new phases formed as reaction products between the $Ca(OH)_2$ and nanostructured Al_2O_3. This resulted in a continuous structure on the granules surface that enhances their mechanical stability without significantly reducing the storage density.

The results obtained in this work show that this reactor concept is very promising and can be considered for the development of a pilot scale reactor with a more efficient heat and gas distribution. Furthermore, different operation settings in which high power densities are achieved by means of higher volume flows but below the fluidisation velocity should be investigated. In order to prevent the reaction bed from fluidising some procedures need to be verified, for example using mechanical barriers or filling the reactor volume completely. In addition, the realisation of the continuous movement of the granules that enables continuous power output should be tested. In parallel, further studies are necessary to better understand the changes occurring in the structure of the granules during the charge and discharge process. Thus, it will be possible to determine when and to what extent the integrity of the granules is lost and if the resulting fragments stabilise in a size range after a larger number of cycles. Moreover, it is necessary to confirm the fluidisation of the bed in practice and analyse the degree of deterioration of the granules in non-fluidising conditions.

Author Contributions: A.C.M.: Conceptualization, methodology, formal analysis, investigation, visualization, writing—original draft. S.A. (Material performance and Morphology and phase composition): methodology, formal analysis, investigation, visualization, writing—original draft; M.L.: conceptualization, methodology, writing—review and editing; M.S.: conceptualization, methodology, investigation (experiments), writing—review and editing, supervision. All authors have read and agreed to the published version of the manuscript.

Funding: This work was partially funded by the European Funds for Regional Development (EFRE Program)—Project-ID EFRE-0801821 and the Deutsche Forschungsgemeinschaft (DFG, German Research Foundation)—Project-ID 279064222—in the frame of the SFB 1244.

Institutional Review Board Statement: Not applicable.

Informed Consent Statement: Not applicable.

Data Availability Statement: Datasets generated during the current study are available from corresponding author on reasonable request.

Acknowledgments: The authors thank Andreas Weigl for his technical support in the preparation of the test bench.

Conflicts of Interest: The authors declare no conflict of interest.

Nomenclature

Symbol	Description	Unit
m	Mass	Kg
d	Diameter	m
p	Pressure	bar
T	Temperature	K
V	Volume	L
g	Gravity	m^2/s
ρ	Density	kg/m^3
P	Power	W
Q	Energy	J
ΔH	Reaction enthalpy	J/mol
M	Molar mass	kg
$\dot{n}$	Molar flow	mol/h
$\dot{V}$	Volumetric flow	m^3/h
$\dot{m}$	Mass flow	kg/h

X	Conversion	-
α	Heat transfer coefficient	W/m^2 K
HTF	Heat transfer fluid	-
U_{mf}	Minimal fluidisation velocity	m/s
MFC	Mass flow controller	-
μ	Dynamic viscosity	Pa.s
ν	Kinematic viscosity	m^2/s
a	Thermal diffusivity	m^2/s
ψ	Void fraction of the reactor	-
Re_{mf}	Reynolds minimal fluidisation	-
Re_{ψ}	Reynolds coefficient in the void fraction	-
Nu	Nusselt number	-
Pr	Prandtl number	-
Ar	Archimedes number	-
C.S	Crushing strength	N
CSP	Concentrated Solar Power	-

References

1. Farulla, G.A.; Cellura, M.; Guarino, F.; Ferraro, M. A Review of Thermochemical Energy Storage Systems for Power Grid Support. *Appl. Sci.* **2020**, *10*, 3142. [CrossRef]
2. Kato, Y.; Sasaki, Y.; Yoshizawa, Y. Thermal Performance Measurement of a Packed Bed Reactor of a Magnesium Oxide/Water Chemical Heat Pump. *J. Chem. Eng. Jpn.* **2003**, *36*, 833–839. [CrossRef]
3. Rosemary, J.K.; Bauerle, G.L.; Springer, T.H. Solar Energy Storage Using Reversible Hydration-Dehydration of CaO-$Ca(OH)_2$. *J. Energy* **1979**, *3*, 321–322. [CrossRef]
4. Ervin, G.J. Solar heat storage using chemical reactions. *J. Solid State Chem.* **1977**, *22*, 51–61. [CrossRef]
5. Schmidt, M.; Gutiérrez, A.; Linder, M. Thermochemical energy storage with $CaO/Ca(OH)_2$ Experimental investigation of the thermal capability at low vapor pressures in a lab scale reactor. *Appl. Energy* **2017**, *188*, 672–681. [CrossRef]
6. Fujii, I.; Tsuchiya, K.; Higano, M.; Yamada, J. Studies of an energy storage system by use of the reversible chemical reaction: $CaO+H_2pÄCa(OH)_2$. *Sol. Energy* **1985**, *34*, 367–377. [CrossRef]
7. Schmidt, M.; Linder, M. A Novel Thermochemical Long Term Storage Concept: Balance of Renewable Electricity and Heat Demand in Buildings. *Front. Energy Res.* **2020**, *8*, 137. [CrossRef]
8. Xu, J.; Wang, R.; Li, Y. A review of available technologies for seasonal thermal energy storage. *Sol. Energy* **2014**, *103*, 610–638. [CrossRef]
9. Schaube, F.; Kohzer, A.; Schütz, J.; Wörner, A.; Müller-Steinhagen, H.M. De- and rehydration of $Ca(OH)_2$ in a reactor with direct heat transfer for thermo-chemical heat storage. Part A: Experimental results. *Chem. Eng. Res. Des.* **2013**, *91*, 856–864. [CrossRef]
10. Roßkopf, C.; Afflerbach, S.; Schmidt, M.; Görtz, B.; Kowald, T.; Linder, M.; Trettin, R. Investigations of nano coated calcium hydroxide cycled in a thermochemical heat storage. *Energy Convers. Manag.* **2015**, *97*, 94–102. [CrossRef]
11. Schmidt, M.; Szczukowski, C.; Roßkopf, C.; Linder, M.; Wörner, A. Experimental results of a 10 kW high temperature thermo-chemical storage reactor based on calcium hydroxide. *Appl. Therm. Eng.* **2014**, *62*, 553–559. [CrossRef]
12. Yan, J.; Zhao, C. Experimental study of $CaO/Ca(OH)_2$ in a fixed-bed reactor for thermochemical heat storage. *Appl. Energy* **2016**, *175*, 277–284. [CrossRef]
13. Funayama, S.; Takasu, H.; Zamengo, M.; Kariya, J.; Kim, S.T.; Kato, Y. Performance of thermochemical energy storage of a packed bed of calcium hydroxide pellets. *Energy Storage* **2019**, *1*, e40. [CrossRef]
14. Kanzawa, A.; Arai, Y. Thermal energy storage by the chemical reaction augmentation of heat transfer and thermal decomposition in the $CaOCa(OH)_2$ powder. *Sol. Energy* **1981**, *27*, 289–294. [CrossRef]
15. Roßkopf, C.; Haas, M.; Faik, A.; Linder, M.; Wörner, A. Improving powder bed properties for thermochemical storage by adding nanoparticles. *Energy Convers. Manag.* **2014**, *86*, 93–98. [CrossRef]
16. Schmidt, M.; Gollsch, M.; Giger, F.; Grün, M.; Linder, M. Development of a Moving Bed Pilot Plant for Thermochemical Energy Storage with $CaO/Ca(OH)_2$. *AIP Conf. Proc.* **2016**, *1734*, 050041.
17. Pardo, P.E.; Anxionnaz-Minvielle, Z.; Rougé, S.; Cognet, P.; Cabassud, M. $Ca(OH)_2/CaO$ reversible reaction in a fluidized bed reactor for thermochemical heat storage. *Sol. Energy* **2014**, *107*, 605–616. [CrossRef]
18. Angerer, M.; Becker, M.; Härzschel, S.; Kröper, K.; Gleis, S.; Vandersickel, A.; Spliethoff, H. Design of a MW-scale thermo-chemical energy storage reactor. *Energy Rep.* **2018**, *4*, 507–519. [CrossRef]
19. Rougé, S.; Criado, Y.A.; Soriano, O.; Abanades, J.C. Continuous $CaO/Ca(OH)_2$ Fluidized Bed Reactor for Energy Storage: First Experimental Results and Reactor Model Validation. *Ind. Eng. Chem. Res.* **2017**, *56*, 844–852. [CrossRef]
20. Fujii, I.; Ishino, M.; Akiyama, S.; Murthy, M.S.; Rajanandam, K.S. Behavior of $Ca(OH)_2/CaO$ pellet under dehydration and hydration. *Sol. Energy* **1994**, *53*, 329–341. [CrossRef]
21. Sakellariou, K.G.; Karagiannakis, G.; Criado, Y.A.; Konstandopoulos, A.G. Calcium oxide based materials for thermochemical heat storage in concentrated solar power plants. *Sol. Energy* **2015**, *122*, 215–230. [CrossRef]

22. Criado, Y.A.; Alonso, M.; Abanades, J.C. Enhancement of a CaO/$Ca(OH)_2$ based material for thermochemical energy storage. *Sol. Energy* **2016**, *135*, 800–809.
23. Sakellariou, K.G.; Criado, Y.A.; Tsongidis, N.I.; Karagiannakis, G.; Konstandopoulos, A.G. Multi-cyclic evaluation of composite CaO-based structured bodies for thermochemical heat storage via the CaO/$Ca(OH)_2$ reaction scheme. *Sol. Energy.* **2017**, *146*, 65–78. [CrossRef]
24. Afflerbach, S.; Kappes, M.; Gipperich, A.; Trettin, R.; Krumm, W. Semipermeable encapsulation of calcium hydroxide for thermochemical heat storage solutions. *Sol. Energy* **2017**, *148*, 1–11. [CrossRef]
25. Afflerbach, S.; Afflerbach, K.D.; Trettin, R.; Krumm, W. Improvement of a semipermeable shell for encapsulation of calcium hydroxide for thermochemical heat storage solutions. *Sol. Energy* **2021**, *217*, 208–222. [CrossRef]
26. Gollsch, M.; Afflerbach, S.; Drexler, M.; Linder, M. Structural integrity of calcium hydroxide granule bulks for thermochemical energy storage. *Sol. Energy* **2020**, *208*, 873–883. [CrossRef]
27. Mejia, A.C.; Afflerbach, S.; Linder, M.; Schmidt, M. Experimental analysis of encapsulated CaO/$Ca(OH)_2$ granules as thermochemical storage in a novel moving bed reactor. *Appl. Therm. Eng.* **2020**, *169*, 114961. [CrossRef]
28. Xia, B.Q.; Zhao, C.Y.; Yan, J.; Khosa, A.A. Development of granular thermochemical heat storage composite based on calcium oxide. *Renew. Energy* **2020**, *147*, 969–978. [CrossRef]
29. Valverde-Pizarro, C.M.; Briones, L.; Sanz, E.; Escola, J.M.; Sanz, R.; González-Aguilar, J.; Romero, M. Coating of $Ca(OH)_2$ /#^{3}-Al_2O_3 pellets with mesoporous Al_2O_3 and its application in thermochemical heat storage for CSP plants. *Renew. Energy* **2020**, *162*, 587–595.
30. Tescari, S.; Moumin, G.; Bulfin, B.; de Oliveira, L.; Schaefer, S.; Overbeck, N.; Willsch, C.; Spenke, C.; Thelen, M.; Roeb, M.; et al. Experimental and numerical analysis of a solar rotary kiln for continuous treatment of particle material. *AIP Conf. Proc.* **2018**, *2033*, 130014. [CrossRef]
31. Risthaus, K.; Linder, M.; Schmidt, M. Experimental investigation of a novel mechanically fluidized bed reactor for thermochemical energy storage with calcium hydroxide/calcium oxide. *Appl. Energy* **2022**, *315*, 118976. [CrossRef]
32. Anantharaman, A.; Cocco, R.A.; Chew, J.W. Evaluation of correlations for minimum fluidization velocity (Umf) in gas-solid fluidization. *Powder Technol.* **2018**, *323*, 454–485. [CrossRef]
33. VDI-Gesellschaft Verfahrenstechnik und Chemieingenieurwesen (VDI-GVC). *VDI Heat Atlas*; Springer: Berlin/Heidelberg, Germany, 2010; pp. 743–744.
34. Samms, J.A.C.; Evans, B.E. Thermal dissociation of $Ca(OH)_2$ at elevated pressures. *J. Appl. Chem.* **1968**, *18*, 5–8. [CrossRef]

3. Discussion and conclusions

The present work investigates the development of a moving bed reactor for the thermochemical cycling of $Ca(OH)_2$. For this purpose, it covers the design and operation of two technical scale reactors and a reaction chamber developed to characterise modified storage material in the form of granules. The investigation involves the thermodynamic analysis of the lab scale reactors, the performance of the storage granules and the experimental demonstration of the movement of the bed of granules after cycling.

In the following subsections, the research objective described in section 1.2 is discussed based on the publications presented in section 2, starting with the conclusions of the characterisation of the storage granules upon the particle stabilisation approach and the potential use at industrial-relevant scale. Next, it continues with the conclusions on the use of a tube bundle reactor for the cycling of $Ca(OH)_2$/CaO granules followed by the considerations for the development of a novel reactor based on the state-of-the-art technology. Following this, the discussion covers the development of a directly heated moving bed reactor and the conclusions on the performance of the concept under the parameters selected. The thesis concludes by describing the potentials and limitations of the test bench and storage granules as well as the upscale of the reactor to a pilot plant.

3.1. Characterisation of the modified $Ca(OH)_2$/CaO-based granules under technical conditions

Three modifications of the storage material in the form of granules were assessed in the present work: CaO granules encapsulated in ceramic shell, $Ca(OH)_2/CaCO_3$ composite granules and granules coated with Al_2O_3 nanostructured particles. Overall, the methods used to stabilise the storage material particles were proven successful since no significant agglomeration or amount of fines were encountered after cycling. However, the resulting performance of the $Ca(OH)_2/CaCO_3$ composites is superior in terms of mechanical stability. This can be explained by the amount of reactive material the samples contain (40 wt% $Ca(OH)_2$). Similar results were found with the CaO granules encapsulated in ceramic shell (39 wt% CaO), as the mechanical stress resulted significantly lower during the dehydration/hydration of the $Ca(OH)_2$/CaO present in the samples.

In terms of cycling stability, the $Ca(OH)_2/CaCO_3$ composites displayed good results along the cycles whereas the ceramic encapsulated CaO showed low conversion probably due to the mass transport resistance caused by its shell. In the case of the granules coated with Al_2O_3, the interaction between the additive and reactive material under reaction conditions leads to the formation of side products which build a layer

on the surface of the granule that enhances its mechanical stability. Furthermore, the side products (mayenite and katoite) hydrate and dehydrate within the parameters used in the experiments. The extent at which they contribute to the overall energy density of the storage granules is currently under research.

To sum up, different degrees of enhanced mechanical stability are achieved by the three methods studied. The highest values are obtained by the $Ca(OH)_2/CaCO_3$ composites and ceramic encapsulated CaO granules although at the expense of energy density. On the other hand, the alumina coating hinders the agglomeration and formation of fines and at the same time offers a sufficiently permeable layer that allows for conversion degrees comparable to reference granules. Such promising results rank this modification as the most suitable for tests in larger scale moving bed reactors.

3.2. Preliminary tests of $Ca(OH)_2$ granules in an indirectly heated reactor

In previous studies, the feasibility of the use of $Ca(OH)_2/CaO$ system at technical scale was investigated and confirmed in fixed bed reactors. However, the exchange of reacted material in this concept is not only difficult but also prevents the continuous operation of the reactor. In addition, the low thermal conductivity of the material requires complex heat exchanger designs. Hence, the upscaling of this reactor concept is technically challenging and costly. For this reason, further investigations aimed at the detachment of the power and capacity. To this end, research was dedicated to the development of moving bed reactors and material modifications that enable the movement of the reaction bed after thermal cycling. One of these experimental investigations is part of the present work. The design of the setup corresponds to a tube bundle reactor, where storage granules are located in the tube side whereas preheated air acting as heat transfer fluid (HTF) streams through the shell side. The test bench includes elements for the controllable flow of the granules, which is intended to be driven solely by gravity assistance. The operation of this reactor concept in the charging and discharging of $Ca(OH)_2$-based granules resulted successful, reaching a thermal power of 0.44 kW. This value is below the nominal power of 1 kW due to the limitations of the heat exchanger. Nevertheless, the primary objective of its design is to enable the movement of the storage granules which was achieved only by the ceramic encapsulated CaO granules due to the reduced volume change given the limited conversion explained in 3.1.

The results of the 6 cycles performed led to some conclusions in the use of indirectly heated reactors for the thermochemical cycling of storage granules. First, the heat exchangers must be of complex design to ensure the heat transport in the porous media due to the low thermal conductivity of the storage material. For this reason, the diameter of the tubes in the heat exchanger are limited to a few millimetres. Second,

the reduced space in the tube side of the heat exchanger is not able to compensate the volume expansion of the reacting granules. As a result, the bed of granules becomes stuck and consequently the movement of the bed does not occur. In conclusion, a gravity assisted moving bed in this tube bundle configuration is not technically feasible for the material modified under the approach selected.

3.3. Considerations for the development of a novel reactor for $Ca(OH)_2$

The material characterisation revealed that the mechanical stability of granules can be enhanced when they are coated with Al_2O_3 additives as almost 50 % maintain their original size after multiple cycles and the agglomeration is hindered. In order to preserve the structural integrity of the granules, the mechanical stress must be minimised during the thermal cycling. Thus, different reactor concepts were assessed upon this condition. For instance, rotary kilns or mechanically assisted fluidised beds involve the continuous mix and erosion of the granules. Fluidised or bubbling beds offer the advantage of the direct heating of the samples but require the use of high gas velocities which lead to the attrition of the granules. In contrast, a tube bundle reactor offers the possibility to hold a stationary bed. However, as described in 3.2, this indirectly heated concept could not be successfully proved.

Based on the assessment of the reactor concepts and the results obtained from the preliminary tests in the indirectly heated reactor, a directly heated reactor concept was chosen for the design of a novel setup. With this concept it appears technically feasible to achieve high heat transfer and the movement of the bed of reacted granules.

3.4. Development of a novel moving bed reactor for $Ca(OH)_2$ -based granules

A directly heated reactor (1.2-3.5 kW_{th}) was developed and set into operation for the thermochemical cycling of 3 L of storage granules in a stationary state. Thus, it was demonstrated that the temperature and gas velocity parameters used produced a sufficiently high heat transfer (α= 248 $W/m^2.K$) between gas and particles. The maximum thermal power obtained in the experiments accounted for -1.76 kW during dehydration which lays in the range of expected values considered in the design phase. At the end of the 10-cycle experimental series, the flowability of the storage granules was reported.

To sum up, after the characterisation and tests in three different reactors, it was proved that the use of Al_2O_3 nanostructured particles contributes positively to the persistent particle stabilisation of $Ca(OH)_2$ -based granules. Nevertheless, in order to preserve the mechanical stability of the granulated material and ensure a desirable bulk behaviour that allows for the free flow of the bed after cycling, a directly heated reactor

must be used. In such reactor concept, the dehydration and hydration can be controlled by the gas volume flows and the difference between the bulk and inlet temperatures. Higher power levels can be obtained by increasing one or the other parameter. However, they must be carefully selected in order to avoid the fluidisation of the bed of granules and therefore higher attrition.

3.5. Outlook

The use of a directly heated reactor in combination with $Ca(OH)_2$ granules coated with Al_2O_3 successfully proved the concept of a moving bed reactor. Therefore, the separation of power and capacity can be investigated at larger scale. For this reason, a pilot plant is envisaged. In this facility, a 5-kW reactor is expected to be operated in a continuous mode for the thermochemical cycling of 100 kg of granulated $Ca(OH)_2$. To this end, the plant requires equipment that enables the transport and continuous feeding and removal of storage granules e.g. large containers for storing unreacted and reacted granules, vacuum conveyors as means of transport and rotary valves to control the mass flow. In this pilot scale facility, a larger number of cycles and the continuous mode can be studied. Different combinations of gas velocities and temperatures can also be tested in order to obtain higher power levels while maintaining a stationary bed. In addition, a hybrid modification approach can be investigated: $Ca(OH)_2/CaCO_3$ composites coated with Al_2O_3. In order to increase the energy density, composites with higher reactive content can be produced. Although this represents more mechanical stress over the structure of the composite, it is expected to be compensated by the proved stabilisation layer given by the Al_2O_3 coating. Furthermore, composites of smaller size diameter can be used to form a larger heat transfer area and thus obtain higher power levels.

The new reactor design must overcome some technical issues encountered during the experiments carried out in this work. For instance, the uneven heat distribution can be addressed by using a nozzle plate which enables a more homogenous gas distribution within the bed, thus preventing the formation of cold spots. Another problem is the increasing pressure drop over the cycles due to the accumulation of storage material in the gas inlet pipe. In order to prevent the gas stream from being blocked, a filter must be installed. Since the formation of dust due to the granules progressive deterioration seems unavoidable, additional control measures must be implemented to prevent the particle matter from being transported to the surroundings of the reactor by the applied gas flow. Thus, in order to contain possible leaks, a casing with a vacuum system can be installed

4. Summary

Calcium hydroxide is regarded as a promising candidate given the advantages it offers for thermal energy storage. However, one of the main challenges is the poor mechanical properties the powder material offers, which worsens after thermal cycling. For this reason, different modifications have been developed to improve the bulk behaviour and thus facilitate its use in moving bed reactors. In this work, two reactors and a reaction chamber were developed and set into operation to assess and test the functionality of stabilised $Ca(OH)_2/CaO$-based granules as thermochemical storage material. The main results of this investigation are summarised as follows:

- Development of a specific setup that enables the rapid cycling and real-time visualisation and tracking of the bulk behaviour of reacting granules. The reaction chamber emulated the reactor conditions for the thermal cycling of a bulk of granules and enabled their characterisation.
- A moving bed reactor for preliminary testing of storage granules was developed and set into operation. The indirectly heated reactor consists of a tube bundle heat exchanger with a nominal power of 1 kW_{th}.
- Development of a novel directly heated moving bed reactor (1.2 kW_{th} nominal power) for the thermal cycling of 2 kg of storage granules. The design of the reactor and the parameters selected prevent the fluidisation of the bed of granules, at the same time ensure enough thermal energy supply for the reactions to occur.
- The characterisation under technical conditions confirmed that the mechanical stability of the granules coated with Al_2O_3 is enhanced. After 20 cycles:
  - the crushing strength resulted almost 50 % higher than reference granules.
  - the share of fines is 65 % lower than reference granules. No significant agglomeration was found.
- In the experiments in the lab scale reactors, the performance of the $Ca(OH)_2$ granules coated with Al_2O_3 resulted comparable to reference granules in terms of conversion and cyclability. In addition, the positive effect of the Al_2O_3 coating for the enhancement of the mechanical stability was confirmed.
- The change in dimensions of the $Ca(OH)_2/CaO$ granules during charge and discharge causes the mechanical stress over the original structure of the granule. This phenomenon can be controlled but at the expense of the energy density of the storage material.
- The heat exchanger geometry in an indirectly heated reactor hinders the movement of the storage granules after reaction. For this reason, it is not suitable when the separation of power and capacity is sought.

- The absence of a heat exchanger in a directly heated reactor provides with more space for the dimension enlargement of storage granules and thus enables the movement of the bed after cycling.

The results described in this dissertation are the base for the development of a pilot plant in which a 5-kW directly heated reactor is expected to cycle 100 kg of storage granules in a continuous mode. Although the continuous cycling of the storage granules is a significant challenge, the author expects that the realisation of a continuous mode is feasible by applying specific procedures to avoid the fluidisation of the bed of granules and technical solutions in the granules transport and control of particle matter emissions. Finally, the storage granules can be subject of further development to improve the storage density and at the same time extend the stabilisation effect.

Bibliography

[1] "Renewables 2021," IEA, Paris, 2021. [Online]. Available: https://www.iea.org/reports/renewables-2021

[2] H. Zhang, J. Baeyens, G. Cáceres, J. Degrève, and Y. Lv, "Thermal energy storage: Recent developments and practical aspects," *Progress in Energy and Combustion Science,* vol. 53, pp. 1-40, 2016/03/01/ 2016, doi: 10.1016/j.pecs.2015.10.003.

[3] D. Fernandes, F. Pitié, G. Cáceres, and J. Baeyens, "Thermal energy storage: "How previous findings determine current research priorities"," *Energy,* vol. 39, no. 1, pp. 246-257, 2012/03/01/ 2012, doi: 10.1016/j.energy.2012.01.024.

[4] C. Villada, W. Ding, A. Bonk, and T. Bauer, "Engineering molten MgCl2–KCl–NaCl salt for high-temperature thermal energy storage: Review on salt properties and corrosion control strategies," *Solar Energy Materials and Solar Cells,* vol. 232, p. 111344, 2021/10/01/ 2021, doi: 10.1016/j.solmat.2021.111344.

[5] A. Bonk, S. Sau, N. Uranga, M. Hernaiz, and T. Bauer, "Advanced heat transfer fluids for direct molten salt line-focusing CSP plants," *Progress in Energy and Combustion Science,* vol. 67, pp. 69-87, 2018/07/01/ 2018, doi: 10.1016/j.pecs.2018.02.002.

[6] D. Weishaupt and K. Müller, "Reliability of Thermal Energy Storage Technologies," *Chemie Ingenieur Technik,* vol. 93, no. 4, pp. 580-584, 2021, doi: 10.1002/cite.202000133.

[7] C. Vaalma, D. Buchholz, M. Weil, and S. Passerini, "A cost and resource analysis of sodium-ion batteries," *Nature Reviews Materials,* vol. 3, no. 4, p. 18013, 2018/03/13 2018, doi: 10.1038/natrevmats.2018.13.

[8] E. K. Hollingsworth, "Karst Regions of the World (KROW)---Populating global karst datasets and generating maps to advance the understanding of karst occurrence and protection of karst species and habitats worldwide," 2009.

[9] "Mineral commodity summaries 2022," in "Mineral Commodity Summaries," Reston, VA, Report 2022, 2022. [Online]. Available: http://pubs.er.usgs.gov/publication/mcs2022

[10] F. Schaube, L. K. Koch, A. Wörner, and H. M. Müller-Steinhagen, "A thermodynamic and kinetic study of the de- and rehydration of Ca(OH)2 at high H2O partial pressures for thermo-chemical heat storage," *Thermochimica Acta,* vol. 538, pp. 9-20, 2012, doi: 10.1016/j.tca.2012.03.003

[11] H. Matsuda, T. Ishizu, S. K. Lee, and M. Hasatani, "Kinetic Study of Ca (OH)2/CaO Reversible Thermochemical Reaction for Thermal Energy Storage by Means of Chemical Reaction," *KAGAKU KOGAKU RONBUNSHU,* vol. 11, no. 5, pp. 542-548, 1985, doi: 10.1252/kakoronbunshu.11.542.

[12] P. E. Halstead and A. E. Moore, "769. The thermal dissociation of calcium hydroxide," *Journal of the Chemical Society (Resumed),* 10.1039/JR9570003873 no. 0, pp. 3873-3875, 1957, doi: 10.1039/JR9570003873.

[13] J. Samms and B. E. Evans, "Thermal dissociation of Ca(OH)2 at elevated pressures," *Journal of Chemical Technology & Biotechnology,* vol. 18, pp. 5-8, 2007, doi: 10.1002/jctb.5010180102

[14] I. Barin, "Thermochemical Data of Pure Substances," 1995, pp. 416-523.

[15] M. W. Chase, Jr., J. L. Curnutt, R. A. McDonald, and A. N. Syverud, "JANAF thermochemical tables, 1978 supplement," *Journal of Physical and Chemical Reference Data,* vol. 7, no. 3, pp. 793-940, 1978, doi: 10.1063/1.555580.

[16] F. Schaube, A. Wörner, and R. Tamme, "High Temperature Thermochemical Heat Storage for Concentrated Solar Power Using Gas–Solid Reactions," *Journal of Solar Energy Engineering,* vol. 133, no. 3, 2011, doi: 10.1115/1.4004245.

[17] H. Ogura, M. Miyazaki, H. Matsuda, M. Hasatani, M. Yanadori, and M. Hiramatsu, "Experimental Study on Heat Transfer Enhancement of the Solid Reactant Particle Bed in a

Chemical Heat Pump Using Ca(OH)2/CaO Reaction," *KAGAKU KOGAKU RONBUNSHU,* vol. 17, no. 5, pp. 916-923, 1991, doi: 10.1252/kakoronbunshu.17.916.

[18] Y. A. Criado, M. Alonso, and J. C. Abanades, "Kinetics of the CaO/Ca(OH)2 Hydration/Dehydration Reaction for Thermochemical Energy Storage Applications," *Industrial & Engineering Chemistry Research,* vol. 53, pp. 12594-12601, 2014, doi: 10.1021/ie404246p

[19] J. K. Rosemary, G. L. Bauerle, and T. H. Springer, "Solar Energy Storage Using Reversible Hydration-Dehydration of CaO-Ca(OH)2," *Journal of Energy,* vol. 3, pp. 321-322, 1979, doi: 10.2514/3.62440

[20] Y. A. Criado, B. Arias, and J. C. Abanades, "Effect of the Carbonation Temperature on the CO2 Carrying Capacity of CaO," *Industrial & Engineering Chemistry Research,* vol. 57, no. 37, pp. 12595-12599, 2018/09/19 2018, doi: 10.1021/acs.iecr.8b02111.

[21] J. Yan, C. Y. Zhao, and Z. H. Pan, "The effect of CO2 on Ca(OH)2 and Mg(OH)2 thermochemical heat storage systems," *Energy,* vol. 124, pp. 114-123, 2017/04/01/ 2017, doi: 10.1016/j.energy.2017.02.034.

[22] N. Wang, Y. Feng, X. Guo, and A. C. T. van Duin, "Insights into the Role of H2O in the Carbonation of CaO Nanoparticle with CO2," *The Journal of Physical Chemistry C,* vol. 122, no. 37, pp. 21401-21410, 2018/09/20 2018, doi: 10.1021/acs.jpcc.8b05517.

[23] N. Koga, L. Favergeon, and S. Kodani, "Impact of atmospheric water vapor on the thermal decomposition of calcium hydroxide: A universal kinetic approach to a physico-geometrical consecutive reaction in solid–gas systems under different partial pressures of product gas," *Physical Chemistry Chemical Physics,* vol. 21, 05/16 2019, doi: 10.1039/C9CP01327J.

[24] R. S. Mikhail, S. Brunauer, and L. E. Copeland, "Kinetics of the thermal decomposition of calcium hydroxide," *Journal of Colloid and Interface Science,* vol. 21, no. 4, pp. 394-404, 1966/04/01/ 1966, doi: 10.1016/0095-8522(66)90005-5.

[25] A. K. Galwey and G. M. Laverty, "A kinetic and mechanistic study of the dehydroxylation of calcium hydroxide," *Thermochimica Acta,* vol. 228, pp. 359-378, 1993/11/15/ 1993, doi: 10.1016/0040-6031(93)80304-S.

[26] J. Tomas and S. Kleinschmidt, "Improvement of Flowability of Fine Cohesive Powders by Flow Additives," *Chemical Engineering & Technology,* vol. 32, no. 10, pp. 1470-1483, 2009, doi: 10.1002/ceat.200900173.

[27] M. Gollsch, S. Afflerbach, B. V. Angadi, and M. Linder, "Investigation of calcium hydroxide powder for thermochemical storage modified with nanostructured flow agents," *Solar Energy,* vol. 201, pp. 810-818, 2020/05/01/ 2020, doi: 10.1016/j.solener.2020.03.033.

[28] I. Fujii, K. Tsuchiya, Y. Shikakura, and M. S. Murthy, "Consideration on Thermal Decomposition of Calcium Hydroxide Pellets for Energy Storage," *Journal of Solar Energy Engineering,* vol. 111, no. 3, pp. 245-250, 1989, doi: 10.1115/1.3268314.

[29] C. Huang, M. Xu, and X. Huai, "Experimental investigation on thermodynamic and kinetic of calcium hydroxide dehydration with hexagonal boron nitride doping for thermochemical energy storage," *Chemical Engineering Science,* vol. 206, pp. 518-526, 2019/10/12/ 2019, doi: 10.1016/j.ces.2019.06.002.

[30] J. Kariya, J. Ryu, and Y. Kato, "Reaction Performance of Calcium Hydroxide and Expanded Graphite Composites for Chemical Heat Storage Applications," *ISIJ International,* vol. 55, no. 2, pp. 457-463, 2015, doi: 10.2355/isijinternational.55.457.

[31] S. Funayama, H. Takasu, S. T. Kim, and Y. Kato, "Thermochemical storage performance of a packed bed of calcium hydroxide composite with a silicon-based ceramic honeycomb support," *Energy,* vol. 201, p. 117673, 2020/06/15/ 2020, doi: 10.1016/j.energy.2020.117673.

[32] S. Funayama, H. Takasu, M. Zamengo, J. Kariya, S. T. Kim, and Y. Kato, "Composite material for high-temperature thermochemical energy storage using calcium hydroxide and ceramic

foam," *Energy Storage*; doi:10.1002/est2.53 vol. 1, no. 2, p. e53, 2019/04/01 2019, doi: 10.1002/est2.53.

[33] M. S. Murthy, P. Raghavendrachar, and S. V. Sriram, "Thermal decomposition of doped calcium hydroxide for chemical energy storage," *Solar Energy,* vol. 36, no. 1, pp. 53-62, 1986/01/01/ 1986, doi: 10.1016/0038-092X(86)90060-5.

[34] J. Yan and C. Y. Zhao, "First-principle study of CaO/Ca(OH)2 thermochemical energy storage system by Li or Mg cation doping," *Chemical Engineering Science,* vol. 117, pp. 293-300, 2014/09/27/ 2014, doi: 10.1016/j.ces.2014.07.007.

[35] A. Maruyama, R. Kurosawa, and J. Ryu, "Effect of Lithium Compound Addition on the Dehydration and Hydration of Calcium Hydroxide as a Chemical Heat Storage Material," *ACS Omega,* vol. 5, no. 17, pp. 9820-9829, 2020/05/05 2020, doi: 10.1021/acsomega.9b04444.

[36] A. Shkatulov and Y. Aristov, "Modification of magnesium and calcium hydroxides with salts: An efficient way to advanced materials for storage of middle-temperature heat," *Energy,* vol. 85, pp. 667-676, 2015/06/01/ 2015, doi: 10.1016/j.energy.2015.04.004.

[37] T. Wang, C. Y. Zhao, and J. Yan, "Investigation on the Ca(OH)2/CaO thermochemical energy storage system with potassium nitrate addition," *Solar Energy Materials and Solar Cells,* vol. 215, p. 110646, 2020/09/15/ 2020, doi: 10.1016/j.solmat.2020.110646.

[38] Y.-T. Li, M.-T. Li, Z.-B. Xu, Z.-H. Meng, and Q.-P. Wu, "Dehydration kinetics and thermodynamics of ZrO(NO3)2-doped Ca(OH)2 for chemical heat storage," *Chemical Engineering Journal,* vol. 399, p. 125841, 2020/11/01/ 2020, doi: 10.1016/j.cej.2020.125841.

[39] Z. Bian, Y. Li, F. Wang, Y. Fang, J. Zhao, and J. Qi, "Understanding the acceleration effect of manganese and cerium doping on the hydration of CaO in CaO/Ca(OH)2 heat storage by density function theory," *Journal of Energy Storage,* vol. 56, p. 105953, 2022/12/01/ 2022, doi: 10.1016/j.est.2022.105953.

[40] J. Kariya, J. Ryu, and Y. Kato, "Development of thermal storage material using vermiculite and calcium hydroxide," *Applied Thermal Engineering,* vol. 94, pp. 186-192, 2016/02/05/ 2016, doi: 10.1016/j.applthermaleng.2015.10.090.

[41] J. Kariya and Y. Kato, "Development of thermal energy storage material using porous silicon carbide and calcium hydroxide," *Energy Procedia,* vol. 131, pp. 395-406, 2017/12/01/ 2017, doi: 10.1016/j.egypro.2017.09.470.

[42] M. Xu, X. Huai, and J. Cai, "Agglomeration Behavior of Calcium Hydroxide/Calcium Oxide as Thermochemical Heat Storage Material: A Reactive Molecular Dynamics Study," *The Journal of Physical Chemistry C,* vol. 121, no. 5, pp. 3025-3033, 2017/02/09 2017, doi: 10.1021/acs.jpcc.6b08615.

[43] C. Roßkopf, M. Haas, A. Faik, M. Linder, and A. Wörner, "Improving powder bed properties for thermochemical storage by adding nanoparticles," *Energy Conversion and Management,* vol. 86, pp. 93-98, 2014, doi: 10.1016/j.enconman.2014.05.017

[44] C. Roßkopf *et al.*, "Investigations of nano coated calcium hydroxide cycled in a thermochemical heat storage," *Energy Conversion and Management,* vol. 97, pp. 94-102, 2015, doi: 10.1016/j.enconman.2015.03.034

[45] S. Funayama, M. Schmidt, K. Mochizuki, M. Linder, H. Takasu, and Y. Kato, "Calcium hydroxide and porous silicon-impregnated silicon carbide-based composites for thermochemical energy storage," *Applied Thermal Engineering,* vol. 220, p. 119675, 2023/02/05/ 2023, doi: 10.1016/j.applthermaleng.2022.119675.

[46] Y. Álvarez Criado, M. Alonso, and J. C. Abanades, "Composite Material for Thermochemical Energy Storage Using CaO/Ca(OH)2," *Industrial & Engineering Chemistry Research,* vol. 54, no. 38, pp. 9314-9327, 2015/09/30 2015, doi: 10.1021/acs.iecr.5b02688.

[47] Y. A. Criado, M. Alonso, and J. C. Abanades, "Enhancement of a CaO/Ca(OH)2 based material for thermochemical energy storage," *Solar Energy,* vol. 135, pp. 800-809, 2016, doi: 10.1016/j.solener.2016.06.056

[48] K. G. Sakellariou, Y. A. Criado, N. I. Tsongidis, G. Karagiannakis, and A. G. Konstandopoulos, "Multi-cyclic evaluation of composite CaO-based structured bodies for thermochemical heat storage via the CaO/Ca(OH)2 reaction scheme," *Solar Energy,* vol. 146, pp. 65-78, 2017, doi: 10.1016/j.solener.2017.02.013

[49] B. Q. Xia, C. Y. Zhao, J. Yan, and A. A. Khosa, "Development of granular thermochemical heat storage composite based on calcium oxide," *Renewable Energy,* vol. 147, pp. 969-978, 2020, doi: 10.1016/j.renene.2019.09.065

[50] R. Guo *et al.*, "Mechanical stability and heat transfer improvement of CaO-based composite pellets for thermochemical energy storage," *Chemical Engineering Science,* vol. 255, p. 117674, 2022/06/29/ 2022, doi: 10.1016/j.ces.2022.117674.

[51] S. Afflerbach, K. D. Afflerbach, R. Trettin, and W. Krumm, "Improvement of a semipermeable shell for encapsulation of calcium hydroxide for thermochemical heat storage solutions Material design and evaluation in laboratory and reactor scale," *Solar Energy,* vol. 217, pp. 208-222, 2021, doi: 10.1016/j.solener.2021.02.005

[52] S. Afflerbach, M. Kappes, A. Gipperich, R. Trettin, and W. Krumm, "Semipermeable encapsulation of calcium hydroxide for thermochemical heat storage solutions," *Solar Energy,* vol. 148, pp. 1-11, 2017, doi: 10.1016/j.solener.2017.03.074

[53] M. Gollsch, S. Afflerbach, M. Drexler, and M. Linder, "Structural integrity of calcium hydroxide granule bulks for thermochemical energy storage," *Solar Energy,* vol. 208, pp. 873-883, 2020, doi: 10.1016/j.solener.2020.08.017

[54] A. Cosquillo Mejia, S. Afflerbach, M. Linder, and M. Schmidt, "Experimental analysis of encapsulated CaO/Ca(OH)2 granules as thermochemical storage in a novel moving bed reactor," *Applied Thermal Engineering,* vol. 169, p. 114961, 2020/03/25/ 2020, doi: 10.1016/j.applthermaleng.2020.114961.

[55] S. Funayama, H. Takasu, M. Zamengo, J. Kariya, S. T. Kim, and Y. Kato, "Performance of thermochemical energy storage of a packed bed of calcium hydroxide pellets," *Energy Storage,* vol. 1, pp. e40, 2019, doi: 10.1002/est2.40

[56] I. Fujii, M. Ishino, S. Akiyama, M. S. Murthy, and K. S. Rajanandam, "Behavior of Ca(OH)2/CaO pellet under dehydration and hydration," *Solar Energy,* vol. 53, pp. 329-341, 1994, doi:10.1016/0038-092X(94)90036-1

[57] C. M. Valverde-Pizarro *et al.*, "Coating of Ca(OH)2 /#³-Al2O3 pellets with mesoporous Al2O3 and its application in thermochemical heat storage for CSP plants," *Renewable Energy,* vol. 162, pp. 587-595, 2020, doi: 10.1016/j.renene.2020.08.095.

[58] L. Briones *et al.*, "Development of stable porous silica-coated Ca(OH)2/γ-Al2O3 pellets for dehydration/hydration cycles with application in thermochemical heat storage," *Journal of Energy Storage,* vol. 51, p. 104548, 2022/07/01/ 2022, doi: 10.1016/j.est.2022.104548.

[59] A. Jashari, S. Afflerbach, K. Afflerbach, and W. Krumm, "Structural stabilization of granular Ca(OH)2 by coating with nanostructured additives for thermochemical cycling in a fixed reaction bed," *Energy Conversion and Management: X,* vol. 18, p. 100367, 2023/04/01/ 2023, doi: 10.1016/j.ecmx.2023.100367.

[60] B. W. Lucke, S. Afflerbach, and W. Krumm, "Optimization of the Coating Process of a Ca(OH)2-Based Thermochemical Energy Storage Material," *Chemie Ingenieur Technik,* vol. n/a, no. n/a, doi: 10.1002/cite.202300081.

[61] A. Solé, I. Martorell, and L. F. Cabeza, "State of the art on gas–solid thermochemical energy storage systems and reactors for building applications," *Renewable and Sustainable Energy Reviews,* vol. 47, pp. 386-398, 2015/07/01/ 2015, doi: 10.1016/j.rser.2015.03.077.

[62] K. Wang, T. Yan, R. K. Li, and W. G. Pan, "A review for Ca(OH)2/CaO thermochemical energy storage systems," *Journal of Energy Storage,* vol. 50, p. 104612, 06/01 2022, doi: 10.1016/j.est.2022.104612.

[63] F. Schaube, A. Kohzer, J. Schütz, A. Wörner, and H. M. Müller-Steinhagen, "De- and rehydration of Ca(OH)2 in a reactor with direct heat transfer for thermo-chemical heat

storage. Part A: Experimental results," *Chemical Engineering Research & Design,* vol. 91, pp. 856-864, 2013, doi: 10.1016/j.cherd.2012.09.020

[64] J. Yan and C. Zhao, "Experimental study of CaO/Ca(OH)2 in a fixed-bed reactor for thermochemical heat storage," *Applied Energy,* vol. 175, pp. 277-284, 2016, doi: 10.1016/j.apenergy.2016.05.038

[65] M. Schmidt, C. Szczukowski, C. Roßkopf, M. Linder, and A. Wörner, "Experimental results of a 10 kW high temperature thermochemical storage reactor based on calcium hydroxide," *Applied Thermal Engineering,* vol. 62, pp. 553-559, 2014, doi: 10.1016/j.applthermaleng.2013.09.020

[66] M. Schmidt, A. Gutiérrez, and M. Linder, "Thermochemical energy storage with CaO/Ca(OH)2 Experimental investigation of the thermal capability at low vapor pressures in a lab scale reactor," *Applied Energy,* vol. 188, pp. 672-681, 2017, doi: 10.1016/j.apenergy.2016.11.023

[67] M. Schmidt, M. Gollsch, F. Giger, M. Grün, and M. Linder, "Development of a Moving Bed Pilot Plant for Thermochemical Energy Storage with CaO/Ca(OH)2." In *AIP Conference Proceedings* ,vol 1734, 2016, doi: 10.1063/1.4949139

[68] M. Schmidt, "Experimental investigation of Ca(OH)2 as thermochemical energy storage at process relevant boundary conditions," Dr, Stuttgart University, 2017.

[69] B.-J. R. Mungyeko Bisulandu and F. Huchet, "Rotary kiln process: An overview of physical mechanisms, models and applications," *Applied Thermal Engineering,* vol. 221, p. 119637, 2023/02/25/ 2023, doi: 10.1016/j.applthermaleng.2022.119637.

[70] M. Neises, S. Tescari, L. de Oliveira, M. Roeb, C. Sattler, and B. Wong, "Solar-heated rotary kiln for thermochemical energy storage," *Solar Energy,* vol. 86, no. 10, pp. 3040-3048, 2012/10/01/ 2012, doi: 10.1016/j.solener.2012.07.012.

[71] S. Tescari *et al.*, "Experimental and numerical analysis of a solar rotary kiln for continuous treatment of particle material," *AIP Conference Proceedings,* vol. 2033, no. 1, 2018, doi: 10.1063/1.5067148.

[72] D. Geldart, "Types of gas fluidization," *Powder Technology,* vol. 7, no. 5, pp. 285-292, 1973/05/01/ 1973, doi: 10.1016/0032-5910(73)80037-3.

[73] D. Kunii and O. Levenspiel, "CHAPTER 1 - Introduction," in *Fluidization Engineering (Second Edition)*, D. Kunii and O. Levenspiel Eds. Boston: Butterworth-Heinemann, 1991, pp. 1-13.

[74] L. F. Marie, S. Landini, D. Bae, V. Francia, and T. S. O'Donovan, "Advances in thermochemical energy storage and fluidised beds for domestic heat," *Journal of Energy Storage,* vol. 53, p. 105242, 2022/09/01/ 2022, doi: 10.1016/j.est.2022.105242.

[75] D. Kunii and O. Levenspiel, "CHAPTER 3 - Fluidization and Mapping of Regimes," in *Fluidization Engineering (Second Edition)*, D. Kunii and O. Levenspiel Eds. Boston: Butterworth-Heinemann, 1991, pp. 61-94.

[76] S. Ergun, *Fluid Flow Through Packed Columns*. 1952.

[77] A. Anantharaman, R. A. Cocco, and J. W. Chew, "Evaluation of correlations for minimum fluidization velocity (Umf) in gas-solid fluidization," *Powder Technology,* vol. 323, pp. 454-485, 2018, doi: 10.1016/j.powtec.2017.10.016

[78] V.-G. V. u. Chemieingenieurwesen, *VDI Heat Atlas*. Heidelberg: Springer Berlin, 2010, pp. 743-744.

[79] Y. A. Criado, M. Alonso, J. C. Abanades, and Z. Anxionnaz-Minvielle, "Conceptual process design of a CaO/Ca(OH)2 thermochemical energy storage system using fluidized bed reactors," *Applied Thermal Engineering,* vol. 73, no. 1, pp. 1087-1094, 2014/12/05/ 2014, doi: 10.1016/j.applthermaleng.2014.08.065.

[80] P. E. Pardo, Z. Anxionnaz-Minvielle, S. Rougé, P. Cognet, and M. Cabassud, "Ca(OH)2/CaO reversible reaction in a fluidized bed reactor for thermochemical heat storage," *Solar Energy,* vol. 107, pp. 605-616, 2014, doi: 10.1016/j.solener.2014.06.010

[81] Y. A. Criado, A. Huille, S. Rougé, and J. C. Abanades, "Experimental investigation and model validation of a CaO/Ca(OH)2 fluidized bed reactor for thermochemical energy storage

applications," *Chemical Engineering Journal,* vol. 313, pp. 1194-1205, 2017/04/01/ 2017, doi: 10.1016/j.cej.2016.11.010.

[82] M. Angerer *et al.*, "Design of a MW-scale thermo-chemical energy storage reactor," *Energy Reports,* vol.4, pp. 507-519, doi: 10.1016/j.egyr.2018.07.005 .

[83] K. Risthaus, M. Linder, and M. Schmidt, "Experimental investigation of a novel mechanically fluidized bed reactor for thermochemical energy storage with calcium hydroxide/calcium oxide," *Applied Energy,* vol. 315, no. 118976, 2022, doi: 10.1016/j.apenergy.2022.118976.